Modeling and Simulation of Efficient Nanoscale MOSFET and Photovoltaic Devices

Thesis Submitted by

TAPAS CHAKRABARTI

DOCTOR OF PHILOSOPHY(ENGINEERING)

Department of Electronics and Telecommunication Engineering
Faculty Council of Engineering & Technology
Jadavpur University
Kolkata, West Bengal, India
2018

Jadavpur University
Kolkata-700032, West Bengal, India

INDEX NO.260/16/E

1. Title of the thesis:

Modeling and Simulation of Efficient Nanoscale MOSFET and Photovoltaic Devices

2. Name, Designation & Institute of the Supervisor:

Prof. Subir Kumar Sarkar
Professor and Former Head of Department
Department of Electronics and Telecommunication Engineering
Jadavpur University
Kolkata-700032, West Bengal, India

3. List of Publications

(International Refereed Journals)
(All UGC approved peer review Journals)

1). **Tapas Chakrabarti**, AnupDey and Subir Kumar Sarkar, "Comparative analysis of Physical Organic and Inorganic Dyesensitized Solar Cell", **Optical Materials** 82 (2018), 141-146, Elsevier DOI: https:doi.org/10.1016/j.optmat.

2) Komol Kumari, **Tapas Chakrabarti**, Abir Jana, DishaBhattachartjee, Bhaskar Gupta, Subir Kumar Sarkar, "Comparative Study on Perovskite Solar cells based on Titanium, Nickel and Cadmium Doped $BiFeO_3$ Active material", Optical Materials Volume 84, October 2018, Pages 681-688, Elsevier, https://doi.org/10.1016/j.optmat.2018.07.071.

3). **Tapas Chakrabarti**, &Subir Kumar Sarkar, "Analytically Performance Study of Newly Modelled HIT solar cell with different materials", International Journal of Latest Technology in Engineering, Management & Applied Science (IJLTEMAS,) Volume VII, Issue IV, April 2018, ISSN 2278-2540 (UGC approved).

4) **Tapas Chakrabarti**, & Subir Kumar Sarkar, "VWF Tool Based T-J Solar Cell Modeling and Analyzing the Performance", Published in International Journal of Innovative Technology and Exploring Engineering (IJITEE) ISSN: 2278-3075, Volume-4, Issue-5, Page 46-50 (UGC Approved).

5) **Tapas Chakrabarti**, Abir Jana, Komal Kumari & Subir Kumar Sarkar, "Dye-Sensitized Solar Cells using Natural Pigments ", Published in International Journal of Innovations in Engineering and Technology (IJIET) http://dx.doi.org/10.21172/ijiet.122.11(UGC Approved).

4. List of Patents :**Nil**

5. List of Presentations in International Conferences / Workshops:

1). **Tapas Chakrabarti**, Akash Jana, AmbarKhanda, Subir Kumar Sarkar, "Modelling High Efficiency H-I-T solar cells with comparative analysis", Published in ICPCSI-2017 at Saveetha Engineering College, Chennai, IEEE Xplore, ***DOI:*** *10.1109/ICPCSI.2017.8392126*

2). **Tapas Chakrabarti**, RudrarupSengupta, NehaSinha and Subir Kumar Sarkar, "Study and Simulation of Energy Efficient Realistic HIT Solar Cell Defect States", Published in IICPE -2016 at Thapar University : IEEE Xplore, ***DOI:*** *10.1109/IICPE.2016.8079502.*

3). **Tapas Chakrabarti**, AmbarKhanda, Malay Saha, Subir Kumar Sarkar, "HIT Solar Cell using ZnTe as an emitter layer", Published in ICPEC -2017 at BNMIT, Bangalore, IEEE Xplore: ***DOI:*** *10.1109/ICSPACE.2017.8343398*.

4). **Tapas Chakrabarti**, Udit Sharma, Suvrajit Manna, TyajodeepChakrabarti, Subir Kumar Sarkar "Design of Intelligent Maximum Power Point Tracking Technique (MPPT) based on swarm intelligence Algorithm", Published in ICPEC -2015 at BNMIT, Bangalore.IEEEXplore***DOI:****10.1109/ICPACE.2015.7274938*

5). **Tapas Chakrabarti**, Udit Sharma, TyajodeepChakrabarti, Subir Kumar Sarkar, "Extraction of Efficient Electrical Parameters of Solar Cell using Firefly and Cuckoo Search Algorithm", Published in IICPE -2016 at Thapar University: IEEE Xplore, ***DOI:*** *10.1109/IICPE.2016.8079503.*

6). **Tapas Chakrabarti**, Malay Saha, AmbarKhanda and Subir Kumar Sarkar, "Modeling of Lead-Free $CH_3NH_3SnI_3$-Based Perovskite Solar Cell Using ZnO as ETL", Published as Book Chapter in Advances in Communication, Devices and Networking, **@ Springer** Nature, through **ICDDN-2017**: *DOI:https://doi.org/10.1007/978-981-10-7901-6_15.*

7). **Tapas Chakrabarti**, RudrarupSengupta, VurikitiPrashant, SubhrajeetDutta and Subir Kumar Sarkar, "Modelling of High Efficiency AlGaInP based PIN solar cells with comparative analysis", Published in **ICAMET- 2014***Proceedings*, December 17-19, 2014 at IIEST Shibpur.

8). RudrarupSengupta, **Tapas Chakrabarti**, VurikitiPrashant, and Subir Kumar Sarkar, "Modelling, Simulation and comparative study new compound alloy based PIN solar cells- an efficient way of energy management", Published in **ICPEC -2015** at BNMIT, Bangalore. IEEE Xplore, ***DOI:*** *10.1109/ICPACE.2015.7274922*.

9). RudrarupSengupta, **Tapas Chakrabarti** and Subir Kumar Sarkar, "Analytical Modelling, Simulation, and Comparative Study of Compound Alloy based Tandem Solar Cells – An Efficient Way", Published in **ICPEC -2017** at BNMIT, Bangalore, IEEE Xplore: ***DOI:*** *10.1109/ICSPACE.2017.8343397*.

10). RudrarupSengupta, **Tapas Chakrabarti** and Subir Kumar Sarkar, "Modelling of cost effective efficient HIT solar cell", Published in ***IEEE Sponsored***, **ICECS-2016***Proceedings*, at Karpagam College of Engineering at Coimbatore.

11). **Tapas Chakrabarti**, & Subir Kumar Sarkar, "Impact of Small AC Signal Superimposed on DC bias on the Performance of Nanoscale SON MOSFETs", Published in ***IEEE Sponsored*** Conference (27-28 July 2018) On Recent Innovations In Electrical, Electronics & Communication Engineering - (ICRIEECE-2018) at Kalinga Institute of Industrial Technology, Bhubaneswar.

Dedicated to

My Parents

Late Hriday Chakrabarti

Late Sandhya Chakrabarti

And My Departed Sister

Late Rama Rani Chakrabarti

&

My Wife

Smt. Latika Chakrabarti

And my beloved Son

Shri Tyajodeep

For their motivation, support and cooperation

CERTIFICATE FROM THE SUPERVISOR

This is to certify that the thesis entitled ***"Modeling and Simulation of EfficientNanoscale MOSFET and Photovoltaic Devices"*** *submitted by* ***Shri. Tapas Chakrabarti*** *who got his name registered on* ***11/05/2016*** *with Regn. No.* ***D-7/E/385/16*** *for the award of Ph.D (Engg.) degree of Jadavpur University is absolutely based upon his own work under the supervision of* ***Prof. Subir Kumar Sarkar*** *and that neither his thesis nor any part of the thesis has been submitted for any degree/ diploma or any other academic award anywhere before.*

Prof. Subir Kumar Sarkar
Supervisor, (Dept. of ETCE)
Jadavpur University
Kolkata-700032,
West Bengal, India

ABSTRACT

The minimization of device size and exploration of alternative energy are the demand of present world. Along with the genre of Mobile computing, smaller handy gadgets, more faster and efficient processors are the requirement of society and this leads towards the exploration into the field of nano-scale MOSFETs. In the same time the use of 'solar energy' through the 'Photovoltaic solar cell' is also the importunity of future life. To feed the demand of these, the device size miniaturization in case of 'MOSFET' or the 'Solar cell structure' is obvious. To incorporate billions of transistors in a single chip, the MOS devices are to be scaled to bring faster speed, but in the same time some unwanted effects do appear. The short channel effect is most prominent, which changes the threshold voltage, surface potential, electric field also. Hence the reliability study of MOS device is an important work which has been done in this research work. On the other hand c-Si solar cell is dominating the solar cell market. The c-Si solar cell efficiency is achieved up to 18% to 20%. To break through this efficiency level and to minimize the uses of c-silicon the 'HIT solar cell', 'Dyesensitized solar cell' 'Perovskite solar cell' new structures modeling have been done, as before fabrication modeling is an important step. In HIT solar cell proposed model the different layers are considered in nanoscale as the thinner layer produced more Voc, which enhanced the efficiency of 27.7%. In 'Dyesensitized solar cell' the nano crystalline semiconductors are used to attract broadband solar spectrum. In the newly modeled 'Perovskite solar cell' the layer of ZnTe is used as HTL whose thickness is 5nm and achieved a remarkable efficiency of 23.54%. The different models are carried out in this research work and achieved good results. At last, some swarm optimization techniques like ABC, FA and CS are applied in PV

panels to derive the minimum duty cycle for the controller to extract the maximum power points and different electrical parameters.

ACKNOWLEDGEMENT

First of all I like to convey my gratitude towards the almighty and my departed parents and elder sister. I would like to express my deep gratitude and indebtedness from my heart to my respected, supervisor Professor Subir Kumar Sarkar, Department of Electronics and Telecommunication Engineering, Jadavpur University, Kolkata-700032 for his valuable guidance, continuous encouragement and inspiration during the course of my Ph.D research work. During the period of this course, I could realize that the blessing of him is there always with me which gives me the boosting energy to achieve the goals by conquering all the hurdles. I am very much fortunate that I got a guide like him, who not only guided me to complete the entire research work and to finish the dissertation in due time, but also he has extended his kind helping hand every time I needed. I learned from him the real quality of a teacher and forgiveness towards the students.

It is also to be mentioned that I am really a fortunate person who has got the help each and every time from all the members of the VLSI Lab of Professor Sarkar.

I have received the support from all the faculties and staff of Department of ETCE and IC Center, and the Faculty of Engineering and Technology (FET), Jadavpur University, during my Ph.D research work.

During the period of this course, there were number of people who directly or indirectly helped me or motivated me to complete the task; I am really indebted to them as their inspiration brought me nearer to my destination.

I am also thankful to my parent Institute, “Heritage Institute of Technology, Kolkata” and specially the authority of the college and the colleagues of this Institute.

Finally I am indebted to my family members, whose love motivation and encouragement always paved the way for me to complete my task. At last, I like to mention the two names; they are my wife Smt. Latika Chakrabarti and my son Tyajodeep who were always beside me with their love, motivation, encouragement and real cordial support during the long research work. Really, without their help and support it would not have been be possible for me to complete the research work and to submit the thesis in due time.

27th June, 2018

Jadavpur University **(TAPAS CHAKRABARTI)**

Kolkata-700032

CONTENTS

LIST OF FIGURES

LIST OF TABLES

LIST OF ABREVIATIONS

ABC	Artificial Bee Colony
AC	Alternating Current
AFORS-HET	Automat FOR Simulation of Hetero-structures
ARC	Anti-Reflection Coating
a-Si:H	Hydrogenated amorphous Silicon
BSF	Back Surface Field
CdS	Cadmium Sulfide
CdTe	Cadmium Telluride
$CH_3NH_3PbI_3$	Methyl Ammonium Lead Iodide
$CH_3NH_3SnI_3$	Methyl Ammonium Tin Iodide
CIGS	Copper Indium Gallium Selenide
CMOS	Complementary Metal Oxide Semiconductor
c-Si	Crystalline Silicon
DC	Direct Current
DMDG SON	Double Metal Double Gate Silicon On Nothing
DMG	Dual Material Gate
DSSC	Dyesensitized Solar Cell
EQE	External Quantum Efficiency
ETL	Electron Transport Layer
FA	Firefly Algorithm
FDSOI	Fully Depleted Silicon On Insulator
FF	Fill Factor
FTO	Fluorine doped Tin Oxide

GaAs	Gallium Arsenide
GaInP	Gallium Indium Phosphide
HCE	Hot Carrier Effect
H-I-T	Heterojunction Intrinsic Thin film
HTL	Hole Transport Layer
ITO	Indium Tin Oxide
LDD	Lightly Doped Drain
LDMOS	Laterally Diffused Metal Oxide Semiconductor
LED	Light Emitting Diode
MOS	Metal Oxide Semiconductor
MOSFET	Metal Oxide Semiconductor Field Effect Transistor
MPPT	Maximum Power Point Tracking
P-I-N	p-type – intrinsic – n-type Semiconductor
PSO	Particle Swarm Optimization
PV	Photovoltaic
QME	Quantum Mechanical Effects
SCAPS	Solar-cell Capacitance Software
SCE	Short Channel Effects
SOI	Silicon on Insulator
STI	Shallow Trench Isolation
TCO	Transparent Conductive Oxide
VLSI	Very Large Scale Integration
ZnO	Zinc Oxide
ZnTe	Zinc Telluride

Symbol	Definition	Unit
∇	Gradient	
Ψ	Electron Wave Function	
k	Wave Vector	
η	Efficiency	
ε_{si}	Dielectric constant	
m	Electron Mass	kg
$\hbar$	Modified Planck Constant	eV.s
E	Energy of the electron	eV
m^*	Electron effective mass	kg
L	Channel Length	Metre
Z	Channel width	Metre
d	Insulated Oxide Thickness	nm
r_j	Junction Depth	nm
V_{TH}	Threshold voltage	V
V_{bi}	Built in potential	Volt
E	Electric field	Volt/cm
i-Si	Intrinsic Silicon	μm
c-Si	Crystalline Silicon	μm
a-Si	Amorphous Silicon	μm
E_g	Band gap	eV
μ_n	Electron mobility	$m^2/(V.s)$

μ_p	Hole mobility	$m^2/(V.s)$
μc-Si: H	Hydrogenated micro crystalline silicon	μm
a-Si:H	Hydrogenated amorphous silicon	μm
J_{sc}	Short circuit current density	mA/cm^2
V_{oc}	Open circuit voltage	mV

CHAPTER 1

INTRODUCTION AND ORGANIZATION OF THE THESIS

- Introduction and Motivation of the Present Research
- Thesis Organization
- Reference

1.1 INTRODUCTION AND MOTIVATION

With the increase of modern society life, the energy requirement is obvious and which is growing exponentially. The smaller device size and ‘alternative energy’ exploration are the demand of future world. The researchers are involved to explore more and more, smaller handy gadgets, more faster and efficient processors which lead to exploration into the regime of nano scale MOSFETs. In the similar time the use of ‘solar energy’ through the ‘Solar Photovoltaic device’ that is the solar cell, is also the importunity of future life. It is perceptible that the intensive research works over the different genere of new model solar photovoltaic cells with advanced optical material is going on. The researchers are investing their new thinking to improve the ‘efficiency’ of ‘solar cell’ with cost effectiveness. The enhancement of ‘efficiency’ is not only the criteria of present research work but also more cost effectiveness, which can only minimize the price of ‘Photovoltaic electrical energy’ unit. The new research in the field of ‘Photovoltaic cell’ is going on to the nanoscale layer thickness of different genre of ‘solar cells’ to increase the ‘efficiency’.

Before physical fabrication, the modeling is very significant critical step.

Down scaling of electronic devices specially MOSFETs in the nano- regime improves device performance, with some constrictions. Due to reduction in size, supply voltage at drain and gate have also been reduced proportionately [1-2]. This situations demand a reliability study of nanoscale device. In 'this research work' a small AC signal of high frequency supply is superimposed on DC biasing, as the uncountable noise sources are inevitable in the VLSI circuits. This 'superimposed signal' changes various electrical characteristics as 'Surface Potential', ' Electric field', 'Threshold Voltage', 'Drain Current' and 'Transconductance' of nano region devices fluctuate but not in bulk. These fluctuations degrade the function of the nanoscale advance MOS devices.

To convert the 'solar light energy' in to 'electrical energy', 'Photovoltaic solar cells' are used which belongs to different generations. In the prevailing 'solar cell' industry, 92% of 'solar cells' are made of 'Silicon', though 'Silicon' is an 'indirect band gap' semiconductor material and it has poor infrared light absorbance. The silicon 'solar cells' are dominating the photovoltaic industry, because of its long term reliability with optimum efficiency.

'Tandem solar cells' of 44.70% efficiency have been achieved at Helmholtz center Derlin [3], which is applicable mainly in satellite powering. These 'Tandem solar cells' are made of optical compound semiconductor with multijunction and multi tunnels which have the lattice mismatch also [4]. The process of compound semiconductor production is complex and costly also. Hence, the output net power price also becomes high. After the reduction of complexity of the multijunction 'Tandem cells', the advanced types of 'single junction Photovoltaic cells' are P-I-N 'solar cells' which also produce the 'efficiency' of 20% using GaAs or GaInP [5-6]. These compound materials have the 'wide band gap' and it may be tuned up to 2.3eV [7]. The 'direct

band gap' property advantages are over shadowed with the increased trap densities. The polarization interfaces of these compound alloys also make difficulty to model these P-I-N solar cells. Moreover these compound optoelectronics semiconductor materials preparation process is very critical which leads to price hike. The researchers are continuously striving their effort for better conversion ratio with the reduction of complexity and cost, which is resulted in development of heterojunction (H-I-T) solar cells. The H-I-T 'solar cells' combine the highly stable crystalline silicon with comparatively low temperature applicable technology of a-Si:H films in a reduced cost with an 'efficiency' of 20.7% [8]. With the motive of minimization of use of silicon, in my research work the new material ZnTe is applied for positive charge transportation emitter layer and the simulated result of this new modeled H-I-T 'solar cell' showed the 'efficiency' of 27.7%.The 'impact of defects' and 'ambient temperature' on the H-I-T 'solar cells' are simulated, for better performance.

In the year of 1991 O'Regan and Gratzel developed a new environment friendly 'Photovoltaic solar cell' using photo sensitizer dye with the name of 'Dyesensitized Solar Cell' [9]. The 'efficiency' of this type of 'solar cell' is very low [10]. Though the 'efficiency' of 'Dyesensitized Solar Cell' is less around 7-8 percent with respect to tandem, P-I-N or H-I-T 'solar cells', but it is becoming popular as the fabrication technology is easier and cheaper too. The conventional DSSCs had the potential to be an alternative of 'silicon solar cells', but the main disadvantage of 'Dyesensitized Solar Cell' is the use of 'liquid electrolytes', which suffers from stability. The 'liquid electrolytes' and dyes are degraded very fast with ambient temperature and hence the overall performance considerations of DSSCs suffer a setback. This problem of stability can be solved by using solid state electrolytes in place of liquid state electrolyte.

From the essence of this draw-back the newer concept of 'solar cells' developed using Perovskite are the alternative significant improvement in terms of 'efficiency' and crossed the level of 20% 'efficiency' [11]. This new concept of 'solar cell' has three parts as the main photosensitizer material Perovskite and other two parts are two different types of charge carriers (electron and hole) transport layer on the top and bottom of Perovskite. The most popular Perovskite material used in solar-cell is $CH_3NH_3PbI_3$ [12]. As lead (Pb) is toxic and hazardous to 'human health' and 'environment', hence a suitable alternative is $CH_3NH_3SnI_3$ used in 'solar cells'. Another important issue of this 'solar cell' is the selection of material suitable for transportation of positive charge carriers, holes.

Mostly used HTL material is high expensive polymer based 'spiro-MeOTAD' [13-14], which pull up the price of 'solar cell'. To achieve a solution, in this research work, effective inorganic II-VI, p-doped Zink Telluride (ZnTe) material is applied as HTL. The new concept of model Perovskite material ($CH_3NH_3SnI_3$) without lead and cheaper HTL material (ZnTe) is applied in the newer 'solar cell' and simulated the same in the SCAPS software and physically fabricated also. In our research work the simulated and fabricated cell has achieved the 'efficiency' of 23.54% and 5.032% respectively.

It is also witnessed that the 'efficiency' enhancement is not the only solution for the production of economical solar power for the prevailing people of society. To draw the maximum electrical energy, it is sensible to utilize the 'PV module' at the 'maximum power point' (MPP) [15]. In this respect the optimization of MPPT (Maximum Power Point Tracking) with the intelligent technique is very much useful. Many Intelligent optimization techniques have been developed recently. 'PSO' is one of them [16] which is applied in this research work. Inspiring from the social behavior of various species the optimization algorithm [17] of ABC (Artificial Bee

Colony) [18], Fire fly algorithm [19] and Cuckoo search [17] [20] algorithm is applied to extract the electrical parameters from the Photovoltaic Panel and tracks the 'Maximum Power Point'.

1.2 ORGANIZATION OF THE THESIS

My research thesis has been outlined in 'eight chapters' including the **1st Chapter** where the Introduction of this work is narrated. In this Introduction Chapter it is illustrated about the 'Nanoscale MOSFETs' as well as the 'Nanoscale' different layer or particles of materials used in 'Photovoltaic Solar cells' of different genre.

In **Chapter 2** an introduction of nanoscale MOS devices and 'solar cell' and their physics is described. The basic, fundamentals, of these devices and brief idea of DMDG SON MOSFET, 'Heterojunction Intrinsic Thin-film', 'Dyesensitized' and 'Perovskite' 'solar cells' are also discussed.

Chapter 3 has described the nano scale DMDG SON MOSFET structures and their reliability study is done while the AC signals like noises are super imposed with the DC signals at the gate.

In **4th Chapter**, the basic concept of Heterojunction Intrinsic Thin Film (HIT) Photovoltaic cells and the different modeling is discussed. The comparison among the different structures and different materials are studied and applied in the new model of H-I-T 'solar cells'.

Chapter 5 consists of 'Dyesensitized solar cell' structures, their working principals and comparison of organic and inorganic dye based 'Dyesensitized solar cells'. The fabrication processes of multiple of cells applying organic and inorganic dyes are discussed and analyses of those cells are also described in this Chapter.

In **Chapter 6**, the different optoelectronics materials are described, including the 'Perovskite materials' which are studied and used in numbers of 'Perovskite solar cells' simulations and

physical fabrications. The details of 'Perovskite solar cell' modeling, construction, simulation and fabrications are postulate in this chapter.

Chapter 7 is framed with the discussion of different 'optimization techniques' and applied to 'extract' the best 'possible solutions' of 'Photovoltaic Panels'. The 'Maximum Power Point Tracking' (MPPT) is an important technique in this domain for best result of output which has been done by intelligent techniques in this work.

In the **8th chapter**, conclusion of works which are carried out in my 'research work' is described with a summery. The future scope of works are discussed which can be the extension of this 'research work' in forthcoming time.

1.3 REFERENCES

[1] H. Matsushita and Y. Tanji, "Application of Independent-minded Particle Swarm Optimization for design of class-E amplifiers," Soft Computing and Intelligent Systems (SCIS) and 13th International Symposium on Advanced Intelligent Systems (ISIS), 2012 Joint 6th International Conference on, Kobe, 2012, pp. 60-64.

[2] J. P. Colinge, "Multiple-gate SOI MOSFETs," Solid State Electron, vol. 48, no. 6, pp. 897–905, Jun. 2004.

[3] Dimroth, F., Grave, M., Beutel, P., Fiedeler, U., Karcher, C., Tibbits, T. N. D., Oliva, E, Siefer, G., Schachtner, M., Wekkeli, A., Bett, A. W., Krause, R., Piccin, M., Blanc, N., Drazek, C., Guiot, E., Ghyselen, B., Salvetat, T., Tauzin, A., Signamarcheix, T., Dobrich, A., Hannappel, T. and Schwarzburg, K. (2014), Wafer bonded four-junction

GaInP/GaAs/ /GaInAsP/GaInAs concentrator solar cells with 44.7% efficiency. Prog. Photovolt: Res. Appl., 22: 277–282. doi: 10.1002/pip.2475

[4] R.Ho, K.W.Mai, and M.A.Horowitz, “The future of wires,” Proc. IEEE, vol. 89, no 4, 2001, pp. 490-504.

[5] Y. G. Xiao, z. Q. Lt, M. Lestrade, and Z. M. Simon, "Modelling of InGaN PIN solar cells with defect traps and polarization interface charges" Li Crosslight Software Inc. , 121-3989 Henning Drive, Burnaby, BC, V5C 6P8, Canada 978-1-4244-5892-9/101$26.00 ©2010 IEEE.

[6] Md. Abu ShahabMollah, Md. Liton Hossain, Md. Imtiaz Islam, Abu FarzanMitul , "High Efficiency InGaN Based Quantum Well & Quantum Dot Solar Cell" ©Academia 2014.

[7] Lu Hongbo, Li Xinyi Zhang Wei., Zhou Dayong, Shi Mengqi, "A 2.05eV AIGainP sub-cell used in next generation solar cells" Lu Hongbo, Li Xinyi Zhang Wei., Zhou Dayong, Shi Mengqi Sun Lijieand Chen Kaijian, Research Center for Photovoltaics, Shanghai Institute of Space Power-Source, Shanghai 200245, China, Journal of semiconductors, September 2014 Vol. 35, No. 9.

[8] H.Sakata, T.Nakai, T.Baba, M.Taguchi, S.Tsuge, K.Uchihashi, S.Kiyama, Proc. 20th IEEE PVSEC (2000), 7.

[9] O’Regan, B.; Gra¨tzel, M. *Nature* 1991, *353*, 737.

[10] Anders Hagfeldt, Gerrit Boschloo, Licheng, Lars Kloo, and Henrik Pettersso, Dye-Sensitized Solar cells , Chem. Rev. 2010, 110, 6595–6663

[11] Peng Qin, Soichiro Tanaka, Seigo Ito, Nicolas Tetreault, Kyohei Manabe, Hitoshi Nishino,Mohammad Khaja Nazeeruddin & Michael Gra¨tzel, " Inorganic hole conductor-

based lead halide perovskite solar cells with 12.4% conversion efficiency ", NATURE COMMUNICATIONS, 5:3834 , DOI: 10.1038/ncomms4834

[12] Y. Shamash, “Stable reduced-order models using Pade type approximation,” IEEE Trans. Autom. Control, Vol. 19, no. 5, pp. 615_616, Oct.1974.

[13] Wonchai Promnopas, Titipun Thongtem, and Somchai Thongtem, "Spiro-MeOTAD Semiconductor-Polymer Gel Composited Electrolyte for Conversion of Solar Energy", Journal of Nanomaterials, Volume 2014, Article ID 529629

[14] Othmane Skhouni, Ahmed El Manouni1, Bernabe Mari, and Hanif Ullah, “Numerical study of the influence of Spiro-MeOTAD thickness on CdS/Spiro-MeOTAD solar cell performance”, Eur. Phys. J. Appl. Phys. (2016) 74: 24602, DOI: 10.1051/epjap/2015150365.

[15] W. Xiao, N. Ozog, and W. G. Dunford, “Topology study of Photovoltaic interface for maximum power point tracking,” *IEEE Trans. Ind.Electron.*,Vol.54, No.3,(2007), pp.1696–1704.

[16] Bijoy Kantha and **Subir Kumar Sarkar**, “Comparative Study Analysis of Particle Swarm Optimization and Genetic Algorithm for the Optimization of Parameter of MEMS based Micro-heater”, Journal of Computational and Theoretical Nanoscience, ASP, Vol-12, pp-1-6, 2015.

[17] X S Yang, “Nature-inspired Metaheuristic Algorithm”, *Luniver Press*, (2008)

[18] X.-S. Yang; S. Deb (December 2009). "Cuckoo search via Levy flights". World Congress on Nature & Biologically Inspired Computing (NaBIC 2009). IEEE Publications. pp. 210–214.

[19] D. Karaboga, “An idea based on honey bee swarm for numerical optimization”, Technical Report-TR06, Erciyes University, Engineering Faculty, Computer Engineering Department, 2005.

[20] Tapas Chakrabarti, Tyajodeep Chakrabarti, Udit Sharma and **Subir Kumar Sarkar**, “Extraction of Efficient Electrical Parameters of Solar Cell using Firefly and Cuckoo Search Algorithm”, in IEEE-7th India ‘International Conference on Power Electronics’ (IICPE) 2016, 17th-19th November, Thapar University, Punjab, India, Volume: IEEE Xplore.

CHAPTER 2

BASICS OF SEMICONDUCTOR PHYSICS AND ADVANCE MOSFET AND SOLAR CELLS

- Introduction
- Semiconductor Physics
- Basics of Nanoscale Advance MOSFET
- Basics of Nanoscale Solar cells
- Reference

2.1. INTRODUCTION

The ‘modern life’ is ameliorating due to technological development. The electronics industry is playing an important role right from the day to day life to the space satellite industry. More ‘energy efficient’ ‘cost effective’ handy, faster devices exploration is going on through the researchers. The ‘semiconductor industry’ is dominating the pace of contemporary development of devices. The MOSFET devices are the paramount of VLSI high density integrated circuits. The newer electronics gadgets are the present challenge in this field and CMOS devices are the building block of ‘low power’ ‘VLSI circuits’. The innovative structures of MOS devices are continuously developed and sizes are also to be miniaturized. The step sub-threshold slope, ‘short channel effect’, ‘threshold voltage fluctuations’ are evolving along with the ‘MOS device’. To address the same ‘DMDG SON MOSFET’ is one of the solutions. In the same time the

reliability study also is a very critical task; along with the sophisticated new device energy management is also an important task. The alternative renewable energies are the future of our civilization. Among the renewable energies the 'solar energy' has the most potential which can be converted to the electrical energy using the 'photovoltaic effect' on semiconductor. The continuous investigations are also going on to develop more efficient solar photovoltaic cell to feed the energy demand.

2.2. SEMICONDUCTOR PHYSICS

The 'electrical conductivity' and resistivity of semiconductor lies in between conductor and insulators. The most common semiconductor used in the 'electronics industry' more precisely in the nano regime devices like MOSFET or Solar cell is Silicon semiconductor. Apart from the silicon there are so many semiconductors that are used in this field like 'Germanium' (Ge), 'Gallium Arsenide' (GaAs), 'Gallium Indium Phosphate' (GaInP) etc. But 'Silicon' is the common and most usable semiconductor as it is abundant in nature in the form of 'silicon dioxide' (SiO_2). The Silicon extraction from the SiO_2 and the fabrication technologies are also well developed. Silicon semiconductor is available in 'mono crystalline', 'poly crystalline' and 'Amorphous Silicon' form. The silicon is also a good choice for fabrication of 'solar cell' due to its good 'absorption coefficient'. The 'silicon' is an 'indirect band gap' material where as 'Germanium' is 'direct band gap' material. The 'silicon' and 'Germanium' are group –IV atoms, which signify that outer orbit of 'these materials' consists of 4 valance electrons making the 'covalent bond', 'each electron' is shared by the 'neighbor atom' also. The 'silicon and Germanium' have a pure diamond lattice as depicted in figure 2.1 [1].

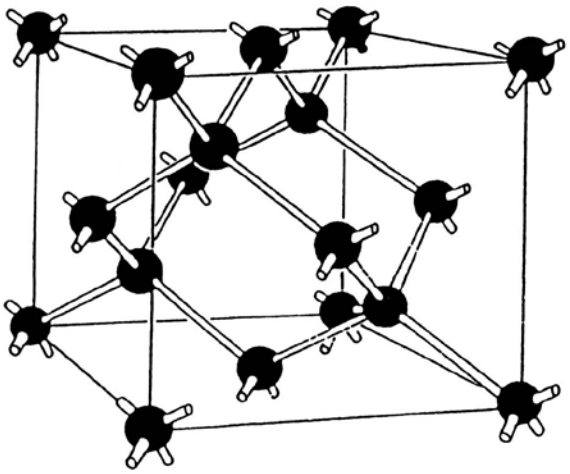

Fig.2.1 Diamond lattice of semiconductor [1]

'Energy Band Structures of Semiconductor':

The dynamic behavior of the 'electron' can be established from the 'electron wave' function, Ψ, which is attained by solving the time-independent Schrodinger equation [2].

$$\nabla^2\Psi + \frac{2m}{\hbar^2}[E - U(r)]\Psi = 0$$

Where, *m* is 'electron mass', $\hbar$ is the 'modified Planck constant', *E* is the 'energy of the electron', and *U(r)* is the 'periodic potential energy' inside the semiconductor.

Solving this quantum-mechanical equation, the relation of electron's energy and momentum that are defined the 'band structure' of the 'semiconductor'.

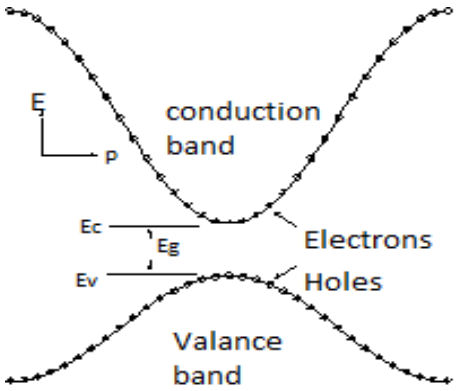

Fig.2.2 'Energy band diagram' of 'direct band gap' material

The ‘Quantum mechanically’ reckoned ‘motion of the electron’ in the ‘crystal’, is free space if its ‘mass’ is **m**, and it is replaced by an ‘effective mass’, $\boldsymbol{m^*}$, and from ‘Newton’s law of motion’ of classical mechanics, the force $F=m*a$, where F is the applied force and ‘a’ is the acceleration of the electron. The allowed ‘electron energies’ Vs ‘crystal momentum’ graph is ‘plotted. The ‘crystal momentum’, $p = \hbar k$, where $\hbar$ is ‘modified plank constant’ and ‘k’ is the ‘wave vector’ corresponding to the ‘wave function’ solutions of the ‘Schrodinger equation’ [2].

The ‘energy bands’ below the ‘valence band’ are speculated to be ‘fully occupied’ by ‘electrons’ and the ‘conduction band’ are speculated to be ‘empty’. These empties are usually termed as holes with positive charge effective mass. The ‘electron effective mass’ is thus defined as

$$m^* = \frac{1}{\left[\frac{d^2E}{dp^2}\right]} = \frac{1}{\frac{1}{\hbar^2}\cdot\frac{d^2E}{dk^2}}$$

2.3 BASICS OF NANOSCALE ADVANCE MOSFET

The basic ‘MOSFET structure’ using Si-SiO_2 was first time proposed by ‘Kahng and Atalla’ in 1960 for the first time [3]. The reduction of device size is the requirement for ‘more density of transistors’ and as well as the ‘performance’ of the ‘electronic gadgets’. The trend of ‘miniaturization’ is shown in Figure 2.3 [4].

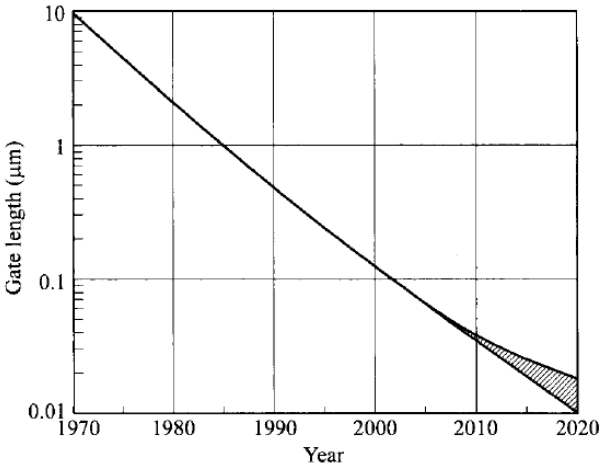

Fig.2.3 Trend of Minimization of Gate dimension in ICs [4]

The ‘structure’ of ‘common MOSFET’ is reflected in figure 2.4. The ‘MOSFET’ is normally four terminals device which are illustrated in the figure consists of ‘p-type’ ‘semiconductor substrate’ in which the ‘source’ and ‘drain’ of n^+ region are there. One ‘Gate terminal’ is connected to the ‘metal’ just above of ‘SiO_2 layer’. The substrate is the another terminal which normally connected to ground. The basic parameters of ‘MOSFET’ are the ‘channel length’ ‘L’ it is the distance between ‘source and drain’, the ‘channel width’ ‘z’, the ‘insulated oxide thickness’ ‘d’, and the ‘junction depth’ ‘r_j’ are illustrated in the figure 2.4. The ‘channel length’ can be modified by ‘modulating’ the ‘Gate to Source voltage’. This ‘channel conductance’ is also rest on the ‘substrate voltage’.

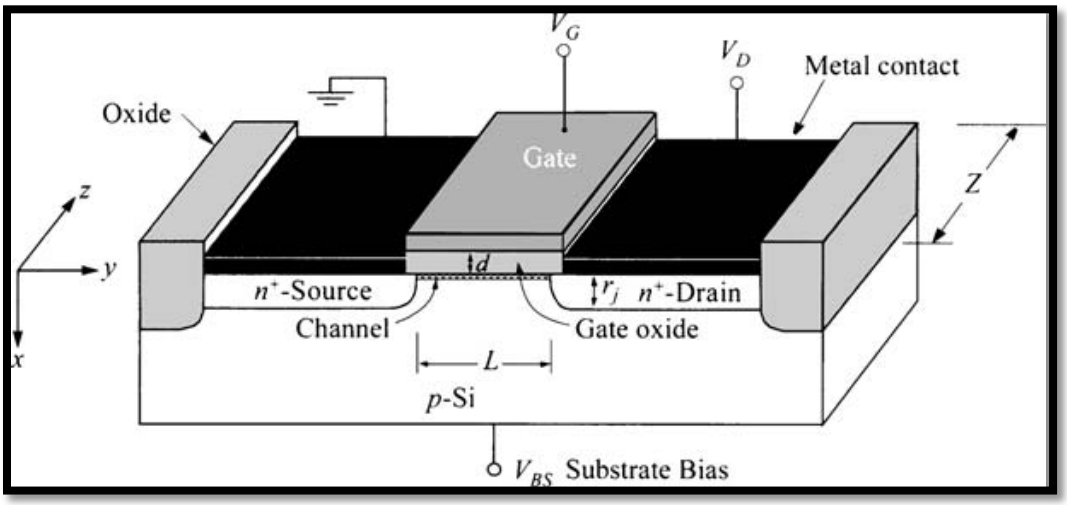

Fig.2.4 Schematic diagram of ‘MOSFET structure’

With the demand of high speed and cost effectiveness, the miniaturization is the obvious choice, but on the contrary ‘several drawbacks’ of the ‘MOS design’ and ‘process’ appear along with benefits. If the ‘thickness’ of ‘silicon dioxide layer’ is brought down around 2nm range, it will start breakdown because of ‘gate leakage current’. The ‘short channel effect’ is the ‘major challenge’ in ‘down-scaling’ of devices. The ‘short channel effect’ shift the ‘pinch off’,

ultimately changes the 'threshold voltage' as well as the 'hot carrier effect', 'drain induced barrier lowering'. To 'overcome' the situations the necessary technological changes are going on as 'SOI devices' or 'SON devices' with 'multiple gates' and 'multiple metals'. The miniaturization also invites the fluctuations of all the 'electrical parameters' like, 'Threshold voltage', 'surface potential', 'Transconductance'; 'electric field' fluctuates along the 'channel length'. The 'double metal', 'double gates', 'silicon on nothing', (DMDG SON) MOSFET structure is shown a breakthrough in recent days. The main concept of a 'DMDG SON MOSFET' is to control the 'channel' very 'efficiently' by selecting the 'channel width' to be 'very small' and by applying a 'gate contact' to 'both sides' of the 'channel'. This idea helps to quell 'short channel effects' and guides to 'higher current density' as compared with a 'MOSFET' having 'only one gate'. The "double metal double gate" 'MOSFET' having 'two gates' and we can modulate the 'gates' from the 'both side' for 'better control' of the 'channel', for this reason 'DMDG' 'MOSFET' is superior to the conventional 'MOSFET' [5].

2.4 BASICS OF NANOSCALE SOLAR CELL

The alternative renewable energy is the prime resource of tomorrow's life. In 1839 'Alexander Edmond Becquerel' discovered the 'Photovoltaic effect' the operating principal of 'solar cell'. The 'solar cells' structures exploration is the mainstream research work in present day. The c-Silicon solar cells' are the 'first generation' 'solar cell' which reached its extreme point of 'efficiency' around 20~22% [6]. The 'thin film solar cells' with newer optical materials and the newer structures have brought a new dimension in this research area. 'Heterojunction thin film' (H-I-T) 'solar cells', 'Dyesensitized solar cells', 'Perovskite solar cells', 'Organic solar cells' and 'Plastic solar cells' are predominant in forthcoming 'energy world'.

'PHOTOVOLTAIC EFFECT IN SOLAR CELL'

The 'Photoelectric effect' is the 'generation' of 'charge carrier' when 'photons' from the 'sun light' are incident on a 'semiconductor material'. The function of 'photovoltaic' is that, the 'incident photons' are the source of 'generation' of an 'electron-hole pair' which can be 'extracted' in to the 'external circuit' that produces 'electricity'. To describe this 'mechanism' more elaborately, and fundamentally, that is the 'light stream' consists of 'photons' and each 'photon' carries one 'quantum of energy'. This 'photon' is 'associated' with just one 'wavelength' or 'frequency'. 'High-frequency photon' has more 'energy' than the 'low frequency'. The 'solar cell' is composed of a 'p-n junction' which is formed by a 'p-doped semiconductor' and 'n-doped semiconductor'. The generated 'charge carriers' in the 'p-n junction' of 'solar cell' are separated by the 'built in potential' of the junction [2].

'Crystalline Silicon Solar Cell'

'Silicon' is one of the most 'abundant elements' in the earth. It is a 'semiconductor material' that very much suitable for 'solar cells' applications, with energy the 'band gap' of 1.1eV. 'Crystalline silicon' is the 'semiconductor material' very popular in the 'solar cell industry', and 'wafer-based' 'c-Si Photovoltaic cells' and modules which influence the 'current solar cells' market. This type of 'solar cells' are used in the form of 'PV Panel' to set up the 'PV Plant' at the rate of several hundred 'Mega Watt' even at the 'Giga Watt' scale due to its stability and large scale production. The 'efficiency' of 'c-Si solar cell' is in the ranges from 14% to 20%, in general [6-7].

‘Amorphous Silicon Solar Cell’

Along with CdTe ‘Photovoltaic cells’, the ‘a-Si solar cells’ are the most developed and ‘widely’ known ‘thin-film solar cells’. ‘Amorphous silicon’ can be deposited on ‘cheap’ and ‘very large substrates’ on ‘continuous deposition techniques’. ‘Different commercial organizations’ are also manufacturing ‘light and flexible’ ‘a-Si module’ ‘perfectly suitable’ for ‘flat’ and ‘curved surfaces’. Currently, ‘amorphous silicon PV modules’ ‘efficiencies’ are ‘in the range’ of ‘4% to 8%’. At laboratory environment, this type of ‘cell’ has attained the ‘efficiencies’ of 12.2%. ‘Thinner layers’ could ‘increase’ the ‘electric field strength’ across the ‘material’ and provide better ‘stability’ and ‘less reduction’ in ‘power output’, but this ‘reduces’ ‘light absorption’ and hence reduces the ‘cell efficiency’. A remarkable alternative of ‘amorphous silicon solar cell’ is the ‘multi-junction thin-film silicon’ (a-Si/μc-Si) ‘solar cell’ which consists of ‘a-Si cell’ with additional ‘layers of a-Si’ and ‘micro-crystalline silicon’ (μc-Si) applied onto the substrate. The ‘advantage’ of the ‘μc-Si layer’ is that it ‘absorbs’ ‘more light spectrum’ through the ‘red’ and near ‘infrared’ of the ‘light spectrum’, thus enhancing the ‘efficiency’ up to 10%. The ‘thickness’ of the ‘μc-Si layer’ is in the ‘order of 3 μm’ and makes the ‘cells thicker’ and ‘more stable’. The ‘current deposition techniques’ enable the ‘production’ of ‘multi-junction thin-films’ [7].

‘Heterojunction with intrinsic thin layer’ (H-I-T)

H-I-T ‘solar cell’ has pulled the attention of ‘’solar cell’ researchers due to its ‘low process temperature’ in comparison to ‘crystalline silicon’ (c-Si) ‘solar cell’ and relatively ‘high efficiency’ (η) (more than 21%). The structure of this type of cell consists of ‘thin intrinsic’ ‘amorphous silicon layers’ as surface passivation, which also acts as ‘buffer layer’ at the ‘top’ as well as ‘bottom surfaces’ of ‘n-type’ ‘crystalline silicon’ (c-Si) wafer. Thin ‘p-type a-Si’ ‘top

layer' acts as an emitter while 'highly doped' 'n+-type' 'bottom layer' is used as a 'back surface field' (BSF) [8-9].

'Dye-sensitized solar cells'

'Photo-electrochemical' function is used in 'Dyesensitized solar cells' which are based on 'semiconductor structures' formed between a 'photo-sensitized' 'anode' and an 'electrolyte'. In a 'Dyesensitized solar cell' the '**Nano crystals'** [10] of semiconductor that harvest the photons and the 'dye molecule' is responsible for the 'charge separation'. It is similar to natural photosynthesis [11] 'These cells' are so attractive because of 'low-cost materials' and simple technology to fabricate. However, their 'performance' can be 'degraded' over time with exposure to 'UV light' and the use of a 'liquid electrolyte' can be problematic. At 'Laboratory' the 'efficiencies' are achieved, more than 10% with the application of 'new broadband dyes' and 'electrolytes' however, 'commercial efficiencies' are become low level of '4% to 5%'. An 'interesting area of research' is the use of '**Nano crystalline'** 'semiconductors' that can allow DSSCs to have a 'broad spectral coverage'. The 'nano-structured materials' used in 'Dyesensitized solar cell' will produce 'high power conversion' 'efficiencies'.

'Perovskite Solar Cells'

The 'working principle' of 'Perovskite solar cells' are very similar to that of DSSC solar cells. The 'generation' of 'electron and hole' pair by 'absorbing light' and 'separation and transportation' of the 'electrons' and 'holes' using two different 'transport layers' is the working function of this type of 'solar cell'. The light is 'absorbed' by the 'Perovskite material' and electron and hole pair is generated. The 'Perovskite material' is 'sandwiched' between 'electron and hole' 'transport layer'. The purpose of the transport layers is to transport 'only one type' of

'carriers' through it and to 'block' the movement of 'other type' of carrier to flow. The 'Perovskite solar cell' showed a record 'efficiency' of 22.1% [12]

2.5 REFERENCES

[1] S . M. Sze and Kwok K. Ng, "Physics of Semiconductor Devices, Chapter-1: Physics and Properties of Semiconductor", John Wiley & Sons.

[2] Robert G.Arns, "The other transistor: early history of the metal-oxide- semiconductor fielld-effect transistor", ENGINEERING SCIENCE AND EDUCATION JOURNAL OCTOBER 1998

[3] S . M. Sze and Kwok K. Ng, "Physics of Semiconductor Devices, 3rd Edition", A John Wiley & Sons (2007)

[4] Jeffery L. Gray, "Handbook of Photovoltaic Science and Engineering: Chapter-3:The Physics of the Solar Cell", John Wiley & Sons.

[5] Pritha Banerjee, Anup Sarkar and Subir Kumar Sarkar, "Exploring the short channel characteristics and performance analysis of DMDG SON MOSFET", Microelectronics Journal, Elsevier, Volume 67, Pages 50-56, September 2017.

[6] M.A. Green et al., "Solar Cell Efficiency Tables (Version 29)," Prog. Photovoltaics Res. Appl., vol. 15, pp. 35-40, 2007.

[7] Khomdram Jolson Singh, **Subir Kumar Sarkar**, "Modeling of an efficient Thermo-Photovoltaic (TPV) cell as a power source for space application", International Symposium on Devices MEMS, Intelligent Systems & Communication(ISDMISC-2011), Sikkim Manipal Institute of technology, Sikkim.

[8]. Khomdram Jolson Singh and **Subir Kumar Sarkar**," A wide band gap In0.5(Al0.7Ga0.3)0.5P Back Surface Field layer increases 6% more efficiency in DLAR Dual Junction InGaP Solar cell " IEEE International Conference on Energy Efficient Technologies for Sustainability – 2016 (IEEE-ICEETS – 2016), 7-9 April, 2016 Nagercoil, TN, India, Volume: IEEE Xplore

[9] Tapas Chakrabarti and Subir Kumar Sarkar, "Analytically Performance Study of Newly Modelled HIT solar cell with different materials", International Journal of Latest Technology in Engineering, Management & Applied Science (IJLTEMAS,) Volume VII, Issue IV, April 2018, ISSN 2278-2540.

[10] Khomdram Jolson Singh, Th. Jayenta Singh, Dhanu Chettri, and **Subir Kumar Sarkar** , "Heterogeneous Carbon Nano-Tube window layer with higher sheet resistance improve the solar cell performance"(ICEPOE 2017) at Thammasat University, Bangkok, Thailand, April 21-23, 2017

[11] Brian O'Regan & Michael Grätzel, "A low-cost, high-efficiency solar cell based on dye-sensitized colloidal TiO2 films", *Nature* 353, 737-740 (24 October 1991) doi:10.1038/353737a0.

[12] Tunahan Işık, "Solar Cells review", DOI: 10.13140/RG.2.1.4298.6404.

CHAPTER 3:

RELIABILITY STUDIES FOR NANOSCALE MOSFET

- INTRODUCTION
- LITERATURE SURVEY OF MOSFETS
- ANALYTICAL STUDY OF NANOSCALE DMDG SON MOSFET
- RESULT AND DISCUSSIONS
- REFERENCES

3.1. INTRODUCTION

The Moor's law postulated in 1965, that the transistors numbers in a single chip would quadruple in every three years. The electronics and communication industry followed the prediction significantly. Advancements in CMOS technologies are primarily manifested through structural modifications in short channel devices.

Outstanding results have been achieved in Silicon based beyond CMOS technologies, including LDMOS and DeMOS with/without STI, DGMOS, High-K/composite material gate, etc. suppressing the Short Channel Effects (SCE) to a great extent. For high speed CMOS devices SOI (silicon on insulator) based MOSFETs are developed. The SOI (Silicon on Insulator) can minimize the parasitic capacitance of MOS devices [1-2].

The additional advantages of fully depleted layer of thin body SOI are the steep sub-threshold slope; lower leakage current through the junction and higher channel mobility and due to lesser impurity concentration the fluctuation of V_{TH} (threshold voltage) can be reduced [1]. In sub-nanometer regime FDSOI MOSFET with multiple gate structures are become more attractive

because of their inherent immunity to short channel effect, improved sub-threshold characteristics and developed current driving capability [2].

Dual Gate (DG) geometry helps in reduction of SCE's by lowering the doping density, whereas, Dual Material Gate (DMG) introduces a step like potential profile, due to the work function of multiple materials used at gate of the device suppressed SCE [3]. A combined compact model structure on dual material dual gate (DMDG) and silicon on nothing (SON) has been established, depicting ultra-low threshold voltage with highly suppressed SCE's [4].

Threshold voltage, low field mobility, drains current, and transient Transconductance are superior in SON MOS compared to its SOI counterparts [1-2]. SON geometry fabrication is easier with standard recipes, epitaxial, RIE, and LDD implantation. The benefits of SON with DMG and DG has been illustrated quite a significant number of times.

Perfect control of SCE's coupled with high drive current, makes SON MOS as a best solutions for integration in deca-nanometer regime. Threshold voltage, low field mobility, drains current, and transient Transconductance are superior in SON MOS compared to its SOI counterparts. SON geometry fabrication is easier with standard recipes, epitaxial, RIE, and LDD implantation. The benefits of SON with DMG and DG has been illustrated quite a significant number of times. These advanced structures, delineated as an excellent gate control with outstanding switching speeds. This drives us to a point the stability and reliability of these transistors, when subjected to small signal noise at gate.

In general noise is a natural method of interference that disturbs a stable switching circuit. Noise can have uncountable sources, ranging from imperfect DC input to parasitic coupling with other L, R components in the circuit. Effect of any random noise is mostly associated to the process of trapping and de-trapping of carrier. Generation and occupation of traps results in discountenance

of conductance.

For semiconductors, typical noise fluctuations are associated with disturbance in conductivity. In MOS/DGMOS, these fluctuations are typically associated with number of carriers and fluctuations, explained by Mc Whorter model, as well as, mobility fluctuations, depicted in Hooge model. Hence, the scaling in device size, supply voltage at drain and gate are also to be reduced proportionately.

To realization of the effect of noise on channel dynamics, for these advanced structures like DMDG SON MOSFET, elaborate study will substantiate the reliability of this advance deca-nanoscale DMDG SON MOSFET [4]. This changed situation demands a reliability study of the nanoscale device.

3.2. LITERATURE SURVEY

The Silicon based MOSFETS sizes are minimized in to a remarkable level to increase in speed and efficiency in mobile computing. These reductions under a certain limit will exhibit some undesirable effects, such as Gate leakage current, Short Channel Effects etc. To overcome these unexpected effects the modifications of device structures are going on.

In sub-nanometer regime FDSOI (Fully Depleted Silicon On Insulator) MOSFET with multiple gate structures are become more attractive because of their inherent immunity to short channel effect, improved sub-threshold characteristics and increase of current driving ability. Improved sub-threshold slope due to volume ‘inversion of charge’ in the channel of dual gate, MOSFET is observed [2].

This type of DG MOSFET intensifies the charge carrier mobility also. The different work functions at the gate are introduced DMG in MOSFET structure the vertical field is modified and step in potential profile also observed [5]. The DMDG MOSFET in SON is another concept of

structure is developed by the researchers.

The DMDG SON MOSFET is more acceptable than the SOI DMDG MOSFET in respect of short channel effects of device. The SON based structure features and improved current driving capability, along with enhanced device scalability, provide opportunity for more device miniaturization, without influencing device performance [6-7].

The downscaling of CMOS transistors in to deca-nanometer scale, 20nm length of channel and the thickness of 5nm is chosen that is an ultra thin body DMDGMOSFET cannot be described by the classical model of charge inversion phenomena. In this structure characteristic the quantum mechanical effects (QME) are required to be considered. As the size is reduced, the supply voltage at drain and gate are also to be reduced proportionately [4].

The CMOS devices are mostly used in VLSI circuits, as the current drive of this type of device is large. Moreover the device with multiple gates have the capability of addressing the short channel effect, sub-threshold slope, drain induced barrier lowering effect which are the function of channel length and film thickness [8]. The performance of multiple gate MOS device can be accounted with different type of analytical physics model [9]. The overall performance of SON MOSFET and SOI MOSFET structure and its comparison can be drawn after solving of 2-D Poisson equation [10]. The multiple metal considering multiple work functions are also used in SON structures improve the SCE of device.

3.3. ANALYTICAL STUDY OF NANOSCALE DMDG SON MOSFET

(A) POTENTIAL MODEL

Analytical Study of Nanoscale DMDG SON MOSFET Potential Model as in Fig.3.1, the model proposed above is ultrathin so carrier quantization appears in this case for two kinds of

confinements, structural confinement, appearing because of ultrathin nature and transverse electric field makes the electrical confinement [11]. Hence, simultaneously 2-D Poisson's equations and Schrodinger equations are solved self consistently, to derive the potential profile [12].

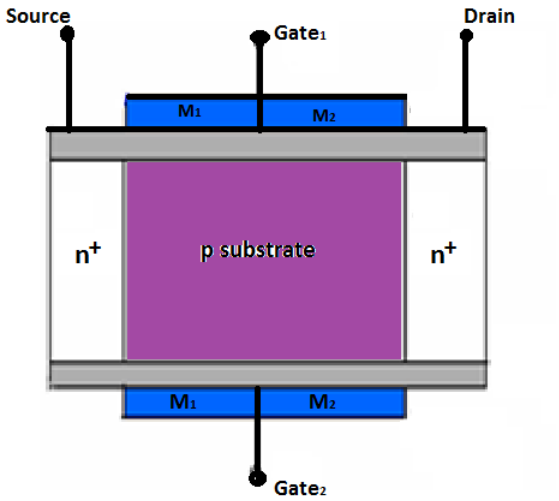

Fig.3.1 Basic structure of DMDG SON MOSFET

The 2-D Poisson equation for such a structure is given by,

$$\frac{\partial^2 \Phi(x,y)}{\partial x^2} + \frac{\partial^2 \Phi(x,y)}{\partial y^2} = \frac{qN_A}{\varepsilon_{si}} \qquad (3.1)\ [12]$$

In the above equation, $\Phi(x,y)$is the 2-D potential profile in the channel, N_A is the acceptor impurity concentration, and ε_{si} is the dielectric constant of silicon. Considering a second order potential approximation, $\Phi(x,y)$ can be expressed in simple parabolic function,

$$\Phi(x,y) = \Phi_s(x) + c_1(x)y + c_2(x)y^2 \qquad (3.2)\ [12]$$

Where, $\Phi_s(x)$ is the surface potential and $c_1(x)$, $c_2(x)$ are the coefficients dependent on x only.

The 1-D Schrodinger equation is given as follows,

$$\frac{\partial^2\psi}{\partial y^2} + \frac{2qm^*_{l,t}}{\hbar^2}(E - E_O)\psi = 0 \qquad (3.3)\ [14]$$

The front gate of the proposed structure consists of two materials M_1 and M_2 with different work functions. So the potential under these two regions will be different. The boundary conditions are to solve (ϕ_1, ϕ_2). The boundary conditions to solve ϕ_1 and ϕ_2 are,

$$\frac{d\Phi_1(x,y)}{dy} = \frac{\varepsilon_{ox}}{\varepsilon_{si}}(\Phi_{s1}(x) - V'_{G1})/t_{ox} \quad \text{under } M_1 \text{ when y=0} \qquad (3.4)$$

$$\frac{d\Phi_2(x,y)}{dy} = \frac{\varepsilon_{ox}}{\varepsilon_{si}}(\Phi_{s2}(x) - V'_{G2})/t_{ox} \quad \text{under } M_2 \text{ when y=0} \qquad (3.5)$$

$$\frac{d\Phi_1(x,y)}{dy} = \frac{\varepsilon_{air}}{\varepsilon_{si}}(V'_{GSb} - \Phi_B(x))/t_{air} \quad \text{under } M_1 \text{ when y=} t_{si} \qquad (3.6)$$

$$\frac{d\Phi_2(x,y)}{dy} = \frac{\varepsilon_{air}}{\varepsilon_{si}}(V''_{GSb} - \Phi_B(x))/t_{air} \quad \text{under } M_2 \text{ when y=} t_{si} \qquad (3.7)$$

$$\Phi_1(L_1, 0) = \Phi_2(L_1, 0) \qquad (3.8)$$

$$\Phi_1(0,0) = \Phi_{s1}(0) = V_{bi} \qquad (3.9)$$

$$\Phi_2(L_1 + L_2, 0) = \Phi_{s2}(L_1 + L_2) = V_{bi} + V_{ds} \qquad (3.10)$$

Where, t_{ox} is the oxide thickness at the dual material gate, ε_{ox} is the dielectric constant of the oxide layer, t_{air} is the thickness of the air layer, ε_{air} is the dielectric constant of air. Also, $V_{G1} = V_{GS}-V_{FB1}$, $V_{G2} = V_{GS}-V_{FB2}$, $V_{GSB} = V_{GS}-V_{FB3}$where V_{GS} is the gate to source bias voltage, V_{FB1}, V_{FB2}, V_{FB3} are the flat band voltages of M_1, M_2 and back substrate respectively. The built in potential (V_{bi}) across the body – source junction, and $\Phi_B(x)$ is the back gate potential function.

After applying all the above boundary conditions, we get four constants as C_{11}, C_{21}, C_{12}, C_{22}.

The surface potential is solved by substituting all the constants found by solving the boundary conditions in the Poisson equation,

$$\frac{d^2\Phi_{s1}(x)}{dx^2} - \alpha\Phi_{s1}(x) = \beta_1 \qquad \frac{d^2\Phi_{s2}(x)}{dx^2} - \alpha\Phi_{s2}(x) = \beta_2 \qquad (3.11)$$

Where,

$$\alpha = \frac{2\left\{1+\frac{C_{ox}}{C_{air}}+\frac{C_{ox}}{C_{si}}\right\}}{t_{si}^2\left\{1+\frac{2C_{si}}{C_{air}}\right\}} \qquad \beta_1 = \frac{qN_A}{\varepsilon_{si}} - \frac{\left[2V'_{G1}\left\{\frac{C_{ox}}{C_{air}}+\frac{C_{ox}}{C_{si}}\right\}+2V'_{GSb}\right]}{t_{si}^2\left\{1+\frac{2C_{si}}{C_{air}}\right\}}$$

$$\beta_2 = \frac{qN_A}{\varepsilon_{si}} - \frac{\left[2V'_{G2}\left\{\frac{C_{ox}}{C_{air}}+\frac{C_{ox}}{C_{si}}\right\}+2V'_{GSb}\right]}{t_{si}^2\left\{1+\frac{2C_{si}}{C_{air}}\right\}} \qquad (3.12)$$

The differential equations (3.11) are solved using normal ODE solving techniques to obtain the surface potential expression. The final equation of surface potential is normalized to get its reduced form as shown below

$$\Phi_{S1} =$$

$$-\frac{\beta_1}{2\sqrt{\alpha}} + \left(4V_{bi}\alpha.e^{(2\sqrt{\alpha}.l_1)}\right) + \left(2V_{ds}\alpha.e^{2\sqrt{\alpha}.l_1}\right) + \left(2\beta_1 e^{\left(L\sqrt{\alpha}.+\sqrt{\alpha}.l_1\right)}\right) - \left(2\beta_2 e^{(L.\sqrt{\alpha}+\sqrt{\alpha}.l_1)}\right) -$$

$$\left(2\beta_1 e^{(-L.\sqrt{\alpha}+2\sqrt{\alpha}.l_1)}\right) + \left(2\beta_1 e^{(-L.\sqrt{\alpha}+3\sqrt{\alpha}.l_1)}\right) - \left(2\beta_2 e^{(-L.\sqrt{\alpha}+3\sqrt{\alpha}.l_1)}\right) - \left(\frac{2V_{bi}\alpha e^{(-L\sqrt{\alpha}.+2\sqrt{\alpha}.l_1)}}{2\sqrt{\alpha}\left(e^{(2L\sqrt{\alpha})}-1\right)}\right) +$$

$$\left(\frac{(\beta_1 e^{\sqrt{\alpha}.x})}{2\sqrt{\alpha}}\right) - \left(2\beta_1 e^{(L.\sqrt{\alpha}+2\sqrt{\alpha}.l_1)}\right) - \frac{\left(2V_{bi}\alpha.e^{(L\sqrt{\alpha}+2\sqrt{\alpha}.l_1)}\right).(\sqrt{\alpha})}{2\sqrt{\alpha}.e^{2L\sqrt{\alpha}}-1} \qquad (3.13)$$

$$\Phi_{S2} = \frac{-\left(\beta_2 e^{(2\sqrt{\alpha}.x)}\right)}{(2\sqrt{\alpha}-\left(2.\beta_2 e^{L\sqrt{\alpha}}\right))} + \left(4.V_{bi}.\alpha.e^{2\sqrt{\alpha}.l_1}\right) + \left(2V_{ds}\alpha.e^{2.\sqrt{\alpha}.l_1}\right) + \left(2\beta_1.e^{L.\sqrt{\alpha}+\sqrt{\alpha}.l_1}\right) -$$

$$\left(\beta_2 e^{-L\sqrt{\alpha}+\sqrt{\alpha}.l_1}\right) - \left(2\beta_1 e^{-L\sqrt{\alpha}+2\sqrt{\alpha}.l_1}\right) + \left(\beta_1.e^{(-L\sqrt{\alpha}+3\sqrt{\alpha}.l_1)}\right) - \left(\beta_2.e^{(-L\sqrt{\alpha}+3\sqrt{\alpha}.l_1)}\right) -$$

$$\frac{2V_{bi}.\alpha.e^{(-L\sqrt{\alpha}+2\sqrt{\alpha}.l_1)}}{2\sqrt{\alpha}.e^{2.L.\sqrt{\alpha}}-1} + \frac{\beta_2 e^{\sqrt{\alpha}.x}}{2\sqrt{\alpha}} + \left(2\beta_2 e^{L.\sqrt{\alpha}}\right) - \left(\beta_2.e^{L.\sqrt{\alpha}+\sqrt{\alpha}.l_1}\right) - \left(2\beta_1.e^{L.\sqrt{\alpha}+2\sqrt{\alpha}.l_1}\right) +$$

$$\left(\beta_1.e^{L\sqrt{\alpha}+3\sqrt{\alpha}.l_1}\right) - \left(\beta_2.e^{L.\sqrt{\alpha}+3\sqrt{\alpha}.l_1}\right) \qquad (3.14)$$

The equations of surface potential Φ_{s1} at 0 to 10nm material (M_1) and Φ_{s2} at 10nm to 20nm material (M_2) are considered here.

Differentiating these two equations with respect to x we get the expression of electric fields,

$$E_1 =$$

$$\left(\beta_1 - \sqrt{\alpha}.e^{(-\sqrt{\alpha}.x)}\right)\frac{\left(\beta_1 e^{(2.\sqrt{\alpha}.x-\sqrt{\alpha}.x)}\right)}{2\sqrt{\alpha}} - \left(2\beta_2 e^{L.\sqrt{\alpha}}\right) + \left(4V_{bi}.\alpha.e^{2.\sqrt{\alpha}.l_1}\right) + \left(4.V_{ds}.\alpha.e^{2.\sqrt{\alpha}.l_1}\right) +$$

$$\left(\beta_1.e^{L.\sqrt{\alpha}+\sqrt{\alpha}.l_1}\right)-\left(\beta_2.e^{L.\sqrt{\alpha}+\sqrt{\alpha}.l_1}\right)-\left(2.\beta_1.e^{(-L.\sqrt{\alpha}+2.\sqrt{\alpha}.l_1)}\right)+\left(\beta_1.e^{(-L.\sqrt{\alpha}+3.\sqrt{\alpha}.l_1)}\right)-$$

$$\left(\beta_2.e^{(-L.\sqrt{\alpha}+3.\sqrt{\alpha}.l_1)}\right)-\frac{(2.V_{bi}.\alpha.e^{\left(-L.\sqrt{\alpha}+2.\sqrt{\alpha}.l_1\right)})}{(2.\sqrt{\alpha}.e^{(2.L.\sqrt{\alpha})}-1)}+\frac{\beta_1.e^{\sqrt{\alpha}.x}}{2.\sqrt{\alpha}}+\left(2\beta_2e^{L.\sqrt{\alpha}}\right)+\left(\beta_1.e^{L.\sqrt{\alpha}+\sqrt{\alpha}.l_1}\right)-$$

$$\left(\beta_2.e^{L.\sqrt{\alpha}+\sqrt{\alpha}.l_1}\right)-\left(2\beta_1.e^{L.\sqrt{\alpha}+2.\sqrt{\alpha}.l_1}\right)+\left(\beta_1.e^{(-L.\sqrt{\alpha}+3.\sqrt{\alpha}.l_1)}\right)-\left(\beta_2.e^{(-L.\sqrt{\alpha}+3\sqrt{\alpha}.l_1)}\right)-$$

$$\frac{2V_{bi}\,\alpha.e^{L\sqrt{\alpha}}.e^{2\sqrt{\alpha}.l_1}}{2\sqrt{\alpha}.e^{2.L.\sqrt{\alpha}}-1} \qquad (3.15)$$

$$E_2=(\beta_2-\sqrt{\alpha}.e^{(\sqrt{\alpha}.x}.)\frac{\beta_2.e^{(-\sqrt{\alpha}.x)}}{2.\sqrt{\alpha}}-\left(2\beta_2.e^{L.\sqrt{\alpha}}\right)+\left(4.V_{bi}.\alpha.e^{2.\sqrt{\alpha}.l_1}\right)+\left(4.V_{ds}.\alpha.e^{2.\sqrt{\alpha}.l_1}\right)+$$

$$\left(\beta_1.e^{(-L.\sqrt{\alpha}+\sqrt{\alpha}.l_1)}\right)-\left(\beta_2.e^{(-L.\sqrt{\alpha}+\sqrt{\alpha}.l_1)}\right)-\left(2.\beta_1.e^{(-L.\sqrt{\alpha}+2.\sqrt{\alpha}.l_1)}\right)+\left(\beta_1.e^{(-L.\sqrt{\alpha}+3.\sqrt{\alpha}.l_1)}\right)-$$

$$\left(\beta_2.e^{(l.\sqrt{\alpha}+3.\sqrt{\alpha}.l_1)}\right)-\frac{2.V_{bi}.\alpha.e^{(-L.\sqrt{\alpha}+2\sqrt{\alpha}.l_1)}}{2.\sqrt{\alpha}.e^{2.L.\sqrt{\alpha}}-1}+\frac{\beta_2.e^{\sqrt{\alpha}.x}}{2.\sqrt{\alpha}}+\left(2.\beta_2.e^{L.\sqrt{\alpha}}\right)+\left(\beta_1.e^{L.\sqrt{\alpha}+\sqrt{\alpha}.l_1}\right)-$$

$$\left(\beta_2.e^{L.\sqrt{\alpha}+\sqrt{\alpha}.l_1}\right)-\left(2.\beta_1.e^{L.\sqrt{\alpha}+2.\sqrt{\alpha}.l_1}\right)+\left(\beta_1.e^{L.\sqrt{\alpha}+3.\sqrt{\alpha}.l_1}\right)-\left(\beta_2.e^{L.\sqrt{\alpha}+3.\sqrt{\alpha}.l_1}\right)-$$

$$\frac{2.V_{bi}.\alpha.e^{L.\sqrt{\alpha}+2.\sqrt{\alpha}.l_1}}{2.\sqrt{\alpha}.e^{2.L.\sqrt{\alpha}}-1} \qquad (3.16)$$

The equation of Electric field E_1 at 0 to 10nm material (M_1) and E_2 at 10nm to 20nm material (M_2) are derived here.

(B) THRESHOLD VOLTAGE MODEL

The quantum threshold voltage can be deduced from the accumulated integrated charge in the virtual cathode under the p+ poly-silicon front gate [15]. The inversion charge carriers are expressed as bellow:

$$Q_{\text{inv},q}^{T}=$$

$$\frac{qkT}{\pi\hbar^2}\sum_i[\sqrt{m_l^*m_t^*}g_t\ln\left[1+\exp\left(-\frac{1}{V_t}\left(E_l^{\sim i}-\emptyset_{S1}(x_m)\right)\right)\right]+m_t^*g_l\ln[1+\exp(-\frac{1}{V_t}(E_l^{\sim i}-$$

$$\emptyset_{S1}(x_m)))]] \qquad (3.17)$$

It is very difficult to solve the equation $Q_{\text{inv,q}}^{T} = Q_T$ directly. Hence, an analytical approach has been utilized. It consists of two parts, first the calculation of classical threshold voltage model taking into account the SCEs, V_{th}^{cl} and secondly we calculate the deviation between the classical and quantum threshold voltageΔV_{th}^{q}. As a result, the final quantum threshold voltage is given by

$$V_{th}^{q} = V_{th}^{cl} + \Delta V_{th}^{q} \quad (3.18)$$

Classical Threshold Voltage

In order to find out the classical voltage threshold model, a graphical approach has been used. In our proposed structure, there exists two different threshold voltages related to each gate material. These threshold voltages are given as under,

$$V_{th2} = V_{FB,fp} + 2\emptyset_F + \left(\frac{Q_{si} + 4VC_{si}}{2}\right) + V_t \ln\left(V_t \frac{4C_{si}}{Q_{si}}\right) \quad (3.19)$$

$$V_{th1} = V_{th2} - \frac{\gamma_{ox} t_f t_{si}}{\gamma_{ox} t_f + \gamma_{air} t_b + t_{si}} \Delta V_{fb} \quad (3.20)$$

It must be analyzed that the overall threshold voltage is derived from the surface potential minima as it is a function of surface potential and occurs at its lowermost value.

$V_{FB,fp}$ is flat-band voltage of the gate, $\gamma_{ox} = \frac{\varepsilon_{si}}{\epsilon_{ox}}$, $\gamma_{air} = \frac{\varepsilon_{si}}{\epsilon_{air}}$, $Q_{si} = qN_A t_{si}$ is total charge across the channel, and ΔV_{fb} is difference between flat-band voltages of the front and the back gates ($\Delta V_{fb} = V_{FB,fp} - V_{FB,bn}$).

Taking into account the SCEs the threshold voltage shift is given by: $\Delta V_{th} = 2\sqrt{\eta_S \eta_{L1}} e^{-\tau}$ where, parameters have the significances as stated.

The final expression of classical threshold voltage after incorporating the threshold voltage shift comes out to be,

$$V_{th}^{cl} = V_{th1} - \Delta V_{th} \quad (3.21)$$

Quantum Threshold Voltage

Considering the classical and quantum inversion charge models at the virtual cathode position, we find out the expression for critical charge, Q_T required to achieve inversion, separately. The difference obtained between the surface potential for the classical and the quantum models is calculated from the expression of critical charge. For classical case, at threshold, we can write,

$$Q_T = Q^T_{\text{inv,cl}} = \int_0^{t_{si}} qn_i \exp\left(\frac{q\phi_1(x_m,y)}{kT}\right) dy =$$

$$qn_i \exp\left(\frac{\phi_{S1}(x_m)}{V_t}\right) \times \int_0^{t_{si}} \exp\left(\frac{(c_{11}(x_m)y + c_{12}(x_m)y^2)}{V_t}\right) dy \qquad (3.22)$$

The value of c_{12} is found to be negative at the virtual cathode position, so we can write $c_{12} = -|c_{12}|$. Hence, the equation on simplification becomes,

$$Q_T = qn_i \exp\left(\frac{\phi_{S1}(x_m)}{V_t}\right) \frac{e^{\frac{c_{11}^2}{4V_t|c_{12}|}}}{2\sqrt{|c_{12}|}} \sqrt{\pi V_t} \left(\text{erf}\left(\frac{-c_{11}+2t_{si}|c_{12}|}{2\sqrt{V_t|c_{12}|}}\right) - \text{erf}\left(\frac{-c_{11}}{2\sqrt{V_t|c_{12}|}}\right)\right) \qquad (3.23)$$

Alternatively, at the weak inversion region where the Fermi level is much below the conduction band, we can approximate the Fermi–Dirac distribution by Boltzmann.

$$Q_T = \frac{qkT}{\pi\hbar^2} \exp\left(\frac{\phi_{S1}(x_m)}{V_t}\right) \sum_i \left[\sqrt{m_l^* m_t^*} g_t \exp\left(-\frac{E_l^{\sim i}}{V_t}\right) + m_t^* g_l \exp\left(-\frac{E_t^{\sim i}}{V_t}\right)\right] \qquad (3.24)$$

Equating (19) and (20), we get the shift in surface potential $\Delta\phi^q_{S1}(x_m)$, This shift allows us to change in threshold voltage from ΔV^q_{th} from $\Delta\phi^q_{S1}(x_m)$.

It can be achieved by allowing non-ideal sub-threshold slope of *S* as,

$$\Delta V^q_{th} = \frac{S}{\left(\frac{kT}{q}\right) ln(10)} \Delta\phi^q_{S1}(x_m) \qquad (3.25)$$

3.4. RESULTS AND DISCUSSION

Most natural method of interference that causes a switching circuit is due to noise. Noise can have uncountable sources, ranging from imperfect DC input to parasitic coupling with other L, R components in the circuit. We are anticipating some significant performance degradation in

DMDG SON MOS, which might be greater than the devices having higher SCE's. To understand the effect of noise in DMDG SON MOS, for the first time, we have taken a sinusoidal component of noise, with varying frequency (1kHz to 1MHz). Sinusoidal signal is a component of an entire noise spectrum. Thereby, at the first step, we are studying the impact of a component of noise. DMDG SON MOS features ultra-low threshold voltage, ideal for DC and high frequency switching applications. Surface states tend to scatter in deep depletion modes. This feature is supposed to be predominant with carriers that are confined with innumerable small potential wells acting as boundary conditions, as is the case with quantum confinement in nanoscale MOS. For this reason, we have operated the device strictly in deep depletion or inversion modes, and studied the impact of sinusoidal signal on the gate, when the drain current saturates. The device features quantum threshold voltage of 0.3458V, in normal DC operations. We have fixed the drain to source voltage (V_{DS}) at 0.5V and, gate to source voltage (V_{GS}) at 0.45V. A sinusoidal voltage (V_{RMS} = 0.707V) is applied at the gate along with V_{GS}. The magnitude of the sinusoid complies with simulated sinusoidal noise applied [16/19]. The total voltage applied at the gate, takes the form, $V_{GS} = V_{GS(DC)} + V_{GS(Sinusoid)} \times \sin(\omega t)$. This ensures that the device stays in inversion regime, with saturating drain current.

Application of this mixed signal is anticipated to bring some change in device performance. Response of surface states with DC and sinusoidal components are analyzed separately, to bring out the underlying factor behind the change in device performance. Moreover, the dissociated DC and sinusoidal constants are convoluted and plotted, to check the fluctuations for different device parameters.

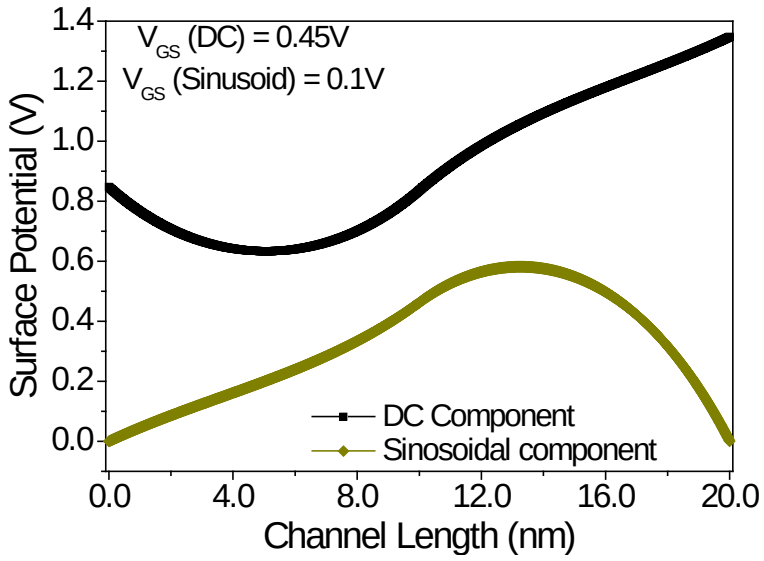

Fig. 3.2 DC and Sinusoidal components of Surface Potential plotted across the length of the Channel

Surface potential directly determines the behavior of surface states. Surface potential plotted against the entire channel length shows the typical profile for a DMDG SON MOS. Both the components are plotted in Fig.3.2. Although fluctuation of surface potential is an expected phenomenon on application of sinusoidal signal at the gate, but the fluctuation seems way to higher, which is almost in the range of 1.3V, even after maintaining the magnitude of sinusoidal signal within safe limits. Fig.3.3 compares the fluctuation of surface potential for a lower (10KHz) and higher frequency (1MHz). Interestingly, we are observing lesser fluctuation at increased frequencies.

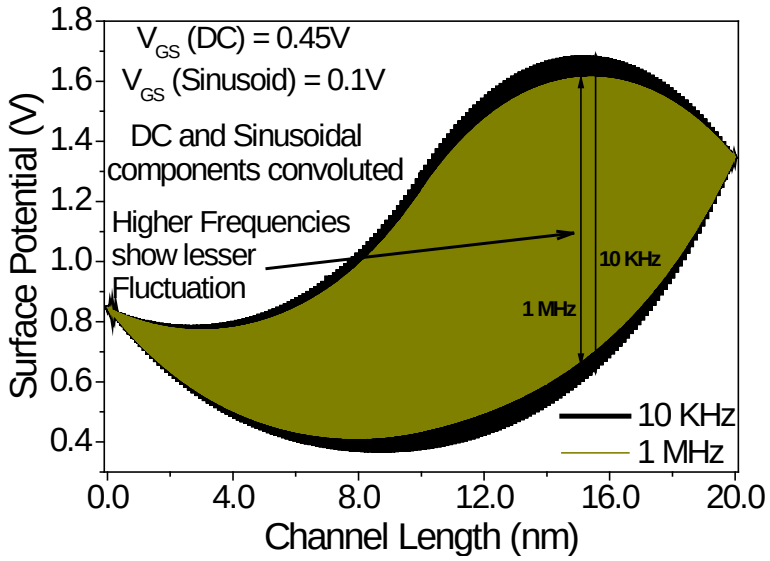

Fig.3.3 Comparison drawn between different frequencies, for convoluted DC and sinusoidal Surface Potential components depicted along the length of the channel. Lesser frequencies show greater potential fluctuations along the channel

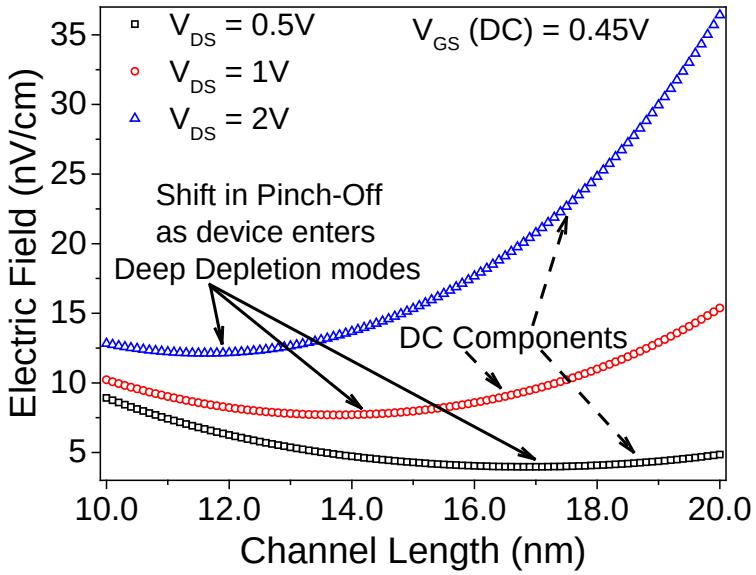

Fig.3.4 Electric Field is plotted along the length of the channel for three different Drain Voltages, indicating levels of Deep Depletion modes, depicting shift in pinch off along the Channel

Electric field profile for deep depletion modes (V_{DS} = 0.5V, 1V, 2V) plotted for the DC component only, shown in Fig.3.4 depicts normal behavior of the channel. The field profile plotted for sinusoidal component depicts an astonishing phenomenon, shown in Fig.3.5. Instead

of saturating near the drain edge, electric field for the sinusoidal component reversers its magnitude, and goes on increasing towards the negative direction, as we approach towards the drain edge. Reversal of magnitude refers to change in direction of field. This phenomenon has never been observed previously for any noise component in any nanoscale MOS structure.

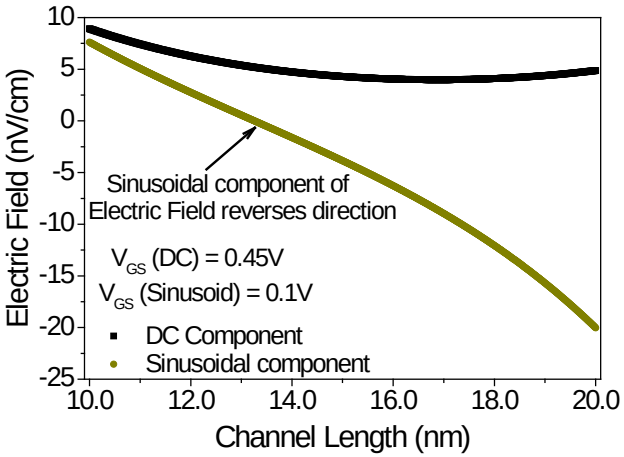

Fig.3.5 DC and Sinusoidal components of Electric Field is plotted along the length of the Channel. Reversal of Field direction for the sinusoidal component is depicted

Fig. 3.6(a), clearly depicts the fluctuation of electric field along the channel, due to the mixed voltage supply at the gate. Interestingly, the fluctuation pinches off at one point in the channel, and then increases drastically towards the drain side. Moreover, the field constantly changes its direction in the drain side, indicating a highly unstable channel dynamics. The comparison between field fluctuations for 10 KHz and 1 MHz, shown in Fig.3.6 (b), depicts lower fluctuation for higher frequencies. Moreover, the interface traps and bounded carriers have responded to lower frequencies significantly, which implies that there will be performance degradation for any component of noise induced in the circuit. Low power devices show significant performance degradation for higher voltages, and higher temperatures. With increase in temperature, the mean free paths for the highly energetic carriers are reduced, which leads to

almost doubling of reverse saturation current for every 10^{o}C rise in temperature. Sinusoidal component is analogous to a transient force which is disturbing the channel dynamics, by opposing the carriers to get collected in the drain side, which in turn, is bound to result in scattering.

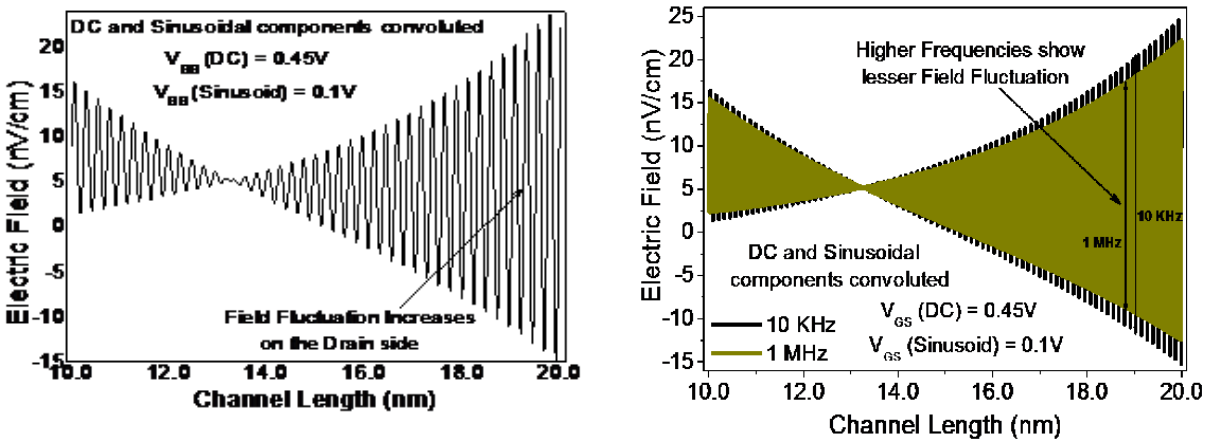

(a) (b)

Fig.3.6(a) DC and Sinusoidal components of Electric Field convoluted to understand their combined effect along the Channel & Fig.3.6(b)Field fluctuation increases drastically in the drain side. The Field even reverses direction quite frequently towards the drain edge

Fig.3.7 shows the expected trend, depicting no temperature variance with the DC component of the field. Whereas, the sinusoidal component is showing clear temperature dependence however the field towards the drain side is increasing in the negative direction with increase in temperature, thereby establishing the fact of high HCE. This phenomenon is clearly depicted in Fig.3.8. Fig.3. 9, clearly depicts the above phenomenon, where a comparison is drawn between the overall impact of both DC and sinusoidal components convoluted together, in 10 Hz, and 10 KHz frequencies.

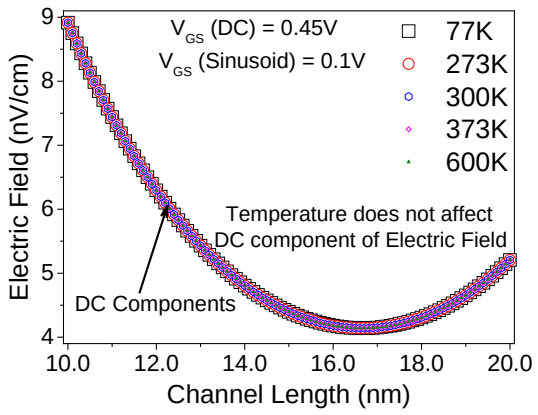

Fig.3.7 DC component of Electric Field plotted across channel length, depicting the invariance of Electric Field with Temperature

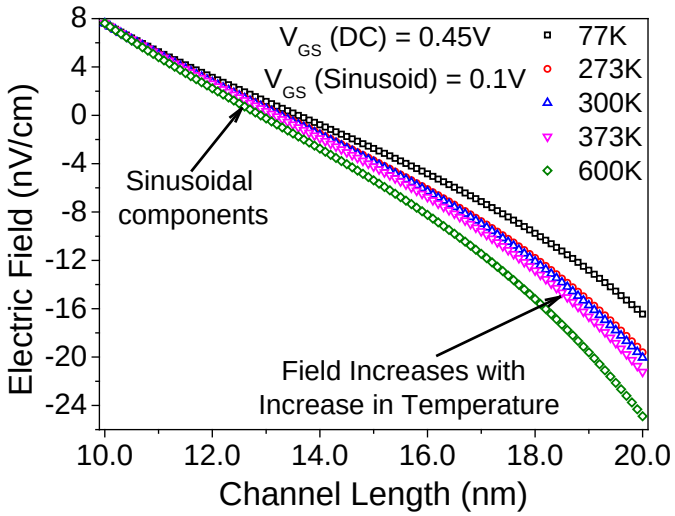

Fig.3.8. Sinusoidal Component of Electric Field plotted across the length of the Channel. Sinusoidal component depicts significant increase of Electric Field in the reverse direction with increase in Temperature

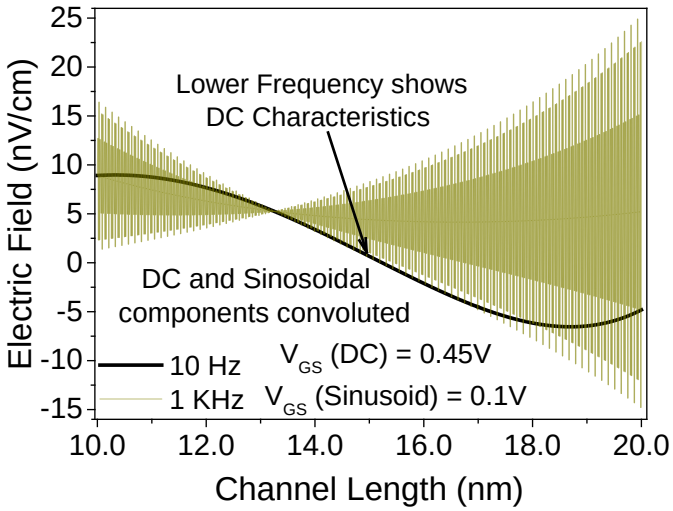

Fig.3.9 Comparison drawn between two frequencies, for convoluted DC and sinusoidal Electric Field components depicted along the length of the channel. Very low frequency plot (10 Hz) shows characteristics analogous to DC component

The phenomenon occurring at the channel due to the combined effect of DC and sinusoidal component of electric field shows highly unstable channel dynamics. It is quite obvious that if the carriers of the channel are not in equilibrium even at gate voltages higher than threshold voltage, and if they are constantly receiving forces in two opposite directions, threshold voltage is bound to fluctuate. To make the model familiar to the phenomenon happening in the channel, we have solved quantum threshold voltage, along the channel, in inversion mode only. Fig.3.10(a) shows the DC and sinusoidal component of the field separately. As expected, the sinusoidal component shows a greater threshold voltage across the channel. This depicts that; the sinusoidal component will have much significant impact in determining the threshold voltage of the device.

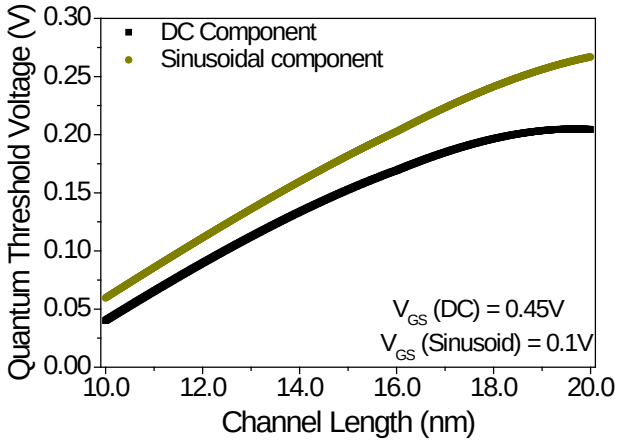

Fig. 3.10.(a) DC and Sinusoidal components of Quantum Threshold Voltage is plotted (a) along the length of the Channel Sinusoidal component shows significant increase in Quantum Threshold Voltage,

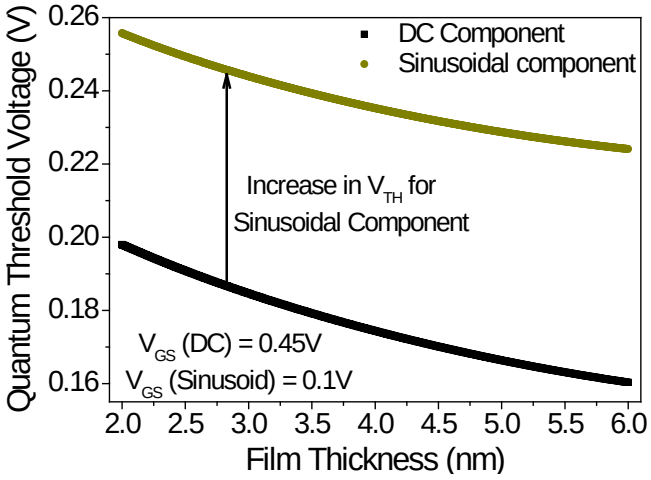

Fig.3.10.(b). Across Film Thickness shows a constant increase in Quantum Threshold Voltage than the DC component

All the above discussions boil down to the fact that, threshold voltage is bound to fluctuate along the channel, if the channel dynamics is disturbed. Moreover, we can observe an increased quantum threshold voltage fluctuation towards the drain edge, which will definitely degrade device performance because of HCE. Fig.3.11, depicts the comparison of threshold voltage fluctuation with change in frequency. An even more interesting phenomenon is observed when we have plotted quantum threshold voltage for both DC and sinusoidal components along the

film, starting from channel to the substrate. As expected, quantum threshold voltages for both the components have lowered on increasing film thickness. But, sinusoidal component of quantum threshold voltage is showing a constant significant increase than the DC component. This infers that, in the combined effect of DC and sinusoidal component, the sinusoidal component will predominate, and will disturb the carrier concentration and orientation throughout the film and the channel. This phenomenon is depicted in Fig.3.10(b), We are observing a change in threshold voltage, which is strictly a DC parameter with a sinusoidal component of noise. This degrades device performance. Fluctuations for electric field and threshold voltage are significantly reduced for simple nanoscale MOS devices, which feature significantly high SCE's. We are reaching at a stage, where structural modifications made to suppress SCE's increases instability of the device when subjected to any component of noise, ultimately resulting in performance degradation and circuit instability.

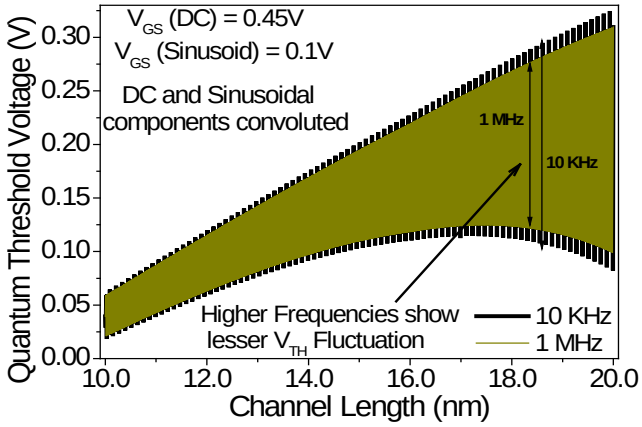

Fig.3.11 Comparison drawn between different frequencies, for convoluted DC and sinusoidal Quantum Threshold Voltage components depicted along the length of the channel. Lesser frequencies show greater Quantum Threshold Voltage fluctuations along the Channel.

3.5 REFERENCES

[1] Priyanka Saha and Subir Kumar Sarkar, "Threshold Voltage Modeling of Linearly Graded Binary Metal Alloy Gate Electrode with DP MOSFET" IETE Journal of Research, Taylor & Francis, DOI.10.1080/03772063.2018.1508374, August 2018.

[2] B. Manna, S. Sarkhel, N. Islam, S. Sarkar, and S. K. Sarkar, "Spatial composition grading of binary metal alloy gate electrode for short channel SOI/SON MOSFET application," IEEE Trans. Electron Devices, vol. 11, no. 3, pp. 472–478, May 2012.

[3] M. Jagadesh Kumar, A. A. Orouji, and H. Dhakad, "New dual-material SG nanoscale MOSFET: Analytical threshold-voltage model," IEEE Trans. Electron Devices, vol. 53, no. 4, pp. 920–923, Apr. 2006.

[4] Sourav Naskar and Subir Kumar Sarkar, Quantum Analytical Model for Inversion Charge and Threshold Voltage of Short-Channel Dual-Material Double-Gate SON MOSFET, IEEE Transactions on Electron Devices, Vol.60, No.9, September 20

[5] M.Jagadesh Kumar, Anurag Chaudhury, Two Dimensional Analytical Modeling of Fully Depleted DMG SOI MOSFET and Evidence for diminished SCEs, IEEE Transactions on Electron Devices, Vol.51, No.4, April 2004.

[6] Sharmistha Shee, Gargee Bhattacharyya, and Subir Kumar Sarkar, Quantum Analytical Modeling for Device Parameters and I –V Characteristics of Nanoscale Dual-Material Double-Gate Silicon-on-Nothing MOSFET, IEEE Transactions on Electron Devices, Vol.61, No.8, August 2014.

[7] Pritha Banerjee, Anup Sarkar and Subir Kumar Sarkar, "Exploring the short channel characteristics and performance analysis of DMDG SON MOSFET", Microelectronics Journal, Elsevier, Volume 67, Pages 50-56, September 2017.

[8] Chi-Woo Lee, Se-Re-Na Yun, Chong-Gun Yu, Jong-Tae Park, Jean-Pierre Colinge, Device design guidelines for nano-scale MuGFETs, Solid-State Electronics 51 (2007) 505–510, DOI: 10.1016/j.sse.2006.11.013.

[9] Te-Kuang Chiang, A Novel Quasi-3-D Threshold Voltage Model for Fully Depleted Quadruple-Gate (FDQG) MOSFETs: With Equivalent Number of Gates (ENG) Included, IEEE Transaction on Nano Technology, Vol. 12, No. 6, November 2013, DOI: 10.1109/TED.2012.2202119.

[10] Nouran M. Ali, Nageh K. Allam, Ashraf M.Abdel Haleem, Analytical modeling of the radial pn junction nanowire solar cells, DOI: http://dx.doi.org/10.1063/1.4886596

[11] V. P. Trivedi and J. G. Fossum, "Quantum-mechanical effects on the threshold voltage of undoped double-gate MOSFETs," IEEE Electron Device Lett., vol. 26, no. 8, pp. 579–582, Aug. 2005.

[12] P. R. Kumar and S. Mahapatra, "Quantum threshold voltage modeling of short channel quad gate silicon nanowire transistor," IEEE Trans. Electron Devices, vol. 10, no. 1, pp. 121–128, Jan. 2011.

[13] K. K. Young, "Short-channel effect in fully depleted SOI-MOSFETs," IEEE Trans. Electron Devices, vol. 36, no. 2, pp. 399–402, Feb. 1989.

[14] R. Shankar, Principles of Quantum Mechanics. New York, NY, USA: Plenum, 1994.

[15] Pritha Banerjee and Subir Kumar Sarkar, "3D Analytical modeling of high-k gate stack dual material tri gate strained silicon –on-nothing MOSFET with dual material bottom gate for suppressing short channel effects", in Journal of Computational Electronics, Springer, Vol.16, No.3, pp-631-639, May 2017.

CHAPTER 4

MODELING OF HIGHLY EFFICIENT HIT SOLAR CELLS

- INTRODUCTION
- LITERATURE SURVEY OF HIT SOLAR CELLS
- THEORY OF HIT SOLAR CELLS
- MODELING OF HIT SOLAR CELLS
- RESULT AND DISCUSSION
- REFERENCE

4.1. INTRODUCTION

A simple 'heterojunction solar cell' means that two semiconductors of different 'band gaps' forming the p-n junction, especially crystalline n-type silicon wafer with amorphous p-type silicon [1].

'Amorphous silicon' is comparatively cheaper silicon material with respect to 'crystalline silicon' (c-Si) technology. Although the 'c-Si solar cells' have high photo-voltaic (PV) conversion efficiency, however, this technology is also associated with higher production cost, thermal budget and requirement of quality Silicon semiconductor. The existing 'defect states' in c-Si wafers manifest further deterioration due to comparatively higher processing temperature. So, the 'crystalline' and 'amorphous' silicon applied in different layer of 'solar cell' and form the 'heterojunction intrinsic thin film' (H-I-T) has become alternative options [2].

The H-I-T ‘solar cell’ was first time developed in 1991, and patented by ‘Sanyo Electric Company’ and it became popular among researchers due to interesting features of the cells like the high PV conversion efficiency (η) and lower processing temperature.

An introduction of ‘thin intrinsic’ layer of ‘hydrogenated amorphous silicon’ (a-Si:H) between the ‘p-type’ and ‘n-type’ ‘silicon’ achieved a remarkable advancement in H-I-T ‘solar cell’ and found better response of the ‘external quantum efficiency’ (EQE). Optimizing the ‘layer thickness’ of intrinsic (i-Si) and emitters (a-Si:H) of H-I-T ‘solar cell’, the ‘Short Circuit Current density’ (Jsc), ‘Fill Factor’ and ‘efficiency’ can be increased up to a level of operation.

The heterojunction a-Si/c-Si interface controls the ‘function of performance’ of the H-I-T ‘solar cell’ and achieved the ‘high efficiency’. Using p-type a-Si:H materials in HIT device structure, ‘high Fill Factor’ along with improved performance observed. The discontinuity of ‘energy band structure’ of heterojunction increase the loss with ‘electron –hole pair’ recombination that is effected to the ‘current density’ but not the ‘open circuit voltage’.

When a light is entered from air to the ‘top surface’ of ‘silicon’, that time a fraction of ‘light’ is returned back to the air by ‘reflection’. Introducing texturization on the top most surface of ‘Silicon layer’ can reduce the ‘reflection’. Textured surface can trap the more light which increase the ‘short circuit current’ but the textured surface becomes more defective, which should be optimized for good response. Comparatively thinner wafers are used in H-I-T ‘solar cells’ like 250 μm, 98 μm thick which leads lower processing temperature. [3].

Charge carrier transportation across the H-I-T cell structure is determined by the various stage ‘drift-diffusion’ of charge carriers, where the high electric field exists, the drift will occur and on account of concentration gradient diffusion of carriers will take place. The ‘heterojunction

interface', the 'energy bands discontinuity' will lead to trap the 'charge carriers' and tunneling the same is an 'important factor' in 'performance' of H-I-T 'solar cells' [2-3].

Exploration of new structures, minimization of silicon is going on. It is evident that newer structures of H-I-T 'solar cell' using 'ZnO', 'ZnSe' and 'ZnTe' materials are showing mentionable results [4].

The 'band gap' of ZnTe is quite wide, which is '2.23–2.28eV' at room temperature, 'absorption coefficient' is also high close to$10^5 cm^{-1}$ and low 'electron affinity' of 3.73eV, which makes the ZnTe as most promising 'compound semiconductor material' (II–VI) in the domain of 'low-cost' and 'high-efficiency' thin film 'solar cells' [4-5]. Another material ZnO is also a 'direct band gap' and sufficiently 'wide band gap' (E_g=3.34eV) semiconductor. But the electron an 'hole mobility' of ZnO is 200 cm2/Vs and 5-50 cm2/Vs respectively, which are not so impressive. In my research work, using ZnTe and ZnO in the 'emitter layer' new models of H-I-T 'solar cells' are developed which reveals that a 'low cost' substitution to traditional 'c-Si solar cells'.

4.2. LITERATURE SURVEY OF 'HIT SOLAR CELLS'

The 'solar cell' industry is dominated by the 'crystalline silicon' (c-Si) 'solar cells' which are most common p-n junction type. Thin-film 'hydrogenated amorphous silicon' (a-Si: H) and 'hydrogenated microcrystalline silicon' (μc-Si: H) semiconductors are popular for 'p-i-n thin-film' structures of 'solar cell' [6].

Different 'band gaps' or work function materials combination called 'Heterojunction materials' like a-Si:H/c-Si, CdS/CdTe and Cds/CIGS are used in H-I-T 'solar cells'. The 'silicon heterojunction' 'solar cells' are a fascinating technology as the amalgamations of 'crystalline silicon' and 'amorphous silicon' are involved [6].

‘Silicon heterojunction’ ‘solar cells’ are engineered of ‘c-Si’ as light absorber along with ‘thin-film silicon’ layers. This type of ‘solar cells’ are achieved the ‘efficiency ~22%’, whereas the ‘theoretical value’ is ~23% for ‘c-Si cells’ [7].

Improving the ‘surface passivation’ of ‘c-Si’ another conceptual configuration is known as ‘Heterojunction Intrinsic Thin-film’ or ‘H-I-T solar cell’, which has showed the result of ‘efficiency’, is ~25%. The ‘typical configurations’ of heterojunction and ‘H-I-T solar cells’ is TCO/a-Si:H(p)/a-Si:H(i)/c-Si(n)/a-Si:H(i)/a-Si:H(n+)/TCO/Al [1].

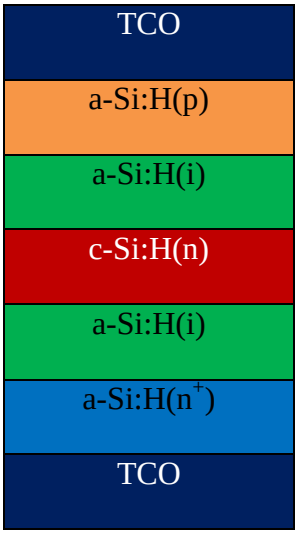

Fig.4.1. Typical Structure of H-I-T Solar Cell

The continuous investigations for betterment of ‘solar cell device’ structures and exploration of materials are also going on. The Sanyo research and development group was the first to apply an a-Si:H heterojunction to a ‘c-Si solar cell’ in 1991 and their first ‘Hetero junction’ ‘solar cell’ by directly depositing ‘a-Si:H(p)’ layer onto ‘n-type-c-Si’ wafer, and was obtained the ‘efficiency’ of 12.3% [6]. Due to the high density ‘defect-state’ at the hetero-interface, the ‘solar cell’ shows relatively low ‘Open circuit voltage’ and ‘Fill Factor’. Inserting of a tiny layer of ‘a-Si:H(i)’ between ‘a-Si:H(p)’ and ‘n-type’ ‘c-Si wafer’ lead to better cell performance. This incorporation of ‘a-Si:H(i)’ lead to passivation of the ‘dangling bonds’ on the ‘c-Si’ surface, which lowered the

a-Si:H/c-Si interface defect-state density. These lower ‘defect-state density’ at the ‘Heterojunction’ interface led to overshadow the ‘Open circuit voltage’ and ‘Fill Factor’. Using a passivated a-Si:H(i) layer, achieved the ‘efficiency’ of 14.8% for H-I-T ‘solar cells’ [6]. A cell efficiency of 18.1% was obtained with the ‘textured wafer surface’ for ‘light trapping’ and the inclusion of a BSF at ‘back side’ of the device [6]. The ‘textured wafer surface’ and the ‘BSF’ is lead to a significant upgrade in ‘short circuit current density’ (Jsc). The H-I-T ‘solar cell’ was further, improved by applying double-side passivated a-Si:H(i) to the wafer. ITO was included in the ‘rear side’ between the BSF and metal-grid electrode for further enhancement of ‘efficiency’ of H-I-T ‘solar cell’ which goes up to 21.3% [3]. Sanyo was also trying to fabricate slim HIT cells with thickness below 100 μm [7]. With these ‘thinner cells’, the ‘short circuit current’ decreases slightly, but the ‘open circuit voltage’ increases significantly, from their existing structure (729 mV to 743 mV). This achievement is accredited to the ‘extremely low’ bulk recombination. From this time, they focused on developing technologies for ‘higher conversion efficiency’ with thin c-Si wafer (98 μm) with the aim of reducing cost. In 2011, Panasonic (Sanyo) obtained a new ‘record of efficiency’ of 24.7% [8]. Innumerable research groups are following Sanyo’s lead to work on H-I-T ‘solar cells’ as high performance and low-temperature processing.

4.3 ‘THEORY OF H-I-T SOLAR CELLS’

The ‘Heterojunction with Intrinsic layer’ (H-I-T) ‘solar cell’ features are adding of a thin layer of ‘intrinsic a-Si:H’ between ‘p-type a-Si:H’ and ‘n-type c-Si’. This ‘solar cell structure’ was initially explored to obtain a ‘thin film’ ‘poly silicon’ or ‘crystalline silicon’ junction of structure for a ‘solar cell’ applying minimum temperature. Here, the emitter is formed of a very ‘thin intrinsic a-Si: H’ layer and put a lid of ‘p-type’ ‘a-Si:H’. The most dominant section is thick ‘n-

type c-Si' where the optical energy is to be assimilated and the 'BSF' is made of a thin 'un-doped a-Si:H' and crowned by 'n-type a-Si'. Indium Tin Oxide is 'sputtered' on the top and bottom of the 'cell' and this ITO will take part as an 'anti-reflection coating' (ARC) and a 'transparent conducting' electrode, enhanced the assembly of carriers density [1] [9-10]. Metals contacts are applied on the frontage, forming a grid to allow light into the cell, however, since 'sun light' enters the 'cell' through the 'front side' only. For maximum collection of 'charge carriers' the back partition of the 'cell' is covered by metal contact as in Fig.4.2.

ITO	TCO Coated Glass Substrate
p-type	a-Si
i-type	a-Si
n-type	c-Si
i-type	a-Si
n^+ -type	a-Si
Back electrode	metal

Figure 4.2 'Basic structure of HIT solar cell'

4.3.1. 'OPERATION OF HIT SOLAR CELL'

The 'principle of operation' of the HIT 'solar cell' is explained by the equation (4.1), with current density (J) versus voltage (V) relation [10]

$$J(V) = J_{01}\left(e^{\frac{q(V-JR_S)}{nkT}} - 1\right) + J_{02}\left(e^{A1(V-JR_S)} - 1\right) + \left(\frac{V-JR_S}{R_{sh}}\right) - J_{Ph} \ldots\ldots\ldots\ldots\ldots\ldots\ldots\ldots (4.1)$$

Where, q is electron charge, J_{ph} is photo current density, J_{01} & J_{02} are 'reverse saturation current' densities, n diode ideality factor, k 'Boltzmann constant', T temperature, R_s series resistance, R_{sh}

shunt resistance, A_1 is a temperature independent constant. The 'equivalent circuit' of 'two diode model' (D_{01}, D_{02}) the 'solar cell' is illustrated in Fig. 4.3.

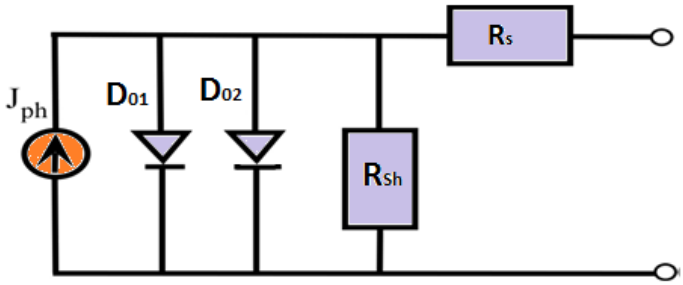

Figure 4.3 'H-I-T Solar cell equivalent circuit'

4.3.2. 'BAND DIAGRAM OF THE a-Si:H/c-Si CELL'

As aforementioned, a 'heterojunction solar cell' is made of two materials with 'different band gaps'. In the junction of 'solar cell' the 'conduction band' and 'valance band' are not in continuous line because of the 'band gap mismatch'. In figure 4.3 demonstrates the 'band structure' of a heterojunction 'a-Si:H/c-Si' where the 'band gap' of 'a-Si' is higher than the 'c-Si' used here.

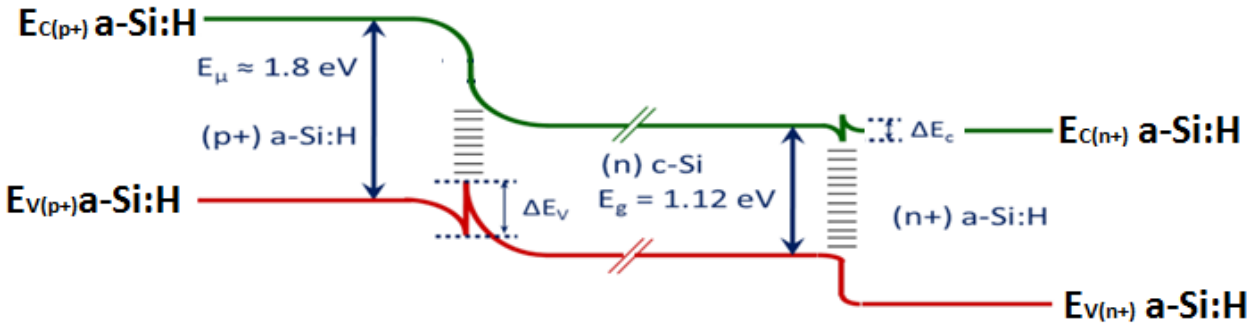

Figure 4.4 'Band diagram' of a (p^+) a-Si:H/(n) c-Si/(n^+) a-Si:H heterojunction

In above fig.4.4, 'ΔE_C' and 'ΔE_V' represents the offsets of 'conduction' and 'valence band' respectively. Considering the 'rear area' of the 'cell', the 'large valence band offset' at the '(n^+)

a-Si:H' interface provides a hindrance to the flow of 'minority holes' whereas, the flow of 'majority electrons' from the '(n)c-Si' to the '(n^+)a-Si:H' is relatively uninterrupted as the offset of 'conduction band' is too small [11].

4.3.3. LOSS MECHANISM OF H-I-T CELL

a). Reduction in 'recombination loss': The H-I-T 'solar cell' technology has its ability to minimize the 'recombination' losses of 'charge carriers' as low temperature budgetary 'amorphous silicon' thin layer is deposited upon the 'charge carrier' generating portion of 'mono crystalline silicon'. The top most 'front layer' of the H-I-T 'solar cell' is formed with a 'thin layer' of 'a-Si', so the probability of 'surface recombination' is become less.

(b). Reduction in optical loss: The 'sun light' is entered in to the 'HIT cell' through the 'transparent ITO' and the 'thin layer' of emitter. Hence the transmission of 'light' is better and the 'sun light' reached in to the 'c-Si' layer to generate the 'charge carriers' with a lesser 'optical loss'. *This has led to improvement in 'short circuit current density' (Jsc) of the 'cell' and ultimately produced 'enhanced efficiency'.*

(c). Minimizing resistance loss: T*he 'photo generated' 'electrical current' is collected through the 'surface grid electrodes'. In H-I-T 'solar cell' the grid is placed in rear, as a result lesser 'resistive loss' and improve the output 'efficiency' of the 'cell'.*

4.4. 'MODELING OF TWO NUMBERS HIT SOLAR CELLS'

'Silicon' H-I-T 'solar cells' combine the 'advantages and stability' of 'c-Si solar cells' such as 'high efficiency' and 'high stability' with those of 'a-Si solar cells' such as low temperature and relatively less costly process. In this 'research work' we have modeled two structure of H-I-T

'solar cells' with 'Zinc Oxide' (ZnO) material and 'Zinc Telluride' (ZnTe) in emitter layer replacing the 'a-Si layer' and optimized the 'layer thickness' of 'different layers' to attain the maximum efficiency.

4.4.1. 'MODELING OF H-I-T SOLAR CELLS WITH ZnO'

'Zinc Oxide' is a 'wide band gap' (II-VI) semiconductor material which has several encouraging 'electronic properties' including, 'good transparency', 'high electron mobility' and 'wide band gap'. These properties are very suitable and important for solar cell. This material is a 'direct band gap' semiconductor with 'Eg=3.4 eV'. The 'crystal structure' of ZnO is hexagonal. The 'electron' and 'hole mobility' of ZnO is 200cm^2/Vs and 5-50 cm^2/Vs respectively. The 'current density' of any kind of 'solar cell' is most critical parameter and dependent on the 'mobility' of 'electron and holes'. The other 'critical parameter' of the 'solar cell' is the 'open circuit voltage' which depends on 'band gap' of the material. The respective parameters are described here.

(a) Current Density

The 'generalized equation' of 'current density' (J_{sc}) of 'solar cell' is depicted below [12].

$$J_{sc} = qG.\sqrt{\frac{kT\tau}{q}}.(\sqrt{\mu_n}+\sqrt{\mu_p}) \dots\dots\dots\dots\dots\dots\dots\dots\dots\dots\dots\dots\dots\dots (4.2)$$

Where, q = 'electron charge'

G= 'Irradiance of light'

K = 'Boltzmann constant'

T = 'Temperature'

μ_n/ μ_p = 'electron/hole mobility'

τ = electron lifetime

From Eq (4.2) the ‘current density’ is ‘directly proportional’ with the ‘square root of mobility’. If we use higher mobility materials then we get higher current density. In Zinc Oxide ‘electron’ and ‘hole mobility’ is ‘higher’ than the ‘amorphous silicon’. ‘Electron mobility’ of ZnO is almost five times greater than the ‘amorphous silicon’. If we use ZnO as an ‘emitter layer’ in a ‘heterojunction solar cell’ then we can expect the ‘higher current density’.

(b) Band Gap

The ‘band gap’ of a semiconductor material is a key factor in respect of ‘solar cell’ absorption of ‘photon energy’ produce the electron hole pair. The photon energy received by the ‘photovoltaic solar cell’ is determined by the ‘band gap’ of that material. The ‘absorption coefficient’ (α) is dependent on the ‘band gap’ which is revealed in following equation.

$$\alpha = \alpha_0 \sqrt{\frac{E(\lambda) - E_g(x)}{E_g(x)}} \ldots\ldots\ldots\ldots\ldots (4.3)$$

Where, $E(\lambda) = \frac{hc}{\lambda}$, ‘h’ is the ‘Plank’s constant’, ‘c’ is the ‘velocity of light’, and ‘λ’ is the ‘wave length’ and E_g is the ‘band gap’.

(c) Open Circuit Voltage:

The maximum ‘open-circuit voltage’ (Voc) of ‘solar cell’ is viewed at the state of zero ‘current’. The ‘open-circuit voltage’ analogous to the ‘amount of forward bias’ on the ‘solar cell’ due to the ‘bias’ of the ‘solar cell junction’ with the ‘light-generated current’.

The ‘equation for Voc’ can be derived at ‘net current’ is zero in the general ‘solar cell’ equation, as follows:

$$V_{oc} = \frac{nkT}{q} \mathrm{l_n} \left(\frac{\mathrm{I_l}}{\mathrm{I_0}} + 1 \right) \ldots\ldots\ldots\ldots\ldots\ldots\ldots\ldots\ldots\ldots (4.4)$$

From equation (4.4) the 'Voc is dependent' on the 'saturation current' (I_o) of the 'solar cell' and the 'light-generated current' (I_l). Again the 'saturation current' is dependent on 'band gap' (E_g) of the material.

An equation for I_o is given below as a 'function of band gap' (E_g) [13]

$$I_0 = \frac{q}{k}\frac{15\sigma}{\pi^4}T^3\int_u^\infty \frac{x^2}{e^{x-1}}dx \ldots\ldots\ldots\ldots\ldots\ldots\ldots\ldots\ldots (4.5)$$

Where 'q' is the 'electronic charge', σ is the 'Stefan–Boltzmann constant', k is 'Boltzmann constant', 'T' is the 'temperature' and $u = \frac{E_g}{kT}$

From equation (4.4) we can analyze that if the 'band gap' is high then the 'saturation current' is low.

Again from the equation (4.2), if the 'saturation current' (I_0) is less, the 'open circuit voltage' is high.

So finally, the 'open-circuit voltage' is increases as the 'band gap' increases.

The 'band gap' of 'ZnO' and 'a-Si' is 3.4 eV, 1.72 eV respectively, the 'band gap' of 'ZnO' is greater than the 'a-Si'. So if we use ZnO as an 'emitter layer' then we can get higher 'open-circuit voltage'.

The proposed H-I-T 'solar cell' structure is "ITO/ZnO(n)/a-Si(i)/c-Si(p)/a-Si(p)/ITO" and the structure as in Fig 4.4. In this proposed structure 'n-doped zinc Oxide' (ZnO) is the 'emitter layer' and a-Si(p), a-Si(i), c-Si(p) 'layers' are BSF, buffer and absorber layers respectively. This structure of H-I-T 'solar cell' is proposed to ameliorate the 'efficiency' of the 'solar cell' and the 'cell structure' is developed in 'AFORS-HET simulation software' environment. In this 'proposed structure', we have taken the optimized 'thickness layer' of the 'ZnO', 'a-Si(i)', 'c-Si(n)' and 'a-Si(n)' is '10nm', '7nm', '300um' and '10 nm' respectively. The 'surface recombination

velocities' of 'electrons' and 'holes' are both has taken as 10^7 cm/s. The 'defect density' in 'c-Si layer' is 0.56eV with a 'concentration' of $1x10^{10} cm^{-3}$ [14-15].

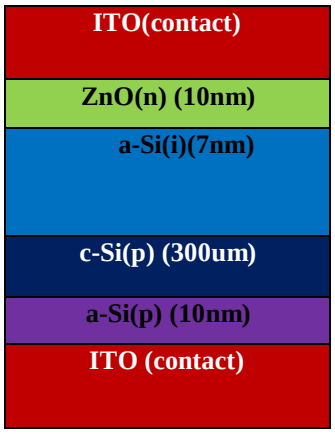

Fig.4.5 'Schematic Structure of Modeled HIT solar cell with ZnO(1st Model)'

4.4.2 'MODELING OF H-I-T SOLAR CELLS WITH ZnTe'

Zinc telluride is a compound chemical with the formula of ZnTe. ZnTe is a 'p-type semiconductor'. 'Zinc telluride' can easily be doped, therefore, the most common semiconductor materials used in optoelectronics is ZnTe. ZnTe is utilized in various semiconductor devices like 'blue LEDs' and 'components of microwave generators'. Zinc telluride (ZnTe) is a 'wide band gap' (II-VI) compound semiconductor. Its 'band gap' remains '2.23eV to2.28eV' at 'room temperature' and it has 'high absorption coefficient' close to$10^5 cm^{-1}$ and 'low electron affinity' 3.73eV. For 'low-cost', 'high-efficiency' 'thin film solar cell' fabrication, Zinc telluride (ZnTe) is becoming most promising 'II–VI compound semiconductor' [16-17]. Most of the 'wide band gap' materials are favorable to n-type doping but resist p-type doping. The 'ZnTe', is easier to 'p-type doping' compared to 'n-type doping' [16]. This is why a 'p-doped ZnTe' layer of 'acceptor concentration' of $1x10^{20} cm^{-3}$ is employed

as ‘emitter layer’ in the ‘proposed structure’. Effective ‘conduction band’ and ‘valance band densities’ of ZnTe are 1.176x10^18 cm^{-3} and 1.166x10^19 cm^{-3} respectively. The ‘electron’ and ‘hole mobility’ of ZnTe is 340cm^2/Vs and 100 cm^2/Vs respectively [17]. Refractive index and extinction co-efficient of ZnTe is 3.56 and 0.2 respectively.

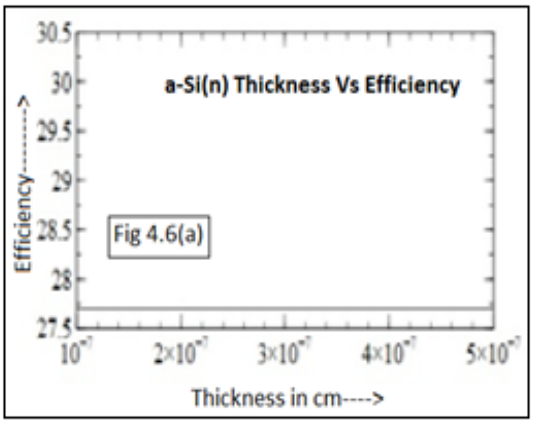

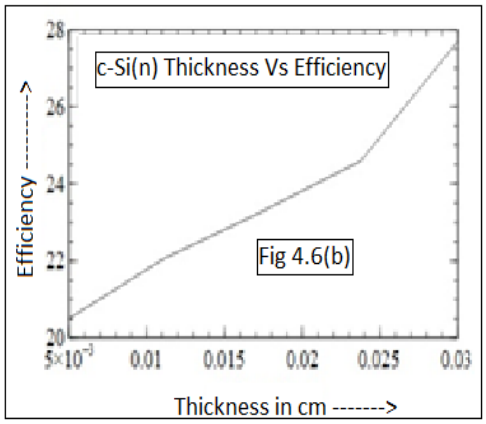

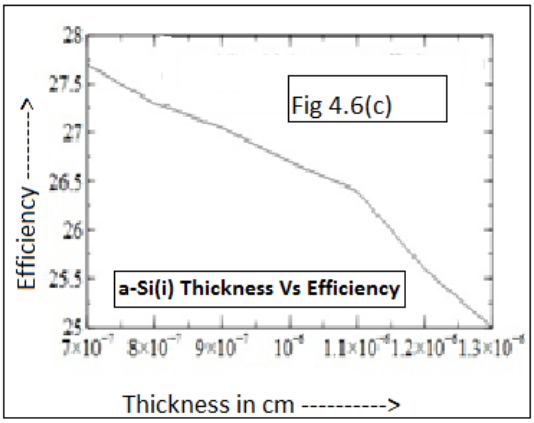

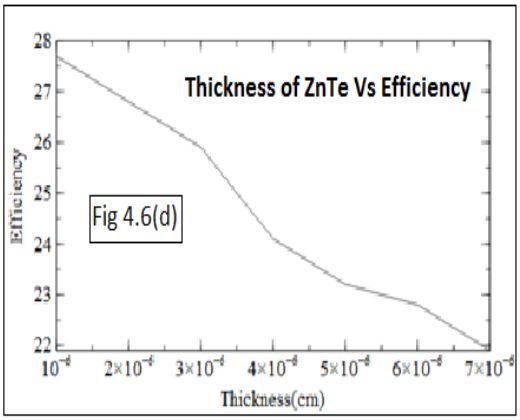

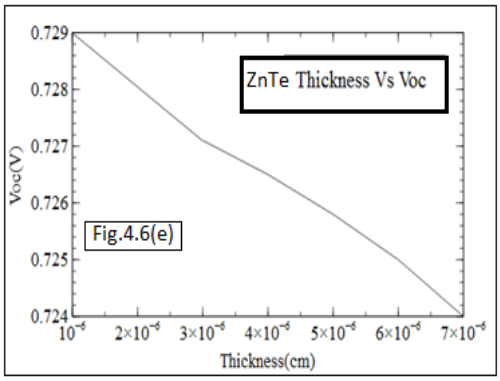

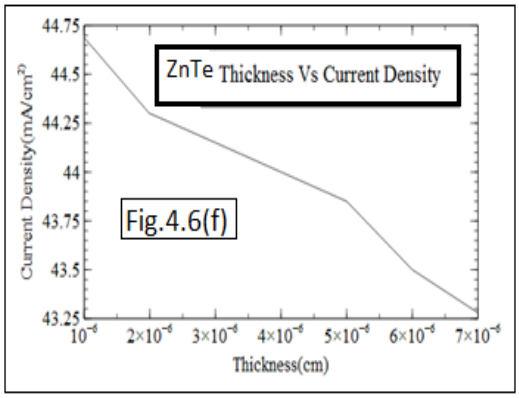

Fig 4.6(a), (b), (c) ,(d), 'Optimization of different layer' of Thickness in respect of Efficiency and Fig.4.6 (e) & (f) Optimized Thickness of ZnTe in respect of V_{oc} & J_{sc}

Considering all optimized thickness value of different layer of the structure is viewed in Fig 4.6 (a),(b),(c) and (d) in "AFORS-HET (Automat FOR Simulation of Hetero-structures) software". The 'thickness' of 'a-Si(n) layer' (fig.4.6.a) will not affect the 'efficiency' but the 'thickness' of 'c-Si(n) layer' (fig.4.6.b) is varied proportionately with 'efficiency'. However the 'efficiency' inversely proportionate with 'thickness' in the 'layer of a-Si(i)' and 'ZnTe(p)' (fig.4.6.c &d). In figure 4.6(e) & 4.6(f) the 'thickness' of 'ZnTe layer' has been optimized with respect to 'open circuit voltage' and 'short circuit current'. Both the 'open circuit voltage' and 'short circuit current' is decreased with the increment of 'thickness of ZnTe layer'. After optimization of 'thickness' of 'different layer' in respect of 'efficiency', 'open circuit voltage' and 'short circuit current', the new model of 'solar cell structure', has been developed using the 'ZnTe as emitter layer' as it is shown in Fig.4.7 and simulated accordingly.

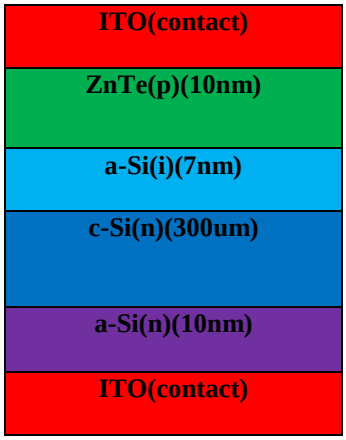

Figure 4.7 Schematic structure of modeled HIT solar cell with ZnTe (2nd Model)

4.5 RESULTS AND DISCUSSIONS

4.5.1 HIT SOLAR CELL WITH ZnO(n) IN EMITTER LAYER

The structure is modeled in 'AFORS-HET simulation software' environment and this modeled H-I-T 'solar cell' using 'ZnO' in 'emitter layer' and simulated consequently. The 'open circuit voltage' (Voc), 'short circuit current density' (Jsc), 'Fill Factor' (FF) and 'efficiency' (Eff) has been achieved 734.6mV, 42.39mA/cm^2, 82% and 25.54% respectively for our proposed structure. The output 'current-voltage curve' (J-V) is simulated and depicted in figure 4.8.

The 'output characteristics' of 'solar cell' is temperature dependent. On this context, the temperature is varied at value of 20^{0}C, 30^{0}C, 40^{0}C, 50^{0}C and 60^{0}C in software environment. From the output 'I-V curve' it is evident from the figure 4.9 that the open circuit voltage of the cell decreases with the increase of temperature. The reason behind the result is that increases in temperature reduces the band gap of a solar cell materials, whereby affecting the solar cell electrical parameters specially the open circuit voltage.

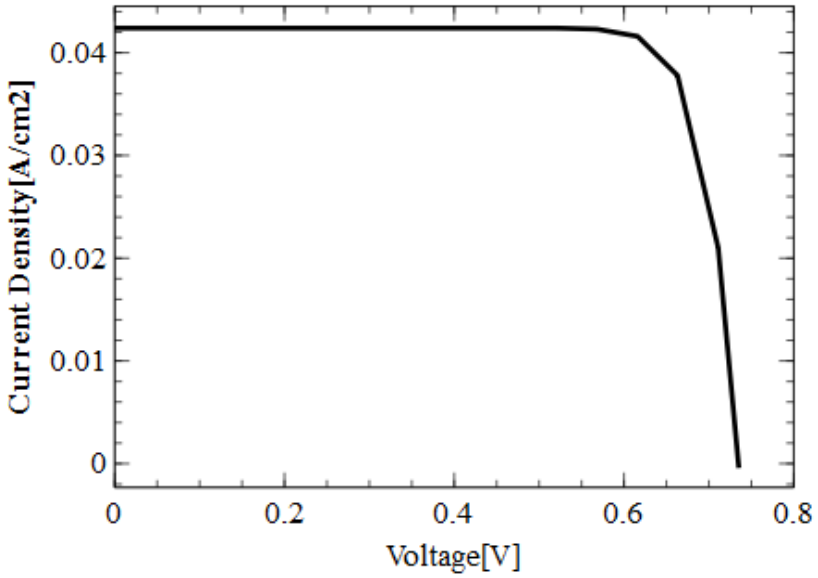

Figure 4.8 The I-V curve of the proposed structure

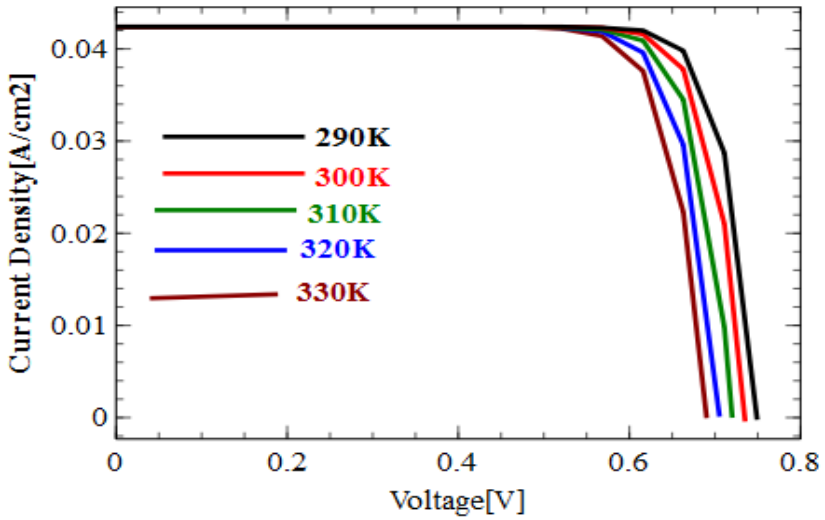

Figure 4.9 I-V characteristics under different temperature

4.5.2 HIT SOLAR CELL ZnTe(p) IN EMITTER LAYER

The 'open circuit voltage' (Voc), 'short circuit current' (Isc), 'Fill Factor' (FF) and 'efficiency' (Eff) has been achieved 729.3mV, 44.69mA/cm^2, 85.03% and 27.71% respectively for our proposed 2nd modeled structure. The output J-V curve is shown in figure 4.10. The result shows a significant improvement in the efficiency of the proposed HIT solar cell in which ZnTe/c-Si

junction is considered instead of a-Si/c-Si junction. The proposed solar cell has shown a significant improvement in 'efficiency' is mainly due to the fact that the absorption coefficient of ZnTe is greater than that of a-Si and the electron and hole mobility of ZnTe is also greater than that of a-Si. The electron mobility of a-Si and ZnTe is 20 cm^2/Vs, 340 cm^2/Vs respectively and the hole mobility of a-Si and ZnTe is 5 cm^2/Vs, 100 cm^2/Vs.

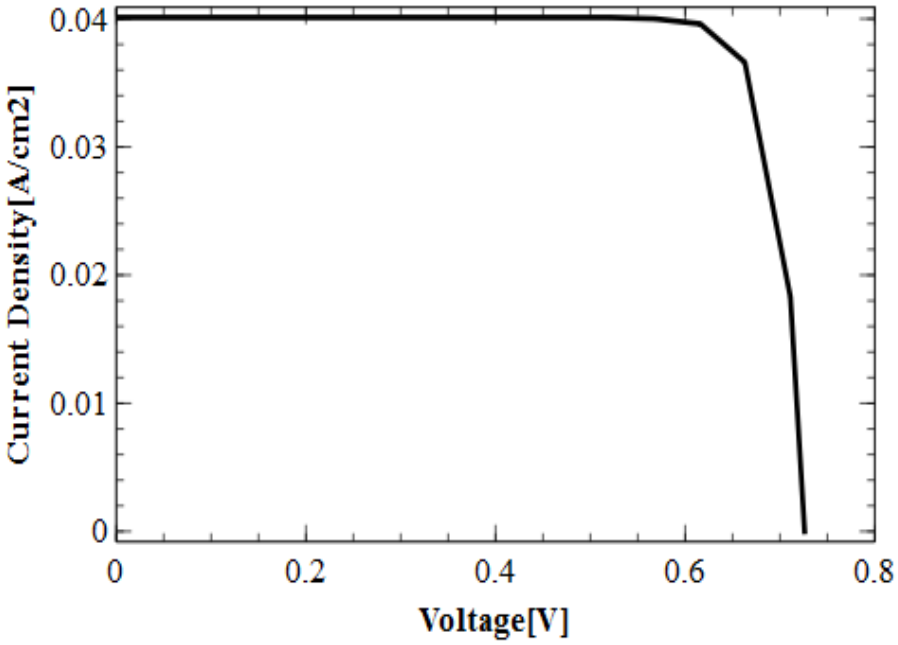

Figure 4.10 J-V curve of the H-I-T solar cell ZnTe as emitter layer(2nd Model structure)

It is well known that the 'band gap' of semiconductors is 'temperature dependent'. While the temperature is increased, it makes the decrement of the 'band gap'. Lower value of external energy is required to 'break the bond'. In the 'bond model' of a semiconductor 'band gap', reduction in the 'bond energy' also reduces the 'band gap'. Therefore increasing the 'temperature' reduces the 'band gap'.

The 'Current-Voltage' characteristics of our second modeled 'solar cell' again simulated in 20^0C, 30^0C, 40^0C, 50^0C & 60 ^{0}C temperatures and the output is shown in figure.4.11. It is

viewed that I-V characteristics of solar cell vary under different temperature. The 'open circuit voltage', 'short circuit current', 'Fill Factor' and the 'efficiency' at different temperature is tabulated in Table4.1.

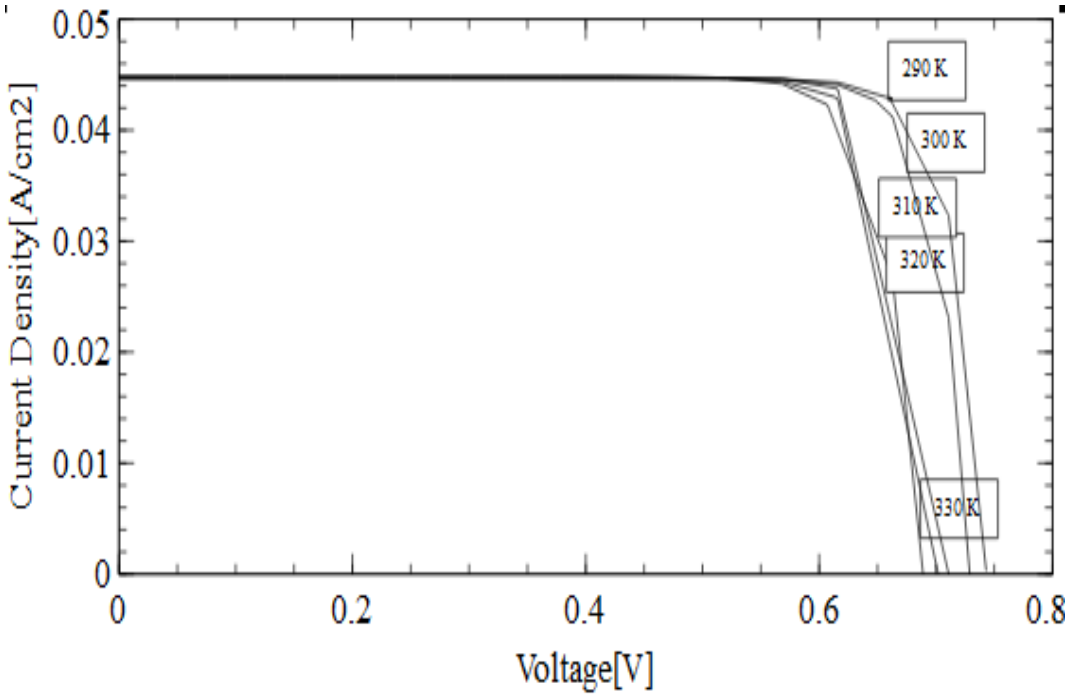

Figure 4.11 J-V characteristics under different temperature

Table 4.1 Output Parameters of 2nd Modeled solar cell ZnTe as emitter layer under different Temperature

Temperature(^{0}C)	Voc [mv]	Isc [Ma/cm2]	FF [%]	η [%]
20	742.7	44.62	85.59	28.37
30	729.4	44.69	84.98	27.7
40	716.1	44.75	83.75	26.84
50	702	44.81	83.87	26.38
60	688.7	44.86	83.14	25.69

4.5.3 COMPARATIVE STUDY WITH PRE EXISTING AND NEW MODELED H-I-T SOLAR CELL

The H-I-T 'solar cell structure' with 'a-Si' and 'c-Si heterojunction' is very common. The Structure is ITO/a-Si(n)/a-Si(i)/c-Si(p)/a-Si(p)/ITO [1] (Model 1) shown in below. In the existing structure 'a-Si(n)' has been used as 'emitter layer', but in the proposed structure (1st Model) 'ZnO(n)' has been used as the 'emitter layer'.

The 'ambient temperature' and the 'defects density' in the 'Hetero-junction with Intrinsic Thin layers' 'solar cells' (H-I-T) are strongly affect their 'performances'. The structure: ITO/a-Si:H(p)/a-Si:H(i)/c-Si(n)/a-Si:H(n)/ITO is presented in Fig.4.12(a). In this H-I-T 'solar cell' structure, "a-Si(p)/ a-Si(i)/ c-Si(n)/ a-Si(n)" layers are used as 'emitter', 'buffer', 'absorber' and 'BSF layers' respectively [18]. The thickness of the "a-Si(p), a-Si(i), c-Si(n) and a-Si(n)" layers are taken as "10nm, 7nm, 300um and 10 nm" respectively. A study of the 'performance evolution' is performed for this structure using 'AFORS-HET simulation software' environment and compared with two other new modeled structure using 'ZnO(n)' and 'ZnTe(p)' in 'emitter layer' substituting the a-Si (n/p) respectively.

The performance comparison of the proposed structure with the existing structures is shown in table 3.

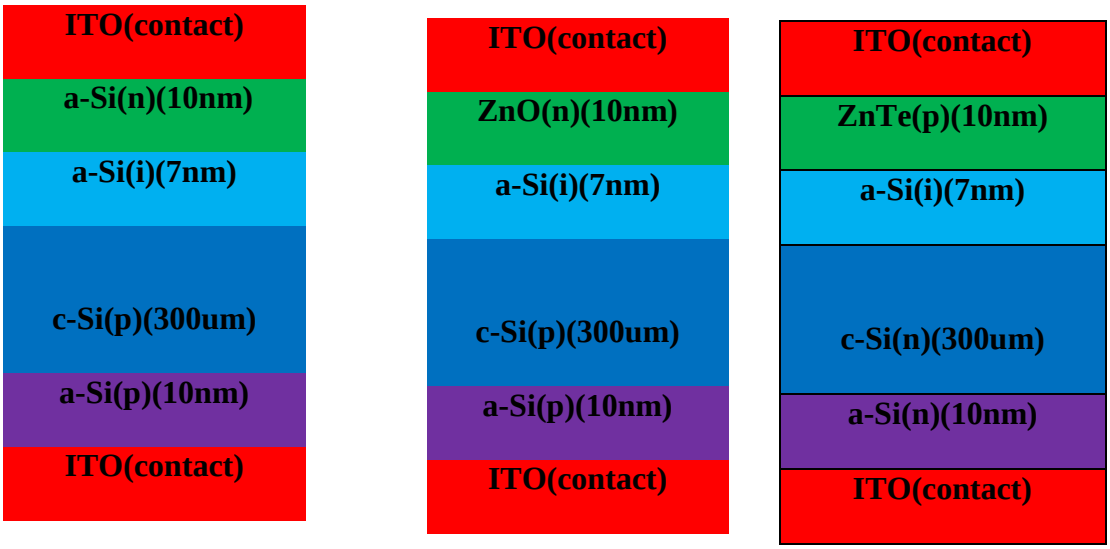

(a) (b) (c)

Figure 4.12: Schematic structure of 3 models (a)Existing Silicon based (b) ZnO in emitter layer & (c) ZnTe in emitter layer HIT Solar cells

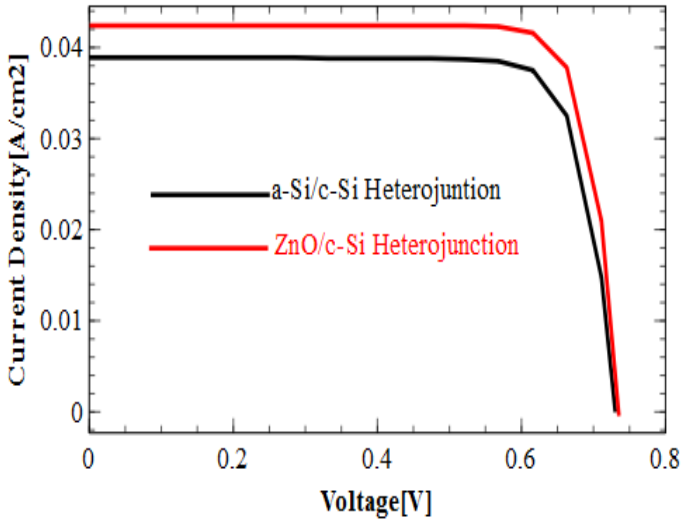

Figure 4.13 J-V curve Comparison between two structure of a-Si and Proposed ZnO in emitter layer

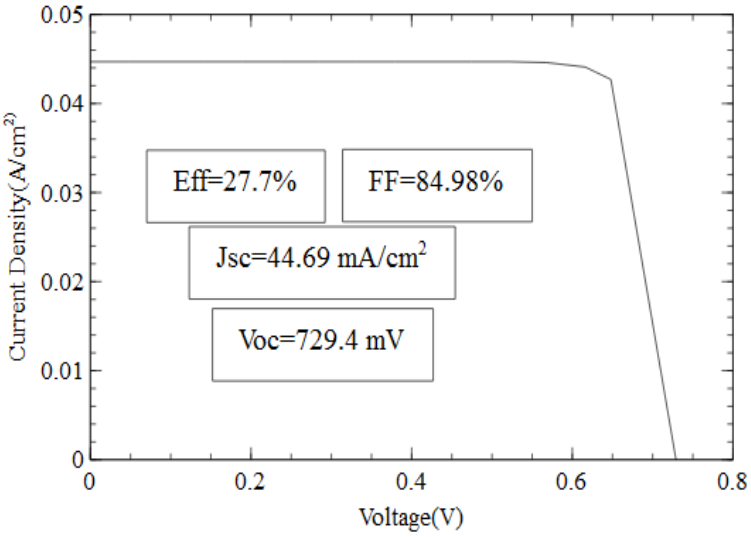

Figure 4.14 J-V curve of the proposed structure HIT Solar cell ZnTe(p) in emitter layer

Table 4.2 Performance comparison of the proposed structures with the existing structure of HIT solar cell

Structure	**Voc [mV]**	**Jsc[mA/cm^2]**	**F.F [%]**	**Eff [%]**
ITO/a-Si(n)/a-Si(i)/c-Si(p)/ /a-Si(p)/ITO [a]	730.1	38.91	81.11	23.04
ITO/ZnO(n)/a-Si(i)/c-Si(p)/a-Si(p)/ITO [b]	734.6	42.39	82	25.54
ITO/ZnTe(p)/a-Si(i)/c-Si(p)/a-Si(n)/ITO [c]	729.3	44.69	85.03	27.71

4.6 REFERENCES

[1] Kamlesh Patel, Pawan K. Tyagi, "Technological Advances in A-Si: H/c-Si Heterojunction Solar Cells", International Journal of Renewable Energy Research,Vol.4, No.2, 2014.

[2] Wakisaka K,Taguchi M, Sawada T, Tanaka M, Matsuyama T, Matsuoka T, Tsuda S, Nakano S, Kishi Y, Kuwano Y, More than 16% solar cells with a new HIT (doped a-Si/no doped a-Si/crystalline Si) structure, Photovoltaic Specialists Conference.1991; 2: 887 – 892.

[3] Tanaka M, Taguchi M, Matsuyama T, Sawada T, Tsuda S, Nakano S, Hanafusa H, Kuwano Y. Development of New a-Si/c-Si Heterojunction Solar Cells: ACJ-HIT (Artificially Constructed Junction-Heterojunction with Intrinsic Thin-Layer). Jpn. J. Appl. Phys. 1992; 31: 3518-3522.

[4] E. Constableand R. A. Lewis, "Optical parameters of ZnTe determined using continuous-wave terahertz radiation", JOURNAL OF APPLIED PHYSICS 112, 063104 (2012)

[5] OthmaneSkhouni, Ahmed El Manouni1, Bernabe Mari, and HanifUllah, "Numerical study of the influence of ZnTe thickness on CdS/ZnTe solar cell performance", Eur. Phys. J. Appl. Phys. (2016) 74: 24602, Eur. Phys. J. Appl. Phys. (2016) 74: 24602

[6] Wakisaka, K., Taguchi, M., Sawada, T., Tanaka, M., Matsuyama, T., Matsuoka, T., Tsuda, S., Nakano, S., Kishi, Y., Kuwano, Y., "More than 16% solar cells with a new "HIT" (doped a-Si/non doped a-Si/crystalline Si) structure," Conference Record of the 22rd IEEE Photovoltaic Specialists Conference, 887-892, IEEE, 1991.

[7] Tsunomura, Y.Yoshimine, Y.Taguchi, M.Baba, T.Kinoshita, T.Kanno, H.Sakata, H.Maruyama, E.Tanaka, M., "Twenty-two percent efficiency HIT solar cell," Solar Energy Material & Solar Cells, Vol. 93, No. 6-7, pp. 670-673,2009.

[8] Mikio Taguchi, Ayumu Yano, Satoshi Tohoda, Kenta Matsuyama, Yuya Nakamura, Takeshi Nishiwaki, Kazunori Fujita, and Eiji Maruyama,"24.7% Record Efficiency HIT Solar Cell on Thin Silicon Wafer",IEEE JOURNAL OF PHOTOVOLTAICS, VOL. 4, NO. 1, JANUARY 2014.

[9] Khomdram Jolson Singh, Th. Jayenta Singh, Dhanu Ch., and **Subir Kumar Sarkar**," A thin layer of Carbon Nano Tube (CNT) as semi-transparent charge collector that improve the performance of the GaAs Solar Cell", **Optik**, ELSEVIER,Vol.135,pp-256-270,April 2017

[10] Khomdram Jolson Singh, Dhanu Chettri, Th. Jayenta Singh, and **Subir Kumar Sarkar**, "Heterogeneous Carbon Nano-Tube window layer with higher sheet resistance improve the solar cell performance"(ICEPOE 2017) at Thammasat University, Bangkok, Thailand, April 21-23, 2017, **IOP Series: Materials Science and Engineering** vol.211, doi:10.1088/1757-899X/211/1/012023, April 2017

[11] S. M. Iftiquar,Youngseok Lee, Vinh Ai Da, Sangho Kim and Junsin Yi , "High efficiency heterojunction with intrinsic thin layer solar cell: A short review", Material and Process for Energy, ©FORMATEX 2013, Pages 59-67

[12] I. Repins, S. Glynn, J. Duenow, T.J. Coutts, W. Metzger, and M.A. Contreras, "Required Materials Properties for High-Efficiency CIGS Modules", *Conference Paper* ,NREL/CP-520-46235,July 2009.

[13] P. Baruch, De Vos, A., Landsberg, P. T., and Parrott, J. E., "On some thermodynamic aspects of photovoltaic solar energy conversion", *Solar Energy Materials and Solar Cells*, vol. 36, pp. 201-222, 1995.

[14] Tapas Chakrabarti and Subir Kumar Sarkar, "Analytically Performance Study of Newly Modelled HIT solar cell with different materials", International Journal of Latest Technology in Engineering, Management & Applied Science (IJLTEMAS,) Volume VII, Issue IV, April 2018, ISSN 2278-2540.

[15] Khomdram Jolson Singh, N. Basanta Singh and **Subir Kumar Sarkar**, "Textured window with DLAR coating design for an effective minimization of electrical and optical losses in an efficient III–V solar cell", Journal of Computational Electronics, Springer, Vol. 14, Issue 1, pp.-288-299, DOI 10.1007/s10825-014-0652-2, 2015.

[16] E.Constableand R. A. Lewis, "Optical parameters of ZnTe determined using continuous-wave terahertz radiation", JOURNAL OF APPLIED PHYSICS 112, 063104 (2012)

[17] Tapas Chakrabarti, Malay Saha, Ambar Khanda and **Subir Kumar Sarkar**,"HIT Solar cell using ZnTe as an emitter layer", IEEE International Conference on Smart Grids, Power and Advanced Control Engineering (ICSPACE-2017), Global Academy of

Technology, 17-19 August, 2017.

[18] Bouzaki Mohammed Moustafa, BenyoucefBoumediene, “Simulation and Optimization of the Performance in Hit Solar Cell”, International Journal of Computer Applications (0975 – 8887) Volume 80 – No 13, October 2013.

CHAPTER 5:

FABRICATION, CHARACTERIZATION AND PERFORMANCE ANALYSIS OF DYESENSITIZED SOLAR CELLS

5.1 INTRODUCTION

The 'crystalline silicon' 'solar cell' is already been commercialized, but the cost of production is quite high, which pull up the tariff of solar power beyond the reach of general people. The continuous exploration on this subject gets high pace, to bring down the production cost of 'solar cell' with high 'efficiency'. The 'dye-sensitized solar cell' can prove itself as a suitable alternative to in the domain of 'solar cells'. It offers a major consideration as a substitute source of unpolluted and green energy being its advantages among innumerable benefits, such low fabrication cost, great mechanical strength (robust), lightweight flexible cell and 'low price' to 'power conversion efficiency' ratio.

A new environment friendly 'low cost solar cell', 'Dyesensitized Solar cell' (DSSC) was first developed in 1991 applying photo sensitizer dye by O'Regan and Gratzel [1]. As the alternative

of conventional C-Si, the DSSCs are becoming very popular as the fabrication technique is very simple and very inexpensive materials are required to fabricate [1-2]. Nature has been a source of inspiration to develop 'Dyesensitized Solar cell' as it uses the principle of stacking in the green leaves, cell stacks thylakoids membranes so that the light will go to many layers of chlorophyll before it gets extinguished and the same trick is used in this solar cell, instead of pilling the thylakoids are using Nano size titanium particles that stacked up for light harvesting. The 'Dyesensitized Solar cell' uses a molecule that is excited by sunlight and generates electric power, but the molecule is not involved in charge conduction, so the charge transport and 'photo induced charge separation' are separated and that's not the case of in all another 'solar cell' which are based on P-N junction semiconductor [3].

Among the 'basic element' used in 'Dyesensitized Solar cell', dye plays a foremost role in absorbing sunlight and converting it into electricity [4-5]. The Ruthenium (Ru) complexes that are used in industries are complex in synthesis, [6-8], hence natural dye finds its way in DSSC. The excellent 'dye' must have 'broad absorption spectrum' and ability to 'inject electron' in semiconductor materials. Natural pigment extracted from flower, anthocyanin, and chlorophyll possess the above excellent qualities [9]. Anthocyanin absorbs light within 450-600 nm range whereas chlorophyll absorbs light in 430-662 nm range [9]. In anthocyanin and carbonyl, the hydroxyl group is present as anchorage agent due to which pigment get attached to TiO2 nanostructures [10-11].

The 'Dyesensitized Solar cell' structures are fabricated on 'ITO coated' 'glass substrate'. The 'wide band gap' 'semiconductor material' TiO_2 film on ITO glass substrate along with a photosensitizer dye is used to make the 'solar cell'. Another predominant part of this 'solar cell' is an 'electrolyte' which is applicable on this film. The different varieties of 'dyes' are the

'charge provider' of 'Dyesensitized Solar cell'. The 'Dyesensitized Solar cell' subsists of a Photo-electrode made of TiO_2 'thin film' on ITO glass and a 'catalytic electrode' on same genre of glass with an 'electrolyte' between them. The 'electrical parameters' like 'Short circuit current density' (J_{sc}), 'Open Circuit Voltage' (V_{oc}), 'Fill Factor' (FF), 'efficiency' (η) and the 'incident photon' to 'current efficiency' (IPCE) depends on the 'morphological properties' of semiconductor, 'spectroscopic properties' of dyes and the 'electrical properties' of 'electrolytes'.

In this research work different inorganic dyes like, Red Colloid Dye $\{FeCl_3[Fe(OH)_3]Fe_3^+\}$, 'Prussian Blue Dye' $\{KFe_3[Fe_2(CN)_6]\}$ and different 'natural pigments' are extracted from natural organic sources like 'Green Chlorophyll Dye' $\{C_{55}H_{72}O_5N_4Mg\}$, 'red dye' from hibiscus and 'blue pigment' from Clitoria-Ternatea is extracted and applied these dyes on TiO_2 thin film, numbers of 'Dyesensitized Solar cells' are fabricated. The 'grain size' of these thin films 'TiO2 particles' are 47 to 67nm. The three samples of dyesensitized solar cell fabrication are narrated using inorganic and organic dye like Red Colloid Dye $\{FeCl_3[Fe(OH)_3]Fe_3^+\}$ and 'Prussian Blue Dye' $\{KFe_3[Fe_2(CN)_6]\}$ of inorganic dye, and in the other hand organic Green Chlorophyll dye $\{C_{55}H_{72}O_5N_4Mg\}$. The best result is observed in the fabricated dyesensitized solar cell using inorganic Prussian blue dye.

5.2 'LITERATURE SURVEY OF DYESENSITIZED SOLAR CELLS'

The environment friendly 'low cost solar cell' using photosensitizer dye was developed by Braian O'Regan and Michel Gratzel in the year of 1991 which is known as Dyesensitized Solar Cell. The device was based on 10µm thick transparent 'TiO_2 particles'. The films were doped with a charge transfer dye for sensitization and light harvesting. The overall 'light' to 'electric energy' 'conversion yield' was 7.1-7.9% in software domain [1].

A basic ‘Dyesensitized Solar cell’ is composed of a ‘semiconductor metal-oxide’ and ‘sensitized’ by a dye, a ‘redox couple electrolyte’ and a ‘counter electrode’ which is generally thermally deposited platinum on ‘fluorine doped tin oxide’ (FTO) to get the maximum ‘efficiency’. While the ‘Dyesensitized Solar cells’ are low cost alternative, the use of costly material Platinum, enhance the price of cells. To address this issue, low cost alternative Cobalt sulfide, Copper sulfide or Nickel sulfide substituted the Platinum material as electrode [12].

The investigation in respect of efficiency and overall performance of DSSC, the morphology of semiconductor materials and optimization of dyes are very important. The exploration of new electrolytes is the continuous process of research work in domain of ‘Dyesensitized Solar cells’. The ‘electrolytes’ are used for appropriate ‘charge propagation’ between the two ‘electrodes’. These electrolytes regenerate the dyes also. Many ‘redox charge relays’ have been proposed as substitution of I^-/I_3^- ‘redox couple’. Recently ‘polymer electrolytes’, ‘organic’ ‘hole transport material’ like ‘spiro-MeOTAD’ is used in some cells [12].

The cost factor, ease of availability of raw materials and variety of colors associated with ‘Dyesensitized Solar cells’. Dyes extracted from natural sources like Capsicum, black rice, spinach, eggplant skin, mulberry, cabbage-palm fruit, gardenia fruit, rhododendron etc. have all been used as sensitizers. On the basis of parameters like ‘short-circuit current density’, ‘open-circuit voltage’, ‘fill factor’ and the ‘efficiency’ the performance for modified chlorophyll (II) with beta-carotene module shows the best result with an efficiency of 4.2% [7].

The ‘TiO_2 nano powder’ has high porosity, so the ‘thin film’ on FTO glass adsorbed the dyes as ‘light sensitizer’. The ‘Prussian blue dye’ is good ‘photosensitizer’ applied on TiO_2 film and achieved the ‘efficiency’ of 0.73% [5].

Some researchers used ZnO instead of TiO_2 for making the 'thin film' on FTO glass. The porosity of ZnO is also substantially high. The DSSCs made of ZnO film with different dye like 'Ru complex dye N719' or 'organic dye D149' are used and observed better result compare to TiO_2 film based 'Dyesensitized Solar cells'[4].

5.3 THEORY OF DYESENSITIZED SOLAR CELLS

'Dyesensitized Solar cells' are belongs to third generation of 'solar cell' which is a very promising in this genre, as 'low cost materials' are involved in fabrication, and the simplicity of structures. The sunlight can be easily absorbed in the 'inner parts' of 'solar cell' through the 'transparent anode' and 'cathode'. It is a mesh or aggregation of nanoparticles of TiO_2 (Titanium di-oxide) or any other material of semiconductor like ZnO (Zinc Oxide) [14], CuO (Copper oxide) etc. through which the electron are transported. A thin film of TiO_2 nano-particles is developed on the conductive glass substrate. As the film is formed with a porous material, the light absorbing dye can be absorbed in this film and that converts the 'incident light energy' into 'electrical energy'. An 'electrolyte' is used between the 'anode' and 'cathode' that replenishes the 'electrons' lost by the 'dye molecules'. The Tio_2 is commonly used 'semiconductor material' which has the unique ability of TiO_2 particles to stay welded together and particle of material is transparent also. Receiving the photons from the solar radiation, the electrons emerged from the dye molecules which are encompassing the TiO_2 particles. 'Dye molecules' are excited from the 'Highest Occupied Molecular Orbital' (HOMO) 'band' to the 'Lowest Unoccupied Molecular Orbital band' (LUMO), after getting excited by the photons from solar radiation [15].

The excited 'dye- molecule' loses an electron and becomes oxidized and the 'electron' goes to the 'conduction band' of the semiconductor, TiO_2 nano-material. This 'injected electron' then gets carried out through the TiO_2 nano-particles which is an electron transport layer, which

depends on the size and the density of the nano-particles. The probability of the 'electron' getting lost in the iodide electrolyte is increased if the nano-particles are small in size; more and more defects are there. Smaller size of nano-particles increases the 'surface area' of covering the nano-particles with dye. If the density of nano-particle is low, then the pathways for the electron to reach the anode are also less. Fabrication of a 'Dyesensitized solar cell' is quite challenging, keeping in view of optimization of size and density of the nano-particles. After excitation of 'dye molecule' emitted 'electron' and it starts to degrade unless the lost electron is replenished. From the 'I^- ions' of 'Iodide electrolyte' the 'dye molecules' are received back the 'electrons' and in this way 'I^- ions' thereby gets oxidized to I_3^- (tri-iodide ions). These tri-iodide ions then move around until they 'come in contact' with the 'cathode' of the DSSC. Once the ions reached in to cathode, they regain their 'missing electrons' from the 'cathode' and get reduced to I^- form again [16]. When all these processes work together, the 'electrons' from the 'dye' reach to the external circuit through 'anode' and then ultimately 'flow back' into the 'cell' through the 'cathode'. The effective electron injection depends on the separation of LUMO and the lower level of conduction band of the semiconductor.

TRANSPARENT CONDUCTIVE OXIDE (TCO):

To get the maximum 'sunlight' to the 'active area', the 'TCO substrates' must be 'highly transparent' (transparency > 80%). The 'efficiency' of 'Dyesensitized solar cell' is also dependent on the 'TCO material' and its 'characteristics' as the efficient 'charge transfer' can 'minimize energy losses'.

1. **SEMICONDUCTOR OXIDE MATERIAL:**

The central part of a 'Dyesensitized solar cell' device subsists of a 'thick nano-particle film' that provides a 'large surface area' for 'light-harvesting'. The efficiency of 'Dyesensitized solar cell'

depends on the ‘electron transfer rates’, which in turn depends on the ‘crystalline’, ‘morphology of surface area’ of the semiconductor. TiO_2 is considered ‘most efficient’ and environmentally benign ‘photo-catalyst’.

2. COUNTER ELECTRODE:

‘Counter electrodes’ are mainly used to ‘regenerate the electrolyte’. The ‘counter electrode’ transports the ‘electron’ that arrives from the external circuit back to the ‘redox electrolyte’ system. Hence, for efficient charge transfer, the counter electrode should exhibit a high catalytic activity and high electrical conductivity.

3. DYE SENSITIZER

An efficient ‘solar cell’ sensitizer should adsorb strongly, to the ‘surface of the semiconductor oxide’ via anchoring groups, exhibit intense ‘absorption’ in the ‘visible part’ of the ‘spectrum’, and possess an appropriate ‘energy level alignment’ of the dye ‘excited state’ and the ‘conduction band edge’ of the semiconductor. The performance of DSSCs mainly depends on the molecular structure of the photosensitization.

4. ELECTROLYTES

In ‘Dyesensitized solar cell’ the ‘electrolyte’ plays an important role, in the process of ‘light-to-electricity conversion’. The ‘electrode’ must be able to ‘transport the charge carrier’ between ‘photo anodes’ and ‘counter electrode’. The electrolytes in ‘Dyesensitized solar cell’ are classified as ‘liquid’, ‘solid-state’, or ‘quasi-solid state’. The ‘conduction band’ of TiO_2 received the ‘electrons’ from the dye, and the ‘dye is oxidized’ and should go to its ‘ground state’ immediately.

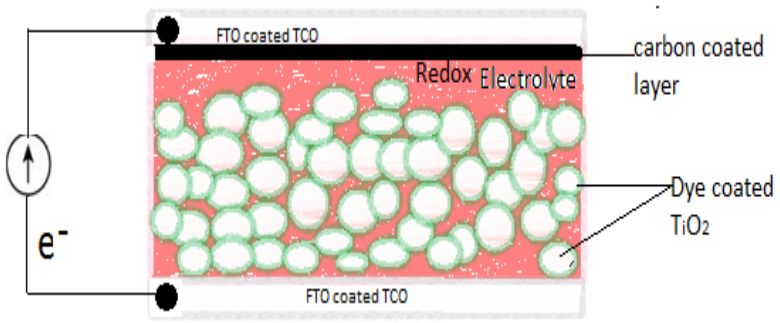

Fig.5.1. Schematic representation of a Dyesensitized solar cell

Equations:

$D + h\nu$ (incoming photon) $\longrightarrow D^*$ [excitation of dye molecule by incoming photon]

$D^* + TiO_2 \longrightarrow e^-(TiO_2) + D^+$ [injection of electron into conduction band]

$D^+ + (3/2)\, I^- \longrightarrow D + (½)\, I_3^-$ [regeneration dye by the electrolyte]

$½\, I_3^- + e^-$ (from load) $\longrightarrow (3/2)\, I^-$ [re-capture of electron]

Where the 'absorption' of the 'light' by the 'dye D' leads to excited state D*

5.4. FABRICATION OF 'DYESENSITIZED SOLAR CELLS'

In my work several type of dye were prepared and used on the 'TiO_2 film' made on 'Indium Tin oxide' 'transparent conductive glass' (ITO) to make these different 'Dyesensitized solar cells'.

A) PREPARATION OF RED COLLOID DYE

The solid block of 'Ferric Chloride' ($FeCl_3$) was crushed in a mortar-pestle to get the fine particles of $FeCl_3$ which is depicted in Fig.5.2(a). Adding 'de-ionized' water to 'Ferric chloride', a solution of 'Ferric Chloride' was made. De-ionized water was added in to 30 % pure 'Ammonia solution' slowly to prepare a 'dilute solution' of Ammonium Hydroxide (NH_4OH). Then the Ammonium Hydroxide (NH_4OH) solution was added 'drop by drop' to the 'Ferric Chloride' ($FeCl_3$) solution. The precipitate of $Fe(OH)_3$ was collected using filter paper which is revealed in Fig.5.2(b), and again mixed with fresh 'Ferric Chloride' ($FeCl_3$) solution, which is

the peptizing agent. The $\mathbf{Fe_3^+}$ ions are absorbed on the surface and breaking up into 'small sized colloidal particles' of $[Fe(OH)_3]$ Fe_3^+ and the colour of dye is red which exhibits in Fig5.2(c). The chemical process for preparation of this 'red dye' is known as peptization.

The Chemical Equations are as follows:

$$FeCl_3 + 3\ NH_4OH \longrightarrow Fe(OH)_3 + 3\ NH_4Cl$$

$$Fe(OH)_3 + FeCl_3 \longrightarrow [Fe(OH)_3]\ Fe_3^+ \text{ (red colloid)}$$

(a).  (b).  (c). 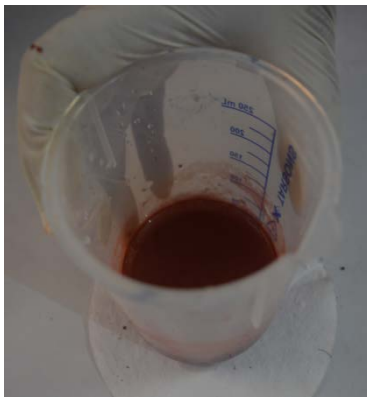

Fig. 5.2 Preparation of Red colloidal dye in Lab (a) Crushing $FeCl_3$ chunks (b) Filtering of $FeCl_3$ solution (c) Red Colloidal Solution

B). PRUSSIAN BLUE $\{KFe_3[Fe_2(CN)_6]\}$ DYE

To prepare this inorganic dye of Prussian blue, two separate solutions were prepared. The first one was 4 gm of 'Ferric Chloride' in '100 ml' of de-ionized water and the 'second solution' was that of 2gm of 'Potassium Ferro cyanide' in 200 ml of de-ionized water. For the first solution, a solid block of 'Ferric Chloride' was weighed and then crushed with a mortar-pestle. DI water was enumerated to it and the 'solution' was subjected to magnetic stirring for some while. In case of second solution, '2 gm' of 'Potassium Ferro cyanide' was taken in a 'beaker' and then DI water was poured to it and then the 'solution' was also subjected to magnetic stirring for some minutes as it is depicted in Fig.5.3(a). The first solution was gradually added into the second

solution with a careful manner. As soon as the two solutions are mixed, the 'precipitate' was formed and collected which was our required 'Prussian blue' {$KFe_3[Fe_2(CN)_6]$}. The precipitate is adjoined to DI water to obtain a colloid like solution of the potent dark blue colour of dye as exhibited in Fig.5.3(b). The compound solution subsists of 'iron ions Fe^{+2}'(ferrous) and 'Fe^{+3} (ferric) states', very rigidly associated with 'CN^- (cyanide) ions'.

Chemical Equations are as bellow:

$$\mathbf{K_4[Fe_2(CN)_6] \longrightarrow K^+ + [Fe_2(CN)_6]4^-}$$

$$\mathbf{FeCl_3 \longrightarrow Fe_3^{+} + 3Cl^-}$$

$$\mathbf{K^+ + [Fe_2(CN)_6]4^- + Fe^{3+} \longrightarrow KFe_3[Fe_2(CN)_6]}$$

(a). 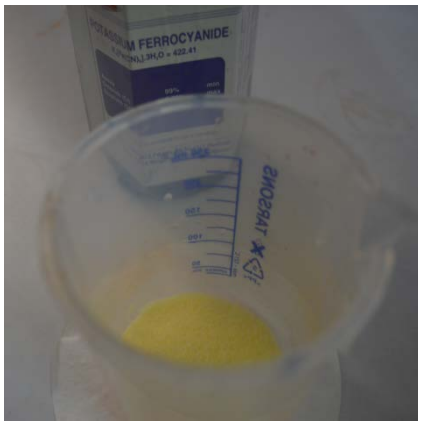

(b). 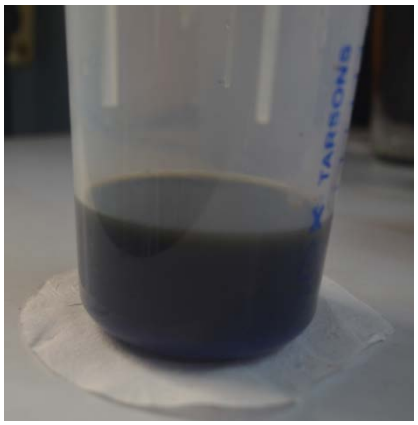

Fig.5.3 Preparation of 'Prussian blue' {$KFe_3[Fe_2(CN)_6]$}Dye (a) 'Potassium Ferro cyanide solution' (b). Formation of 'Prussian Blue Dye'

C) PREPARATION OF GREEN DYE FROM CHLOROPHYLL

Few bunch of spinach leaves were washed with 'DI water' and cut into small pieces to increase the 'surface area' of the target. The immense grinding of leaves was done in a mixer grinder at very high speed. 50 ml of DI water was mixed while grinding. The obtained solution was filtered and the precipitate was separated. The dilute filtrate solution was heated at 100 degree Celsius for 5 minutes. The solution started simmering and the Chlorophyll automatically being separated from the solution. The 'solution' was 'filtered' again, and the precipitate that we obtained was

the chlorophyll. The obtained chlorophyll was diluted with ethanol and thus the final dye was made which is exhibited in Fig.5.4. In spinach there are two types of chlorophyll are found as bellow:

Chlorophyll-A ($C_{55}H_{72}O_5N_4Mg$) & Chlorophyll-B ($C_{55}H_{70}O_6N_4Mg$) [8].

Spinach leaves being cut into small pieces

Chlorophyll obtained from the leaves

Green Dye obtained from the leaves of Chlorophyll

Fig.5.4. Extracted Green Chlorophyll from spinach

D). PREPARATION OF ELECTROLYTE

The 'iodide electrolyte solution' was prepared by dispersing "0.127 g of 0.05 M Iodine (I_2)" in "10 ml of water free Ethylene Glycol" and then 'adding 0.83 g of 0.5 M Potassium Iodide (KI)'. The 'solution' was subjected to magnetic stirring and 'stored in a dark container' which is displayed in Fig.5.5

Addition of
Ethylene Glycol in KI + I2 powder

Final Iodide electrolyte solution

Fig.5.5. Preparation of Electrolyte in Lab

5.5 EXPERIMENTAL DETAILS OF SOLAR CELLS WITH DIFFERENT DYE:

The 'ITO coated conductive glass' was considered for the cell fabrication. Initially the glass was washed 'two times' with 'de-ionized water' and 'Isopropyl alcohol' (IPA) to clear the dust and 'impurities from the surface'. One paste of 3 gm of TiO_2 nano powder was made by adding 'drop by drop' Ethanol until the paste attained the state of a watery shampoo. The 'conductive side' of the glass was checked and carefully the ITO coated conductive glass was taped from the edge of two end and the 'conductive side' was kept 'facing up'. The taping was done as 0.4 cm was taped from edges and 0.8 cm was taped from other edge. Using spin coater the 'film of TiO_2' was developed on the ITO glass. The TiO_2 layer was initially left to dry and settle on its own for '10 minutes' and then was mounted on a 'hot plate' for '20 minutes' at '350 (+) degree Celsius'. These steps resulted in a properly deposited uniform 'layer of TiO_2' on the 'conductive side' of the ITO glass is exhibited in Fig.5.6.

These spin coated TiO_2 glasses were immersed in different three colours of dye which are already prepared in the lab as 'red', 'Prussian blue' and 'Chlorophyll green' for different time span. The 'red dye' and the 'Prussian blue dyes' are inorganic dyes, where as the 'green dye' is organic dye.

TiO2 nano-powder

Deposited TiO2 film on ITO glass

TiO_2 coated ITO glass mounted on a furnace

Fig.5.6 Coating of TiO_2 thin film on ITO doped conductive Glass Substrate.

(A). Solar Cell-1: The immersion time of 'TiO$_2$ coated' 'conductive glass' in 'red dye' was '30 minutes' and after then the 'TiO$_2$ coated glass' was taken out carefully. It was left to 'soak for 10 minutes' and mounted on a 'hot plate' for '5 minutes' to dry the glass slide properly. 'Two drops' of the 'electrolyte' were enumerated to the TiO$_2$ and dye coated first slide and immediately the 'second slide' with 'carbon coating' was placed over it, which shown in Fig.5.7(a).

(a). 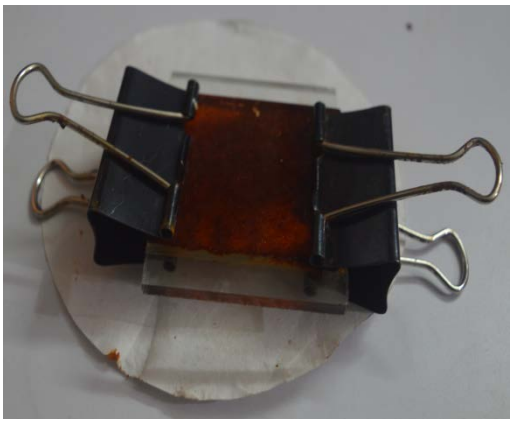

(b). 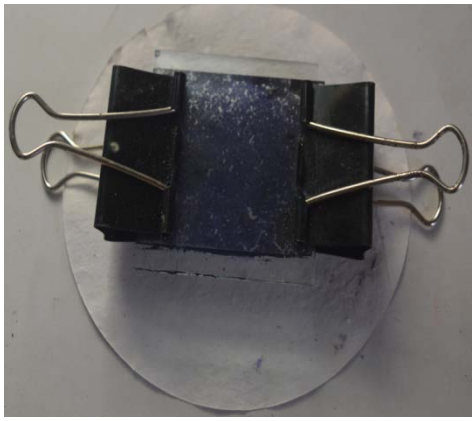

(c). 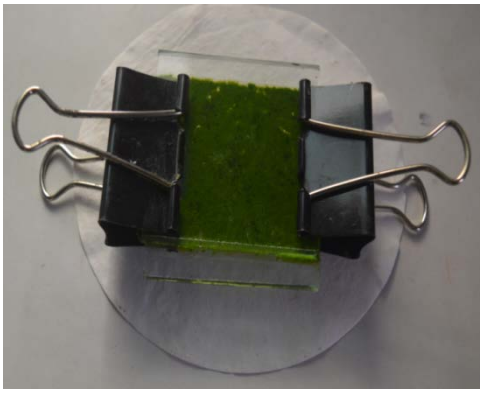 (d) 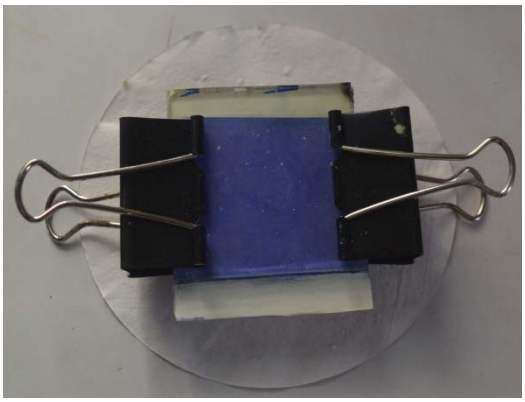

Fig. 5.7 Fabrication of Dyesensitized solar cell with (a). Red Colloidal dye (b). Prussian Blue dye (c). Green dye from Chlorophyll (d) Blue dye extracted from Clitoriaternatea

(B). Solar Cell-2: The second sample of TiO_2 coated glass was immersed in the blue dye for '45 minutes' and then taken out carefully. It was left to 'soak for 10 minutes' and mounted on a 'hot plate' for '5 minutes' to dry the glass slide properly.

A second ITO coated glass was again taped to a plate such that three edges, portions of width 0.4cm and one from one edge a 'portion of 0.8 cm' were covered. Again, same as the previous cell, 'two drops' of the 'electrolyte' were applied to the TiO_2 and dye coated first slide and immediately the 'second slide' with 'carbon coating' was placed over it. The binding clips were used to the sides and the sides with 0.8 cm of exposed glass surface were left open to attach the electrodes for electrical measurement purposes as exhibited in Fig.5.7(b).

(C). Solar Cell-3: The third sample of TiO_2 coated glass was immersed in the green dye of Chlorophyll for '45 minutes' and then taken out carefully. Similarly it was left to 'soak for 10 minutes' and mounted on a 'hot plate' for '5 minutes' to dry the glass slide properly.

The electrolyte was poured carefully on the chlorophyll 'TiO_2 coated slide' and the 'carbon coated slide' was immediately 'placed on top' in such a way that 0.8 cm remained exposed on

'either side' to attach the clips for electrical characterization. The binding clips are used in the other sides of the glass substrates as shown in Fig.5.7(c).

In similar way we have fabricated another two 'Dyesensitized solar cells' with Red color dye' extracted from Hibiscus and 'Blue dye' extracted from Clitoriaternatea as depicted in Fig.5.7(d).

5.6 RESULTS AND DISCUSSIONS

I. SURFACE MORPHOLOGY

The spin coated 'TiO_2 film' on the ITO doped Glass substrate has been examined through FE-SEM result in Fig.5.8 (a). The Morphology of this film is revealed that the TiO_2 grain structures are stay welded and very much suitable for application of dyes. Average nano-particles size of 'TiO_2 thin film' are estimated to be about 47-63nm. It is much cleared that 'TiO_2 nano-particles' were successfully and 'uniformly deposited' onto the 'ITO glass substrates' and their concentration and size depended on the 'thickness' of the deposited 'TiO_2 thin films'. The different colors of dyes are applied on these films. Fig 5.8(b) explained the XRD peaks of 'TiO_2 thin film' layer, deposited on ITO coated glasses and sintered at above 350^0C for 30 minute. In this peaks is obtained at $2\theta=25.2^0$, 37.10, 38^0, 38.40, 47.80, 54.90 and 55.1^0. Both 'anatase and rutile' phase is observed when annealing at above 350^0C. No anatase phase peak is observed when 'annealing temperature' is below 350^0C. All the peak of 'TiO_2 thin film' is clearly indicates that small size of nano particles are presents in samples.

(a) 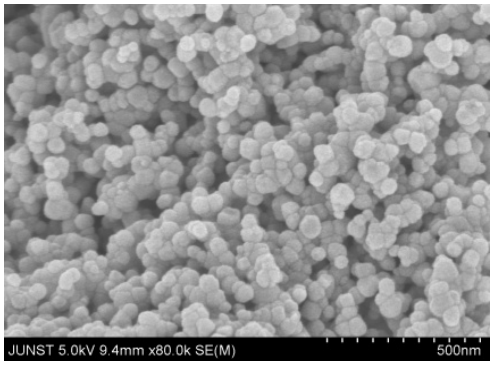

(b). 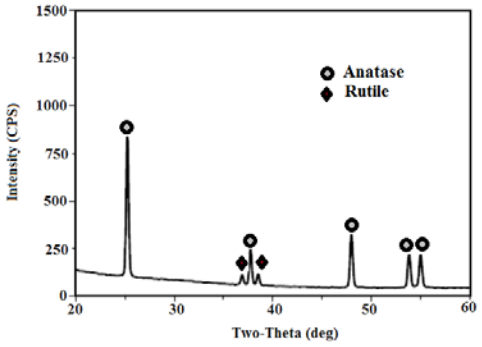

Fig. 5.8. (a). FE-SEM of TiO_2 coated thin film & (b). XRD patterns of TiO_2 nano-particles

The 'Dyesensitized solar cells' are fabricated with different dye like inorganic Red Colloid dye and Prussian blue dye, and green dye made of Chlorophyll, which is organic. It is viewed from the previous authors that for the DSSC solar cells made of Red Turnip extracted red dye and Wild Sicilian extracted purple dye, the 'short circuit current density' (J_{sc}), 'open circuit voltage' (V_{oc}) and 'Fill Factor' of these cells are 9.5mA and 8.2mA, 430mV and 380mV, 37% and 38% respectively [11].

In our work, the 'Dyesensitized solar cells' with red colloid dye displayed a 'short circuit current density' (J_{sc}) of 7.5mA/cm^2, an 'open circuit voltage' (V_{oc}) of 570mV and 'Fill factor' of 40.65% whereas the another two solar cells fabricated with 'Prussian blue dye' and 'Green dye' made of Chlorophyll have shown the 'Short circuit current density' (J_{sc}) 13.5mA and 6.5mA, 'open circuit voltage' (V_{oc}) 730mV and 473mV and 'Fill Factor' 69.55% and 25.83% respectively.

With the comparison of 'electrical parameters' like 'Short Circuit current' (I_{sc}), 'Open circuit voltage' (V_{oc}) and 'Fill Factors' of these 'fabricated solar cells' and the previous 'solar cell', it is revealed that the Solar Cell-2 of our work, using the 'Prussian blue dye' has exerted the maximum 'Fill Factor' of 69.55% in 'comparison to others'. In Fig.5.9 (a), (b), (c) & (d) are exhibited the output 'I-V curve' of these 'Dyesensitized Solar Cells'.

In the Table-1, the different 'electrical parameters' of newly 'fabricated solar cells' of our works and the previously 'fabricated solar cells' done by the other authors are shown. From the 'comparison of the solar cells' with the previously published authors' 'solar cell' with 'Prussian blue dye' [4] the 'short circuit current density' (J_{sc}) 1.7 mA/cm^2, 'open circuit voltage' (V_{oc}) 0.63V and 'FF' is 69% where as in our work with same dye we observed the 'short circuit current density' (J_{sc}) 13.5 mA/cm^2, 'open circuit voltage' (V_{oc}) 0.73V and 'FF' is 69.5%. The 'fabricated solar cells' in our work used 'Carbon coated' counter 'electrode of ITO glasses', which is increased the 'conductivity'. The 'Short Circuit Current density' (J_{sc}) is significantly high from previous author's published 'solar cells', which is the novelty of this work.

The current voltage characteristics of these 'fabricated cells' have been 'measured at AM 1.5G' and irradiance of '1000w/m^2'. The 'short circuit current' and 'open circuit voltage' have been measured with the digital multimter. The maximum 'voltage and current' is also measured connecting '1kilo ohm' series resistance along with the cell. The 'I-V curves' are plotted in 'Matlab' with the measured value mentioned in the table-5.1.

Table5.1. Electrical Parameters of our fabricated solar cells and previous authors' solar cells

Solar Cells with Different Dyes	Short Circuit Current density (J_{sc}) mA/cm^2	Open Circuit Voltage (V_{oc}) in Volt	Fill Factors
Red Colloid Dye [17]	7.5	0.57	0.41
Red color dye extracted from Hibiscus	0.970	0.370	0.18
Red Turnip [9]	0.49	0.43	0.51
Prussian Blue Dye [17]	13.5	0.73	0.695

Blue dye extracted from Clitoriaternatea	3.910	0.721	74.21
Purple colour dye of Wild Sicilian [10]	9.50	0.43	0.37
Green (Chlorophyll) Dye [17]	6.5	0.47	0.26
Green Dye from Spinach [12]	0.35	0.44	0.49

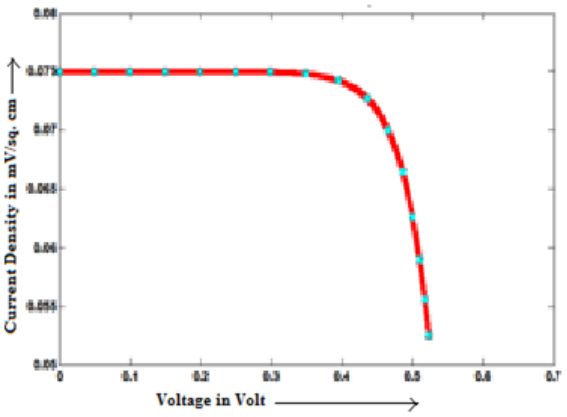

Fig.5.9(a). I-V curve of DSSC with Red Dye

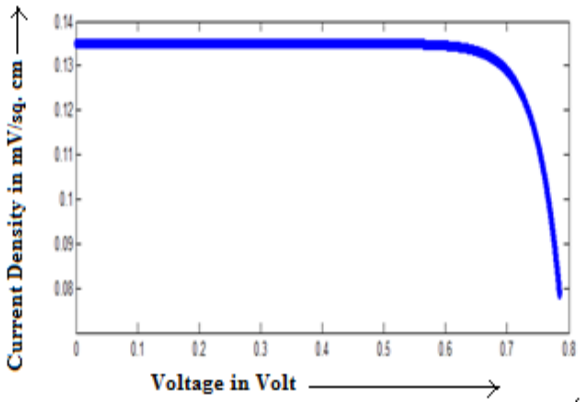

Fig.5.9(b). I-V curve of DSSC with Prussian Blue

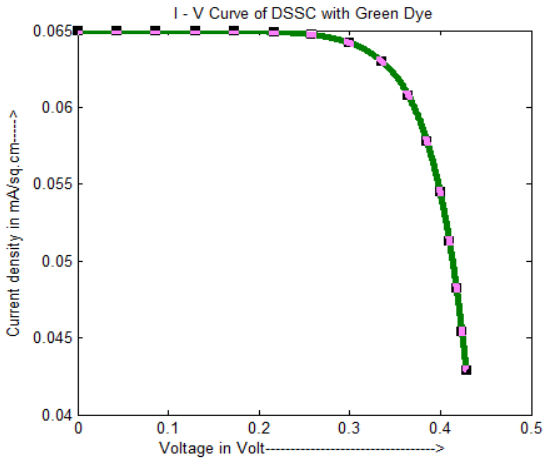

Fig. 5.9(c). I-V curve of DSSC with Green Dye

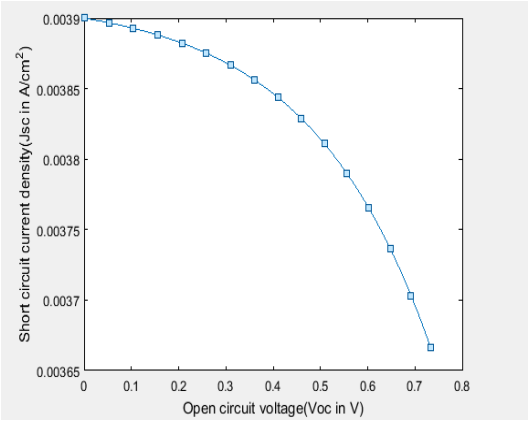

Fig. 5.9(d) I-V characteristics of dye extracted from Clitoriaternatea (blue dye)

5.7 REFERENCES

[1] Brian O'Regan & Michael Grätzel, "A low-cost, high-efficiency solar cell based on dye-sensitized colloidal TiO2 films", *Nature* 353, 737-740 (24 October 1991) doi:10.1038/353737a0;

[2] Bayron Cerda, R. Sivakumar, M. Paulraj "Natural dyes as sensitizers to increase the efficiency in sensitized solar cells", doi:10.1088/1742-6596/720/1/012030.

[3] Khomdram Jolson Singh, Munan Kr.Thakur, N.Sanjeev, L.Aneka, Basob Roy and **Subir Kumar Sarkar**, " Numerical Design and Analysis of Graphene based a-Si/c-Si HIT Solar Cells", International Conference on Advances in Nanotechnology (ICAN) 2017, Don Bosco University,Assam, 9-13 January 2017.

[4] Nobuya Sakait Et.al., "Efficiency Enhancement of ZnO-Based Dye-Sensitized Solar Cells by Low-Temperature TiCl4 Treatment and Dye Optimization", *J. Phys. Chem.*C, 2013, 117 (21), pp 10949–10956 DOI: 10.1021/jp401106u,

[5] P.Naresh, Kumar, K.Sakthivel,"Preparation and Characterization of Low Cost Prussian Blue Sensitized Solar Cell, *Journal of Ovonic Research* Vol. 11, No. 4, July - August 2015, p. 169 – 173

[6] In Chung, Byunghong Lee, Jiaqing He, Robert P. H. Chang& Mercouri G. Kanatzidis, "All-solid-state dye-sensitized solar cells with high efficiency" , *Nature* 485,486–489,(24 May 2012)doi:10.1038/nature11067

[7] Hubert Hug , Michael Bader, Peter Mair, Thilo Glatzel, "Biophotovoltaics: Natural pigments in dye-sensitized solar cells", *J. Applied Energy* 115 (2014) 216–225, http://dx.doi.org/10.1016/j.apenergy.2013.10.055

[8] Seung I. Cha, Yuhyun Kim, Kyu Hyeon Hwang, Yun-Ji Shin, Seon Hee Seo and Dong Yoon Lee, "Dye-sensitized solar cells on glass paper: TCO-free highly bendable dye-sensitized solar cells inspired by the traditional Korean door structure *Energy Environ. Sci.*, 2012, 5, 6071-607 DOI: 10.1039/C2EE03096A

[9] P.Naresh Kumar, K.Sakthivel, Preparation and Characterization of low cost Prussian blue sensitized solar cell, Journal of Ovonic Research, Vol. 11, No. 4, July - August 2015, p. 169 – 173

[10] D D Pratiwi , F Nurosyid , A Supriyanto and R Suryana, Efficiency enhancement of dye-sensitized solar cells (DSSC) by addition of synthetic dye into natural dye (anthocyanin), IOP Conf. Series: Materials Science and Engineering 176 (2017) 012012 doi:10.1088/1757-899X/176/1/012012.

[11] Umer Mehmood, Saleem-ur Rahman,1 Khalil Harrabi, Ibnelwaleed A. Hussein, and B. V. S. Reddy, Recent Advances in Dye Sensitized Solar Cells, Advances in Materials Science and Engineering, Volume 2014, Article ID 974782, 12 pages, DOI: http://dx.doi.org/10.1155/2014/974782.

[12] Iwona A. Rutkowska & Adam Andrearczyk & Sylwia Zoladek & Monika Goral & Kazimierz Darowicki & Pawel J. Kulesza, Electrochemical characterization of Prussian blue type nickel hexacyanoferrate redox mediator for potential application as charge relay in dye-sensitized solar cells, J Solid State Electrochem (2011) 15:2545–2552, DOI 10.1007/s10008-011-1509-2

[13] R. Syafinar Et. al., Chlorophyll Pigments as Nature Based Dye for Dye-Sensitized Solar Cell (DSSC), ScienceDirect Energy Procedia 79 (2015) 896 –902, doi:10.1016/j.egypro.2015.11.584.

[14] Khomdram Jolson Singh, Ch. Akendra Singh, Th. Jayenta Singh, Dhanu Chettri, and **Subir Kumar Sarkar** , " ZnO based homojunction p-i-n solar cell to self-power UV detector

"IEEE International Conference on Inventive Communication and Computational Technologies (ICICCT 2017), Coimbatore, India ,10-11, March 2017

[15] M.S. Su'ait, M.Y.A. Rahman, A. Ahmad, "Review on polymer electrolyte in dye-sensitized solar cells (DSSCs)", Solar Energy 115 (2015) 452–470, http://dx.doi.org/10.1016/j.solener.2015.02.043

[16] Hemant Kumar Mulmudi, Sudip Kumar Batabyal, Manohar Rao,Rajiv Ramanujam Prabhakar, Nripan Mathews, Yeng Ming Lam and Subodh Gautam Mhaisalkar, "Solution processed transition metal sulfides: application as counter electrodes in dye sensitized solar cells (DSCs)", Phys. Chem. Chem. Phys., 2011, **13**, 19307–19309, DOI: 10.1039/c1cp22817j

[17] Tapas Chakrabarti and Subir Kumar Sarkar, "Analytically Performance Study of Newly Modelled HIT solar cell with different materials", International Journal of Latest Technology in Engineering, Management & Applied Science (IJLTEMAS,) Volume VII, Issue IV, April 2018, ISSN 2278-2540.

CHAPTER 6

MODELING, FABRICATION AND CHARACTERIZATION OF PEROVSKITE SOLAR CELLS

6.1. INTRODUCTION

New solid state material, Perovskite used in 'solar cells' are called 'Perovskite solar cell', which are Organic-inorganic-metal tri halide materials. The 'Chemical formula' of compound material of Perovskite is ABX3 and the crystal structures of these materials are similar to 'calcium titanium oxide' (CaTiO3) [1].

In recent exploration of 'solar cells' the 'Perovskite solar cells' are exhibited a remarkable breakthrough in terms of 'efficiency'. These types of 'solar cells' are passed the 'efficiency level' of more than 20% in last few years. A 'Perovskite solar cell' structural formation is a 'Perovskite material layer' in a center and two 'layer' as a 'hole transport layer' (HTL) and 'electron transport layers' are in two side. All the materials layers are build up on TCO glass substrate [2-3].

The ‘active region’ that is the ‘Perovskite layer’ of the ‘Perovskite solar cells’, receive the ‘solar irradiation’ and generates the ‘electron and hole pairs’. The generated ‘electrons and holes’ in the ‘Perovskite layer’ is required to collect in the outer circuit separating the ‘charge-carriers’ from the ‘Perovskite layer’ to the ‘electrodes’. To get a ‘net current’ from the ‘Perovskite solar cell’ the two different ‘charge-carrier’ transportation ‘layers’ are predominant. Hence, the ‘HTL’ and ‘ETL’ are selected with suitable ‘effective materials’ to collect and transport the ‘holes’ and ‘electrons’ to the ‘electrodes’ ‘efficiently’. These two layers not only ‘transport’ the ‘charge-carriers’ but also offer a ‘resistance’ to opposite ‘charge-carriers’. Therefore the ‘probability’ of ‘recombination’ at those ‘layers’ get reduced. As a result the ‘Perovskite solar cell’ can produce more ‘current’ and more ‘efficiency’ [4].

6.2. LITERATURE SURVEY OF PEROVSKITE SOLAR CELL

In the year of 2009, the first ‘Perovskite solar cell’, was developed and published by ‘Miyasaka et al.’ based on ‘Dyesensitized architecture’. The ‘Perovskite layer’ was developed on ‘Titanium dioxide layer’ as electron-collector (ETL) and the ‘power conversion efficiency’ was only 3.8% [5].

This ‘Perovskite solar cell’ was stable only for a ‘few minutes’ due to use of ‘liquid electrolyte’. In 2011 ‘Park et al.’ reported 6.5% PCE in similar architecture of cell [6]. The first stable ‘Perovskite solar cell’ was published by Henry Snaith and Mike Lee of the University of Oxford in 2012 using ‘solid state’ ‘hole transport layer’ [4][7]. They achieved almost 10% ‘efficiency’ using the ‘sensitized TiO2 architecture’ with the ‘solid-state’ ‘hole transport’ material. More than 10% of ‘efficiency’ was achieved using an inert scaffold instead of the ‘hole transport materials’ [4]. In 2014 with some new ‘deposition techniques’ the ‘efficiency level’ was attained in a higher range.

Using the ‘thin film architecture’ and ‘reverse scan method’ the 19.3% ‘efficiency’ was ‘achieved’ by ‘Yang Yang’ [8-9]. Some researchers of (KRICT) ‘Korea University of Science and Technology’, developed a ‘solar cell’ device in November 2014, and achieved 21.1% of ‘record efficiency’ but it was ‘non-stabilized’ [10].

In March 2016, researchers from KRICT and (UNIST) ‘Ulsan National Institute of Science and Technology’ achieved 22.1% of ‘efficiency’ using ‘single-junction’ ‘Perovskite solar cell’ which is the highest ‘certified record’ for ‘Perovskite solar cell’ [10]. ‘Methyl ammonium-lead iodide’ ($CH_3NH_3PbI_3$) is the ‘most popular’ ‘Perovskite material’ in ‘solar cells’ and showed impressive results of ‘efficiency’. But as the ‘lead’ is hazardous material to ‘human health’ due to its ‘toxicity’. Hence the alternative ‘Perovskite materials’ exploration has been started and found ‘Methyl ammonium tin iodide’ ($CH_3NH_3SnI_3$) is an alternative ‘Perovskite material’ suitable to ‘Perovskite solar cells’ and showed significant good results [11-13].

6.3. THEORY OF PEROVSKITE SOLAR CELL

‘Perovskite solar cell’ is based on ‘Perovskite materials’ which are ‘Organic-inorganic-metal tri halide materials’, having ‘chemical formula’ ABX3 and having specific ‘crystal structure’ as ‘calcium titanium oxide’ ($CaTiO_3$). In last few years ‘Perovskite solar cells’ have shown ‘significant improvement’ in terms of ‘efficiency’ more than 20% ‘efficiency level’. A ‘Perovskite solar cell’ is consists of a ‘Perovskite material’ which remain in center and in two side an ‘electron transport layer’ (ETL) and a ‘hole transport layer’ (HTL), on the top of TCO.

6.3.1 PEROVSKITE MATERIAL

The ‘mineral’ ‘Perovskite’ ($CaTiO_3$) is named from the name of ‘Russian mineralogist’, ‘Count Lev Aleksevich von Perovski’.

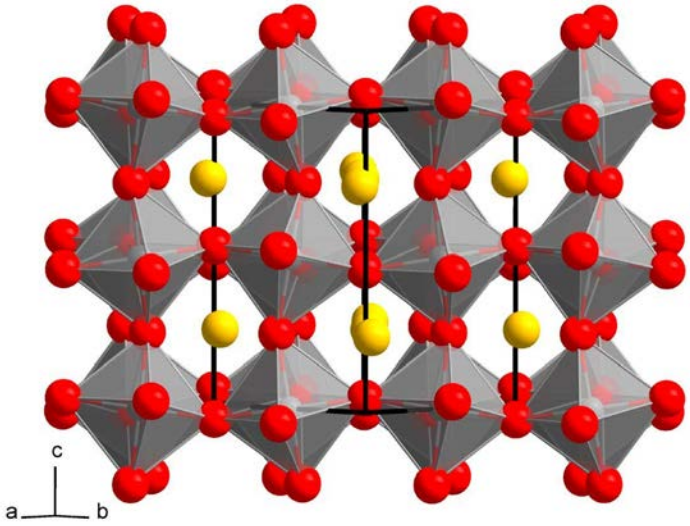

Fig6.1: Perovskite material structure [1]

The basic ‘building block’ of the ‘organic-inorganic Perovskite’ are the ABX_3 structure, where A is commonly a ‘large cation’ coordinated to ‘12 X^-anions’. The structure consists of a ‘network’ of ‘corner-sharing’ BX_6 octahedral, where the ‘B atom’ is a ‘metal cation’ (tin or lead) and X is the ‘hybrid anion’ (bromine or iodine). The ‘hinged octahedral’ allow for ‘wide accommodation’ of the B-X-B ‘bond angle’, and several ‘sets of cooperative rotations’, known as ‘tilt transitions’, which shows, different structures at different temperatures. Experimentally, the ‘organic-inorganic super lattices’ are easily customized by modifying the ‘combination’ of the ‘organic and inorganic’ components in the starting solution from which the hybrids are crystallized. Hence, changing the parameters of the ‘material properties’ and tuning the same the ‘different order of structure’ will appear at ‘different temperature’. The $CH_3NH_3BX_3$ compound at high temperature, it will be ‘pseudo cubic’, ‘tetragonal’ at ‘medium temperature’, and ‘orthorhombic’ at ‘low temperature’, respectively [14]. ‘Perovskite materials’ are used in ‘solar cells’ due to its ‘high absorption coefficient’.

6.3.2 ZnTe as 'HOLE TRANSPORT MATERIAL'

The increase in 'efficiency' of different types of 'Perovskite solar cells', the 'hole transport layers' (HTL) were mainly limited to 'organic compounds' such as "spiro-MeOTAD" and other conducting 'polymers'. But these types of 'organic hole-transport materials' are usually 'quite expensive' compared to 'Perovskite materials' and 'n-type semiconductor materials' employed in the 'Perovskite solar cells', due to intricate 'synthetic procedure' and 'high-purity' requirement [1]. In present times, the focus of the researchers are on an 'effective inorganic material' as 'hole transport layer' to overcome this challenge. In this 'research work', 'p-doped Zinc Telluride' (ZnTe), an inorganic group II-VI material is propound as the 'hole transport layer' for 'lead free' ($CH_3NH_3SnI_3$) 'Methyl Ammonium-tin iodide' based 'Perovskite solar cells'.

The ZnTe is a 'wide band gap' (~2.6 eV) II-VI material, which 'band structure' satisfy the 'necessary condition' to be employed as 'hole transport layer'. The most predominant reason behind the investigation of ZnTe as 'hole transport layer' is its very 'high hole mobility'. The 'hole mobility' of the 'p-doped ZnTe' is 80-100cm^2/Vs which is almost 100 times more than that of 'CuSCN' and 1000 times more than that of 'spiro-MeOTAD' [5][9].

6.3.3 ZnO as 'ELECTRON TRANSPORT LAYER'

'Electron' and 'hole pairs' are produced in the 'Perovskite layer' of the 'Perovskite solar cells'. After that the 'electrons' and 'holes' need to be collected at the 'electrodes' to get a 'net current' at the 'outer circuit'.

For a material to be maneuvered as 'electron transport layer' (ETL) in 'Perovskite solar cells' the materials should satisfy few important properties as postulated below:

(i) 'Conduction band' of the 'ETL material' should be 'less' than the 'HOMO (highest occupied molecular orbital) level' of the 'Perovskite material'

(ii) 'High electron mobility'

(iii) 'Higher band gap'.

The 'electron mobility' of the 'n-doped ZnO' is almost 200cm^2/Vs and the 'band gap is 3.4eV [10]. The 'properties of ZnO' are satisfied to the above three conditions, therefore it is a suitable material for 'ETL'.

6.3.4 ARCHITECTURE AND WORKING PRINCIPLE OF 'PEROVSKITE SOLAR CELLS'

The basic working principle of 'Perovskite material' is very similar to that of 'Dyesensitized solar cells'. The 'Perovskite solar cell' working function is 'generation' of 'electron and hole pair' by absorbing 'light' in 'Perovskite layer' and then 'separation and transportation' of the 'electrons' and 'holes' using two different 'transport layers'. The 'Perovskite material' is 'sandwiched' between 'electron' and 'hole' transport 'layers'. The function of the 'transport layer' is to transport only 'one type' of 'charge carriers' through it and to 'offer a resistance' to the other one. 'Hole transport layer' means that it will allow 'holes' to 'pass through' and block the 'electrons'. Similarly, 'electron transport layer' allows electrons and opposes the holes movement. Due to use of two separate types of 'transport layers', the chances of 'recombination' of 'charge carriers' are also decreased. Figure-2, shows the basic 'schematic structural diagram' of 'Perovskite solar cell'. The 'cell' can also be utilized by inverted configuration. 'Perovskite solar cells' have many 'distinct advantages' over traditional 'silicon solar cells'. The main advantage of 'Perovskite solar cell' is that this type of 'solar cell' can deliver 'high efficiency' and it is 'cost effective' also, compared to traditional 'Silicon solar cells'. The 'fabrication processes of 'Perovskite photovoltaic is 'much cheaper' and 'simpler' than 'silicon solar cell'

production. The ‘wafer processing’ and ‘cell fabrication’ associated with ‘silicon’ require ‘expensive equipment’ and ‘facilities’. In comparison, ‘Perovskite cell fabrication’ can be attained with ‘simpler methods’ like ‘solution spin coating’ and ‘vapor deposition’ methods.

The relation between current density, J_{sc} and mobility is given by the equation,

$$J_{sc} = qG\left(\sqrt{\mu_p} + \sqrt{\mu_n}\right)\left(\sqrt{\frac{KT}{q}}\tau\right) \ldots\ldots\ldots\ldots\ldots\ldots\ldots\ldots\ldots\ldots\ldots\ldots\ldots\ldots\ldots\ldots (6.1)$$

Where q = electron charge,

k = ‘Boltzmann constant’

T = ‘temperature’

μ = ‘electron mobility’ and τ = ‘carrier lifetime’.

From the above equation (6.1) it is found that the higher ‘carrier mobility’ will lead to the increased ‘short circuit current’ of the ‘cell’ and hence will improve the overall ‘performance of the cell’.

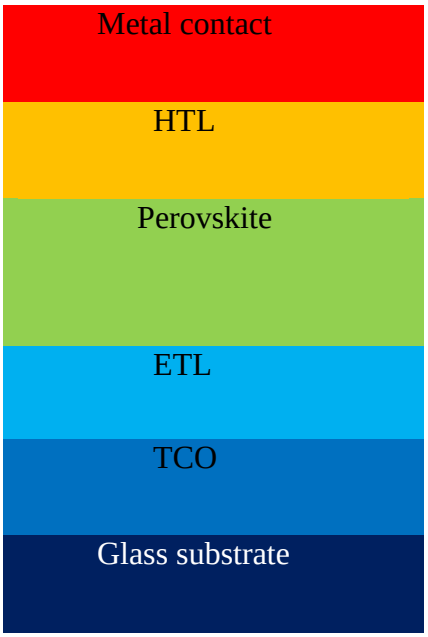

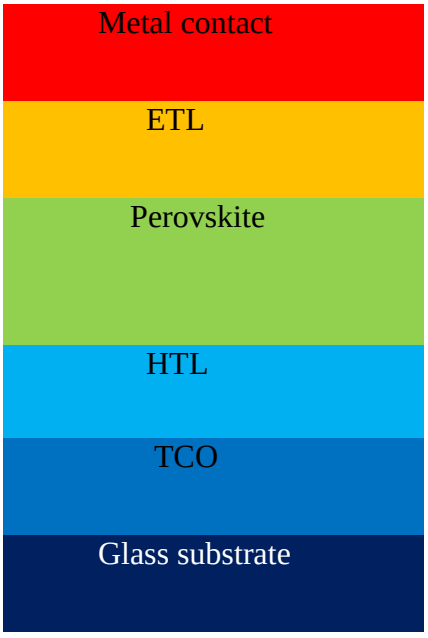

Fig 6.2: (a) Perovskite solar cell structure Fig.6.2.(b) Inverted Perovskite solar cell structure

6.4 MODELING & FABRICATION OF 'PEROVSKITE SOLAR CELLS'

During last few years, the researchers have devoted extensive 'research effort' into 'inorganic/organic' 'solar cells' like 'Dye-sensitized solar cells' (DSSC) due to its 'cost effectiveness' and simple 'fabrication process', over the 'conventional solar cells' made of different materials like 'Silicon', 'Germanium', 'Gallium-Arsenide', 'Gallium Indium Phosphate' etc. The exploration of 'different materials' as 'electron transport layer' of the 'Perovskite solar cells' to improve the performance of the 'solar cells' is going on among the researchers. The popular 'Perovskite material' used in 'solar cell' is 'Methyl Ammonium-lead iodide' ($CH_3NH_3PbI_3$) along with 'top and bottom' layer of 'HTO' and 'ETO'.

In my 'research work', two numbers of 'Perovskite solar cells' have been modeled in software environment and one of them is physically fabricated in Lab. We have applied the ZnO as an 'electron transport layer' (ETL), in one model and in another model, ZnTe is introduced as a 'hole transport layer' substituting the costly compound HTL material 'spiro-MeOTAD'.

6.4.1 PROPOSED MODELED 'PEROVSKITE SOLAR CELL' with ZnO as ETL

In this proposed 'solar cell' a planer 'p-i-n heterojunction architecture' with 'layer configuration' of "metal contact/TCO /ZnO(n) /CH_3NH_3SnI3/*spiro-MeOTAD*(p)/metal contact" as depicted in figure 6.3 is modeled, where 'n-doped ZnO' and 'p-doped Spiro-MeOTAD' 'layers' are used as 'electron transport layer' and 'hole transport layer' respectively. The parameters considered in simulation of this 'Perovskite solar cell' structure are described in table 6.1.

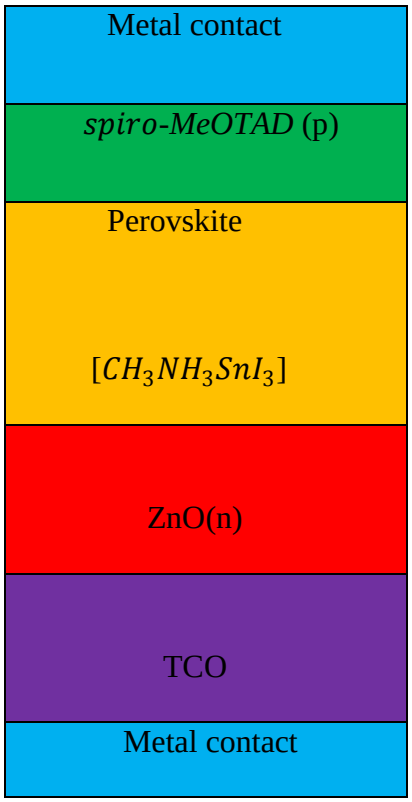

Figure 6.3: Schematic of the proposed cell

Table 6.1: layer parameters used for the simulation [15-16]

Parameters	**Spiro-MeOTAD (HTL)**	**Perov-skite ($CH_3NH_3SnI_3$)**	**ZnO (ETL)**	**TCO**
Band gap	2.25	1.23	3.4	3.5
Dielectric constant	7.3	8.2	8.12	9
Electron affinity	3.73	4.17	4.29	4.4
Electron mobility	300	1.6	200	20
Hole mobility	100	1.6	5	10
Acceptor 'doping concentration' (N_A)	2*10^18	Self doped	0	0
Donor 'doping concentration' (N_D)	0	0	1*10^19	2*10^19
Layer thickness	0.25 um	0.40 um	0.5 um	0.5 um

6.4.2 PROPOSED MODELED 'PEROVSKITE SOLAR CELL STRUCTURE' WITH ZnTe as HTL

In this 'solar cell' a planer 'n-i-p heterojunction' architecture with 'layer configuration' of "metal contact/ TCO/TiO2(n)/CH3NH3SnI3/ZnTe(p)/metal contact" as exhibited in figure 6.4 is modeled, where 'n-doped TiO2' and 'p-doped' ZnTe 'layers' are employed as 'electron transport layer' and 'hole transport layer' respectively. 'Zinc telluride' (ZnTe) is a 'wide band gap' II-VI 'semiconductor material' [13-14][18]. The 'band gap' of ZnTe is 2.23–2.28 eV at 'room temperature', 'high absorption coefficient' (close to$10^5 Cm^{-1}$) and very 'high hole mobility' (80-100cm^2/Vs) 'Zinc telluride' (ZnTe) is best promising 'semiconductor candidates' for the 'hole transport layer' in 'Perovskite solar cell'. Most of the 'wide band gap' 'II-VI materials' are favorable to 'n-type doping' and resist 'p-type doping'. But in the case of ZnTe, 'p-type doping' is much easier compared to 'n-type doping' [20]. This is why a 'p-doped ZnTe' layer of 'acceptor concentration' of $1*10^{19}$ cm^{-3} is used as 'hole transport layer' (HTL) in the proposed structure. 'Effective Conduction band' and 'valance band densities' of ZnTe are $1.176x10^{18}$ Cm^{-3} and $1.166x10^{19}cm^{-3}$ respectively [21]. 'Thermal velocities' of the 'electron' and 'hole' are both set to be equal to 10^7 cm/s. The parameter values of all the layers applied for the Structure simulation are depicted in Table 6.2.

$CH_3NH_3SnX_3$ (where X = Cl, Br, I) is unstable in 'ambient atmosphere' and the 'Sn^{2+} ion' will rapidly oxidize into more stable 'Sn^{4+} ion', which is a 'p-type dopant' within the material in 'self-doping process'. So, instead of intrinsic, the 'Perovskite layer' can be simulated as 'p-doped material' during the simulation due to the present of 'Sn^{4+} impurities' [11][15]. For this proposed structure an 'acceptor doping concentration' of $1*10^{15}$ cm^{-3} is assumed for the 'Perovskite material' during the structure simulation.

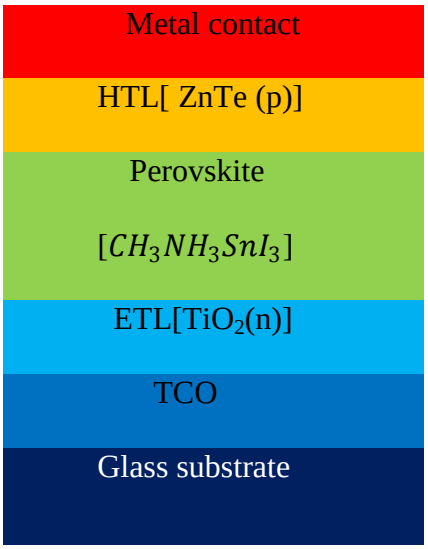

Figure 6.4: Schematic 'structure of the proposed cell'

6.4.3 PHYSICAL FABRICATION OF 'PEROVSKITE SOLAR CELL' with ZnTe:

The FTO coated glass was cleaned with 'Alconox' in an 'ultrasonic bath' for '20 minutes', followed by 'rinsing the glass' with DI water. After that, it was transferred in a 'beaker' containing 'acetone' and 'sonicated with ethanol' for 10 minutes. The glass was 'cleaned' and 'dried' to use as the 'substrate of solar cell'. The 'resistance' of the 'glass substrate' was checked to find the conductive side which is found of 21 Ω. Generally the 'resistances' of 'conductive glass' substrates remain in between 10 Ω to 30 Ω.

Six (6) gram of 'titanium dioxide' powder was measured and 9 ml of 'nitric acid' was poured into the powder and 'crushed the mixture' with a crusher until the mixture was consistent. Then, the suspension was kept in a dark container for 10 min to attain the 'equilibrium state'. In order to break the masses into 'separate particles', the 'powder' was ground in a 'ceramic mortar' with a 1 ml of 'water' and 0.1 ml of 'acetic acid' to prevent 'aggregation of the particles'. After the dust had been disseminated by the high 'shear forces' in the 'viscous paste', it was mitigated by

'slow addition' of water up-to 4 ml under constant grinding. Finally, 'few drops' of 'detergent liquid' were added to smooth the spreading of the 'colloid' on the 'substrate'.

To get the active area on the 'conductive side' of FTO glasses, the TiO_2 paste was 'spin coated' on the 'conductive side' of the glass surface, the 'spinning' rate was kept '3000 rpm' for '30 sec'. The resultant sample was 'annealed' at 400 °C for 30 min, which is presented in Fig 6.5(a).

For deposition of 'lead-free Perovskite' (active material), "SnI_2" and "$CH_5N.HI$" were separately deposited in two different phase. Initially 0.5 gm of SnI_2 was loaded in cleaned 'tungsten boat' and then it was heated indirectly by passing current through the 'electrode' at 'vacuum pressure' of 10-5 Torr, as a result, thin 'layer of SnI_2' (yellow colored) was deposited on the 'surface of TiO_2' which are utilized as 'electron collector', that was kept on 'substrate holder' (normal to material containing tungsten boat) by 'thermal evaporation technique' as presented in Fig 6.5(b).

After deposition of SnI_2 on the 'surface of TiO_2', the sample was transferred in 'nitrogen clove' to prevent it from 'decomposition' in air. Afterward, 0.5 g of $CH_3NH_3SnI_3$ was mixed in 1.5 ml of 2-propanol, the mixture was vigorously stirred for 15 min, the 'resultant mixture' was 'spin coated' on the 'surface of TiO_2', with a spin rate of '3000 rpm for 30 sec'.

Next step was 'deposition' of 'hole collector layer', ZnTe which was deposited on the sample prepared above.

'Zinc' (Zn) and 'Telluride' (Te) metals of 'high purity' were weighed by an 'electronic balance' in the 'stoichiometric ratio'. The material was 'mixed and ground' using agate 'mortar and pestle' and then the 'resultant mixture' was kept in cleaned 'tungsten boat'. The material loaded 'tungsten boat', was heated indirectly by passing current through the 'electrodes' at a vacuum pressure of 10-5 Torr, as a result of heating ZnTe it evaporates and settles on the surface of substrate kept on the 'substrate holder' as shown in Fig 6.5(c). For ZnTe deposition on the

'surface of active Perovskite' ($CH_3NH_3SnI_3$), which acts as a 'hole collector layer' displayed in fig.6.5(d). Through the different 'steps of fabrication' the 'Lead-free' solution-processed 'solid-state' 'photovoltaic devices' based on 'methyl ammonium tin iodide' ($CH_3NH_3SnI_3$) 'Perovskite semiconductor' as the 'light harvester' is used as 'active layer'. Here TiO_2 is used as common 'Electron Transport Layer'. 'Hole transport Layer' 'Zinc telluride' (ZnTe) is used in the newly fabricated 'Lead (Pb) free Perovskite solar cell' is exhibited in fig.6.5(e).

Fig. 6.5(a) Spin coating of TiO2

Fig.6.5(b)Deposited SnI_2 by Thermal Evaporation

Fig. 6.5(c) ZnTe by thermal deposition

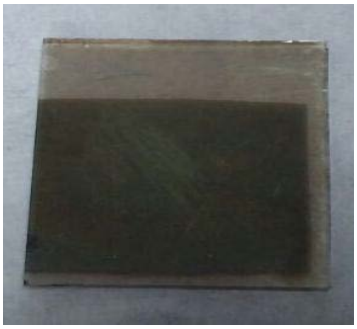

Fig. 6.5(d) ZnTe layer By thermal deposition

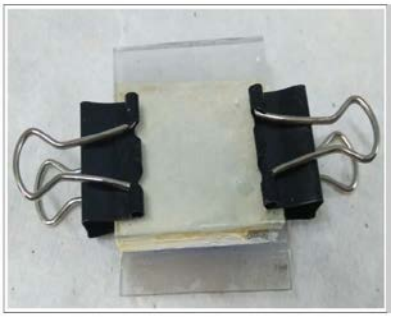

Fig. 6.5(e) Fabricated complete Perovskite Solar Cell

6.5 RESULTS & DISCUSSIONS

The proposed two structures of 'Perovskite solar cells' as exhibited in figure 6.3 and 6.4 are simulated in 'SCAPS simulating' software tool.

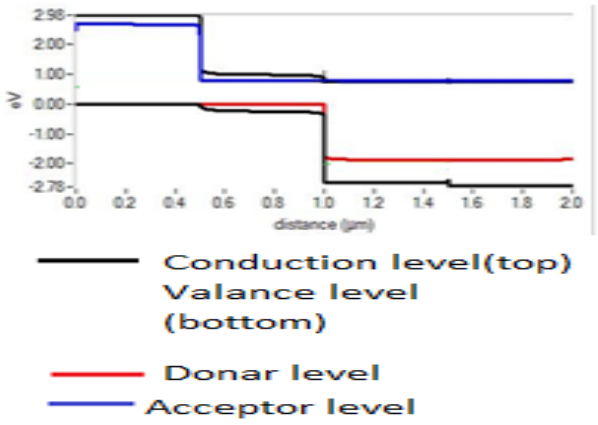

Figure 6.6: Band diagram of the proposed cell

The 'band diagram' of the proposed structure is derived in figure 6.6. For any 'Perovskite solar cell' the 'valance level' of the 'electron transport layer' which is marked by 'blue line' need to be 'lower' than the 'HOMO level' that is drawn on the top as 'black line' of the 'Perovskite material' and the 'conduction level' of the 'hole transport layer' marked as 'red line' need to be 'higher' than the 'LUMO', indicated by the bottom 'black line'. Our proposed structures (Fig.6.3) have satisfied the necessary condition, which is depicted in the above figures 6.6.

(i) 1st Modeled 'Perovskite solar cell'

The 'doping level' of the ZnO is varied to optimize the 'performance' of the proposed 'solar cell'. Figure 6.7 has stated the relation between the 'doping level' of ZnO and the 'efficiency' of the 'cell'.

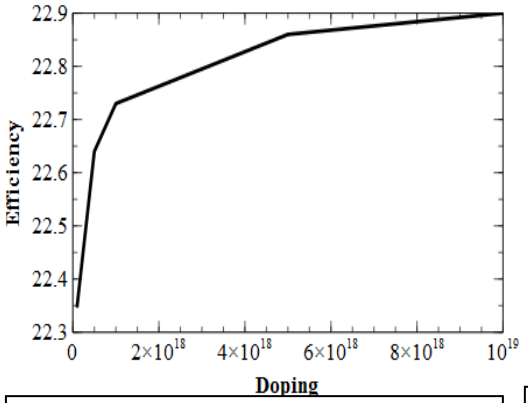

Figure 6.7: Doping of ZnO Vs Efficiency

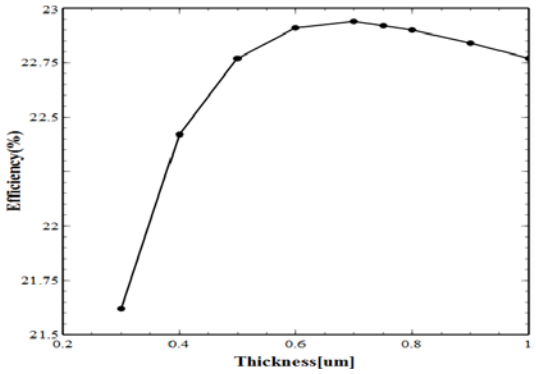

Figure 6.8: Efficiency Vs Thickness of the Perovskite layer

From the above curve, figure 6.7, it is observed that the 'efficiency' of the 'cell' is increased with the increment of doping level and accordingly the 'donor doping-concentration' of ZnO is optimized.

The 'thickness' of the 'Perovskite layer' is also varied to optimize the 'solar cell performance' and the 'result shows' that with the increase of 'Perovskite layer thickness', the 'solar cell' 'performance' is improved up to a certain value and then it is decreased which is clearly viewed in the figure 6.8. This 'observation' can be verified from the fact that, with increasing 'thickness' of the 'Perovskite layer', the 'carrier' 'generation rate' will be increased and hence the 'solar cell performance' will be improved. But the Perovskite layer thickness must be optimized in accordance with the 'carrier lifetime' to minimize the 'recombination rate' and maximize the number of 'charge-carriers' transferred to the 'transport layers'. The figure 6.9 exhibited the relation between the 'Perovskite layer' 'thickness' and 'solar cell' 'efficiency' for the proposed structure.

After optimization of doping level of the ZnO layer and the 'Perovskite layer' of the 'cell' is simulated under the 1.5G 'solar spectrum illumination' and found 22.94% 'efficiency', 34.23 mA/cm^2 'current density', 0.87 V 'open circuit voltage' and 74.77% fill factor. The simulated

output ‘J-V curve’ of our 1st modeled ‘Perovskite solar cell’ using ZnO as ETL has been drawn in figure 6.10.

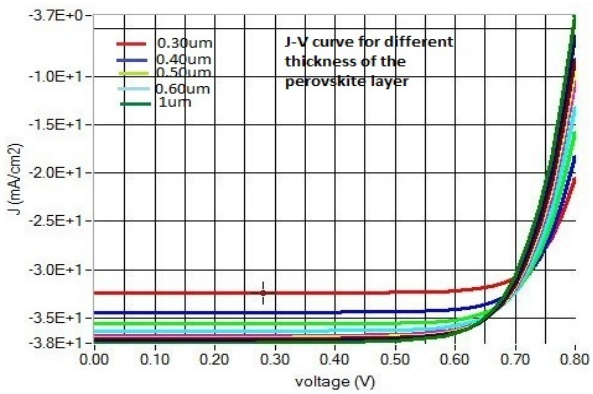

Figure 6.9: J-V curve for different thickness variation of Perovskite layer for the proposed cell

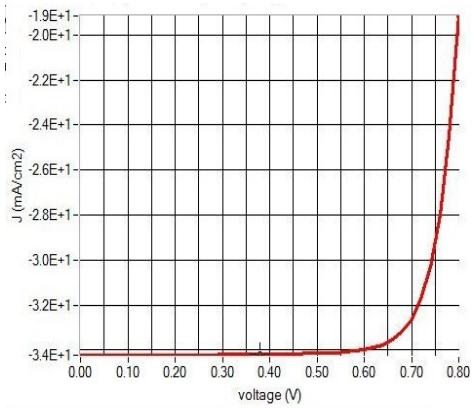

Figure 6.10: J-V curve of the proposed cell

(ii) 2nd Modeled ‘Perovskite solar cell’ with ZnTe as HTL

The ‘Perovskite solar cell’ with ZnTe as ‘hole transport layer’ is modeled with the similar ‘optimization technique’ applied in 1st modeled ‘solar cell’. Another important parameter ‘electron affinity’ is considered in ZnTe ‘layer optimization’ as most ‘critical function’ of HTL is the ‘blocking of electron’ and to allow the ‘hole’. The relation between ‘electron affinity’ of HTL and efficiency of ‘solar cell’ is viewed in figure 6.11.

After parameter optimization (ZnTe) for the proposed structure, 23.54% solar cell efficiency, 76.21% fill factor, 36.88 mA/cm^2 current density and 0.87V open circuit voltage are observed. Figure 6.12 shows the J-V curve for the proposed solar cell after optimizing the different ‘layer thickness’ as described in table 6.2.

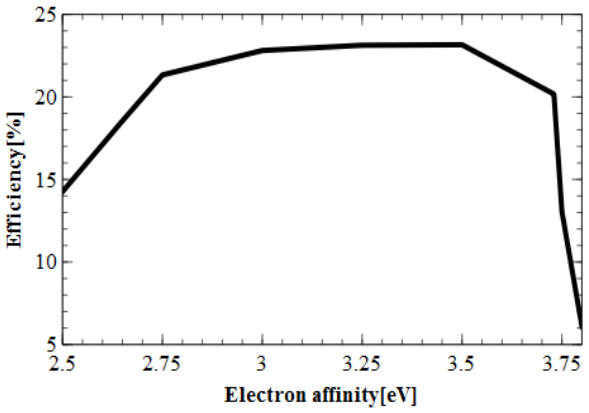

Fig 6.11: Effect of electron affinity of HTL over Efficiency of the cell

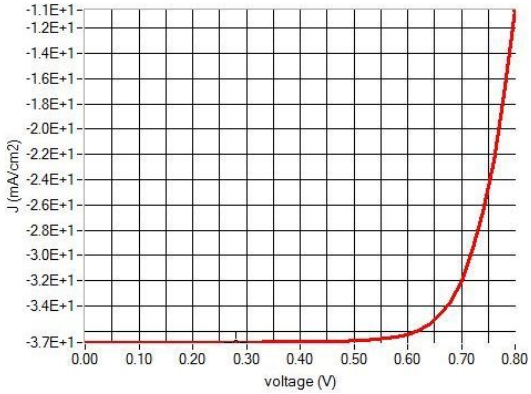

Fig.6.12: J-V curve of the proposed cell with ZnTe as HTL

Table 6.2: Layer parameters used for the simulation of 'solar cell with ZnTe as HTL [15] [21]

Parameters	ZnTe (HTL)	Perovskite ($CH_3NH_3SnI_3$)	TiO_2 (ETL)	TCO(SnO_2 doped)
Band gap	2.25	1.23	3.2	3.5
Dielectric constant	7.3	8.2	9	9
Electron affinity	3.73	4.17	4.26	4.4
Electron mobility	300	1.6	20	20
Hole mobility	80-100	1.6	10	10
Acceptor doping concentration (N_A)	$1*10^{19}$	Self doped	0	0
Donar doping concentration (N_D)	0	0	$1*10^{17}$	$2*10^{19}$
Layer thickness	0.50 um	0.70 um	0.5 um	0.5 um

(iii) Results of Fabricated Solar Perovskite Solar Cell:

The 'lead free' 'Perovskite ($CH_3NH_3SnI_3$) solar cell' with the ZnO (n) as 'electron transport layer' and ZnTe as the 'hole transport layer' is obtained the 'open circuit voltage' of 0.74 V and 'short circuit current' 7.48 mA. The Fill Factor and efficiency of this solar cell are attained 49.06% and 2.717% respectively from the physically fabricated 'PV cell'.

In case of ZnTe(p) as hole transport layer and conventional TiO_2 as the ETL the Perovskite cell gives the open circuit voltage, that is 0.79 V and 'short circuit current' is 11.57 mA, and Fill factor and efficiency are 55.05% and 5.0317% respectively.

The J-V characteristics curve of these two 'Perovskite solar cells' as mentioned above paragraph are presented in figure 6.14(a) and 6.14(b).

Using ZnTe as a 'Hole Transport Layer', the 'efficiency' is achieved 22.94% by 'Simulation software' 'SCAPS', but the 'fabricated cell' with same materials profile the 'efficiency' comes down to 5.031%, as the physical 'fabrication procedure' could not keep the 'layer thickness' as per simulated structure due to some constraints. However the 'fabricated solar cell' with the 'lead free' 'Perovskite' and ZnTe in 'hole transport layer' is significantly promising. The comparison of simulated results of 'lead free' 'Perovskite solar cell' with 'ETL' and 'HTL' non silicon layer of ZnO and ZnTe respectively as well as the fabricated same structures of cells are depicted in Table.6.3.

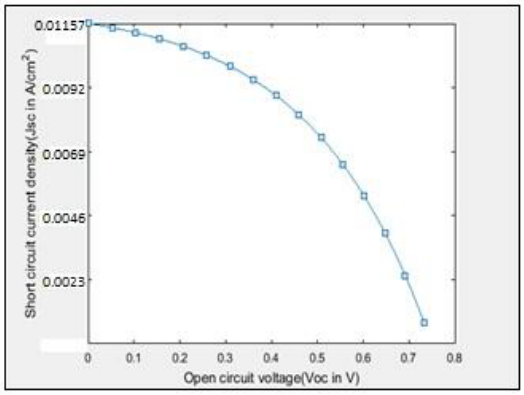

Fig.6.14(a). J-V Characteristics of fabricated Perovskite Solar Cell with ZnTe as HTL

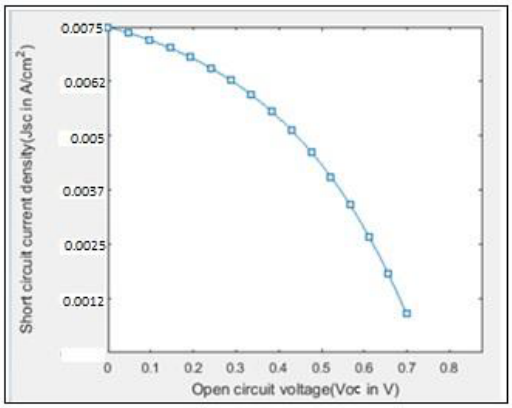

Fig.6.14(b). J-V Characteristics of fabricated Perovskite Solar Cell with ZnO as ETL

Table 6.3. Comparison of simulated and fabricated solar cell

Sl No	Cell structure	Open circuit Voltage (V_{oc}) in volt	Current density J (mA/cm^2)	Fill Factor (%)	Efficiency (%)	Remarks
1	metal contact/TCO /ZnTe(p) /CH_3NH_3SnI3/ TiO_2(p)/metal contact	0.87	36.88	76.21	23.54	Simulated
2	**metal contact/TCO /ZnTe(p) /CH_3NH_3SnI3/ TiO_2(p)/metal contact**	**0.79**	**11.57**	**55.05**	**5.032**	**Fabricated**
3	Metal-contact/TCO/ZnO(n) /CH_3NH_3SnI3 /*spiro-MeOTAD*(p)/ metal contact	0.87	34.23	74.77%	22.94	Simulated
4	**Metal-contact/TCO/ZnTe(p)/**	**0.74**	**7.48**	**49.06**	**2.71**	**Fabricated**

	CH_3NH_3SnI3/ ZnO(n)/metal contact					

The 'crystal structure' of 'methyl ammonium tin iodide' ($CH_3NH_3SnI_3$) modified with ZnTe and TiO2 are exposed in 'XRD patterns' as viewed in figure 6.15(a) in which the patterns of 'Zn', 'Te', 'C', 'I'and 'Sn' samples contain matches orthorhombic. In figure 6.15(b) the patterns 'Ti', 'Oxide', 'C', 'I', 'Sn' samples contain matches 'orthorhombic'. The other peaks are just below due to 'background noise'. So, these survivals of the clear dominant peak of ZnTe, TiO2 modified 'methyl ammonium tin iodide' must be sufficient to justify the deposited layers.

The grown 'nano crystalline' average size is achieved by XRD results. It can be calculated by the 'Scherrer's equation' as follows: $D = \frac{k\lambda}{\beta cos\theta}$

Where k is equal to 0.9 (constant), it denotes x-ray wavelength, θ denotes 'Bragg angle', and β denotes 'full width of the diffraction line' at the half of the 'maximum intensity'. In figure 6.16(a), figure 6.16(b), 6.16(c) and figure 6.16(d) are the FESEM result of film made of ZnTe, ZnO and the layers of 'Perovskite'. The figures 6.16(a) is the FESEM result of ZnTe film and figure 6.16(b) the nano rod of ZnTe which are 10~15 nm dia. In figure 6.16(c) the FESEM of 'film' made of ZnO is shown and figure 6.16(d) it is revealed the three layer of the fabricated solar cell consists of 'Perovskite material', '$CH_3NH_3SnI_2$' on 'TiO2 film' and along with the 'hole transport layer' of 'ZnTe' have been observed.

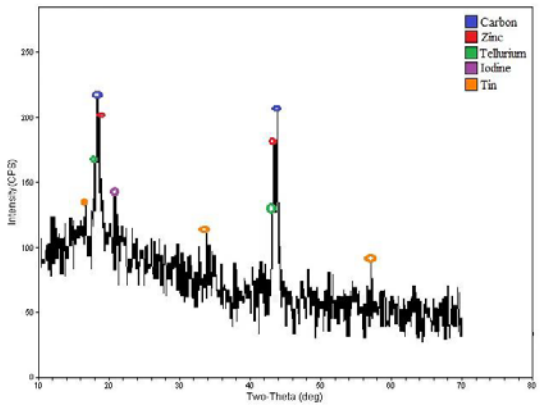

Fig.6.15(a) XRD pattern of $CH_3NH_3SnI_3$ modified with ZnTe

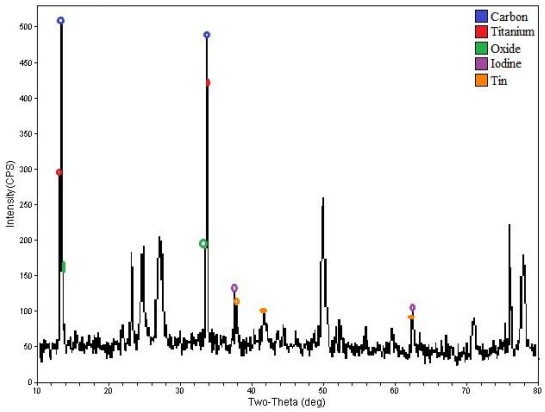

Fig 6.15 (b) XRD patterns of $CH_3NH_3SnI_3$ after modification of TiO_2

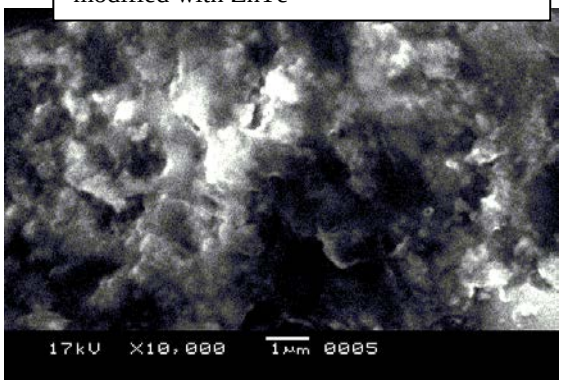

Fig.6.16(a) SEM Result of ZnTe film

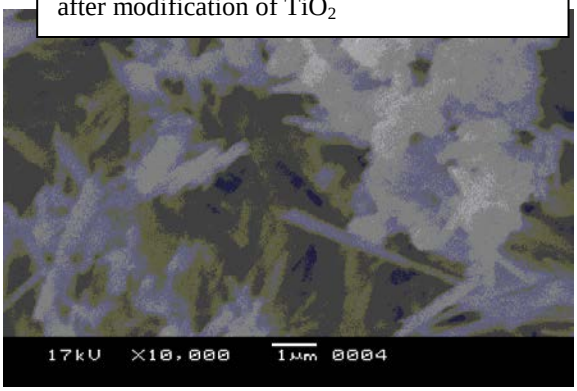

Fig.6.16(b) SEM Results of ZnTe Nano-tube

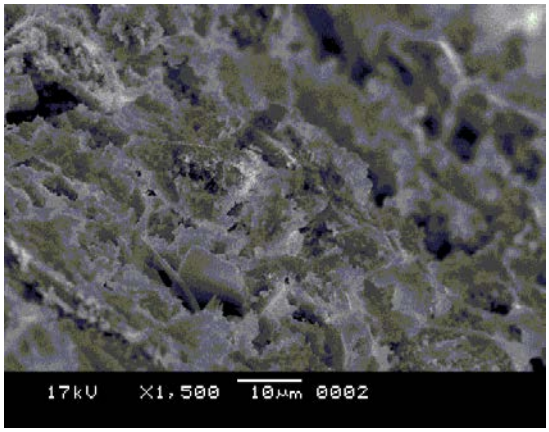

Fig.6.16(c) SEM Result of ZnO film

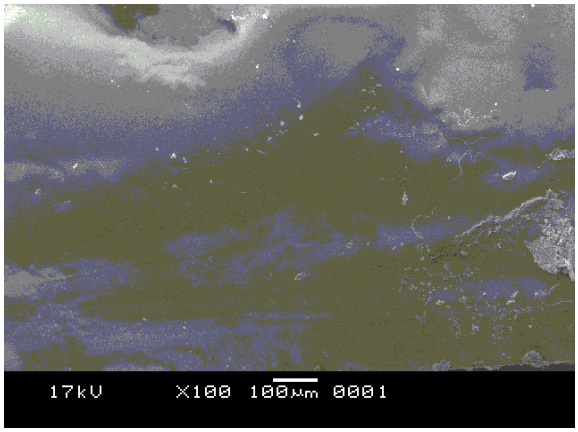

Fig.6.16(d). SEM Results of TiO2, CH3NH3SnI2 & ZnTe

6.6 REFERENCES

[1] Peng Gao, Perovskites: crystal structure, important compounds and properties, GMF Group Meeting.

[2] *Lee, M. M.; Teuscher, J.; Miyasaka, T.; Murakami, T. N.; Snaith, H. J. (October 4, 2012). "Efficient Hybrid Solar Cells Based on Meso-Superstructured Organometal Halide Perovskites". Science.338(6107):643647.*doi*:*10.1126/science.1228604 .PMID 23042296.

[3] Komal Kumari, Tapas Chakrabarti, Abir Jana, Disha Bhattachartjee, Bhaskar Guptaa and **Subir Kumar Sarka**r ,"Comparative Study on Perovskite Solar Cells based on Titanium, Nickel and Cadmium doped BiFeO3 active material", Optical Materials , Elsevier, Vol. 84, pp.681-688, August 2018

[4] Kim, Hui-Seon; Lee, Chang-Ryul; Im, Jeong-Hyeok; Lee, Ki-Beom; Moehl, Thomas; Marchioro, Arianna; Moon, Soo-Jin; Humphry-Baker, Robin; Yum, Jun-Ho; Moser, Jacques E.; Grätzel, Michael; Park, Nam-Gyu (August 21, 2012). "Lead Iodide Perovskite Sensitized All-Solid-State Submicron Thin Film Mesoscopic Solar Cell with Efficiency Exceeding 9%". Scientific Reports. 2. doi:10.1038/srep00591. PMC 3423636 PMID 22912919.

[5] Kojima, Akihiro; Teshima, Kenjiro; Shirai, Yasuo; Miyasaka, Tsutomu (May 6, 2009). "Organometal Halide Perovskites as Visible-Light Sensitizers for Photovoltaic Cells". Journal of the American Chemical Society. 131 (17): 6050–6051. doi:10.1021/ja809598r. PMID 19366264.

[6] Jeong-Hyeok; Lee, Chang-Ryul; Lee, Jin-Wook; Park, Sang-Won; Park, Nam-Gyu (2011). "6.5% efficient perovskite quantum-dot-sensitized solar cell". Nanoscale. 3 (10): 4088–93. doi:10.1039/C1NR10867K. PMID 21897986.

[7] Hadlington, Simon (October 4, 2012). "Perovskite coat gives hybrid solar cells a boost". RSC Chemistry world.

[8] Khomdram Jolson Singh, Chelsea Leiphrakpam, Nongthombam Palbir Singh, N.Basanta Singh and **Subir Kumar Sarkar, "**3D single GaAs co-axial nanowire solar cell for nanopillar-array photovoltaic device**",** International Journal on Computational Science and Application (IJCSA), AIRCC, Australia, Volume: 4, No.3, Pp 91-100, June 2014.

[9] Zhou, H.; Chen, Q.; Li, G.; Luo, S.; Song, T.-b.; Duan, H.-S.; Hong, Z.; You, J.; Liu, Y.; Yang, Y. (July 31, 2014). "Interface engineering of highly efficient perovskite solar cells". Science. 345 (6196): 542–546. doi:10.1126/science.1254050. PMID 25082698

[10] "NREL efficiency chart".

[11] Nakita K. Noel, Samuel D. Stranks, Antonio Abate, Christian Wehrenfennig, Simone Guarnera, Amir-Abbas Haghighirad, Aditya Sadhanala, Giles E. Eperon,a Sandeep K. Pathak, Michael B. Johnston, Annamaria Petrozza, Laura M. Herza and Henry J. Snaith, " Lead-free organic–inorganic tin halide perovskites for photovoltaic applications ", Energy Environ. Sci., 2014, 7, DOI: 10.1039/c4ee01076k

[12] Anastasiia Iefanova, Nirmal Adhikari, Ashish Dubey, Devendra Khatiwada, and Qiquan Qiao, " Lead free CH3NH3SnI3 perovskite thin-film with p-type semiconducting nature and metal-like conductivity", AIP Advances 6, 085312 (2016); doi: 10.1063/1.4961463

[13] Chong Liu, Jiandong Fan, Hongliang Li, Cuiling Zhang & Yaohua Mai, "Highly Efficient Perovskite Solar Cells with Substantial Reduction of Lead Content", Scientific Reports, 6:35705,DOI: 10.1038/srep35705

[14] Jing Feng Mechanical properties of hybrid organic-inorganic $CH_3NH_3BX_3$ (B = Sn, Pb; X = Br, I) perovskites for solar cell absorbers,APL Materials 2, 081801 (2014); doi: http://dx.doi.org/10.1063/1.4885256

[15] Hui-Jing Du, Wei-Chao Wang, and Jian-Zhuo Zhu, " Device simulation of lead-free CH3NH3SnI3 Perovskite solar cells with high efficiency", Chin. Phys. B, Vol. 25, No. 10 (2016) 108803.

[16] E. Constableand R. A. Lewis, "Optical parameters of Spiro-MeOTAD determined using continuous-wave terahertz radiation", JOURNAL OF APPLIED PHYSICS 112, 063104 (2012).

[17] Khomdram Jolson Singh and **Subir Kumar Sarkar,** "Highly efficient ARC less InGaP/GaAs DJ solar cell numerical modeling using optimized InAlGaP BSF layers", Optical and Quantum Electronics,Springer ,Volume 43, Issue 1-5, pp 1-21, DOI :10.1007/s11082-011-9499-y , 2011.

[18] Khomdram Jolson Singh and **Subir Kumar Sarkar,** "An Effective Modeling Approach for High Efficient Solar Cell Using Virtual Wafer Fabrication Tools", Journal of Nano and Electronic Physics, Volume 3, Number 1, Part 4:792-801, 2011.

[19] Khomdram Jolson Singh, Dhanu Chettri, Th. Jayenta Singh, and **Subir Kumar Sarkar**, "A Performance Optimization and Analysis of Graphene based Schottky Barrier GaAs Solar Cell" (ICEPOE 2017) at Thammasat University, Bangkok, Thailand, April 21-23,

2017

[20] E. Constableand R. A. Lewis, “Optical parameters of ZnTe determined using continuous-wave terahertz radiation”, JOURNAL OF APPLIED PHYSICS 112, 063104 (2012)

[21] Othmane Skhouni, Ahmed El Manouni1, Bernabe Mari, and Hanif Ullah, “Numerical study of the influence of ZnTe thickness on CdS/ZnTe solar cell performance”, Eur. Phys. J. Appl. Phys. (2016) 74: 24602, DOI: 10.1051/epjap/2015150365

CHAPTER 7

APPLICATION OF SOFT COMPUTING TOOL IN PHOTO-VOLTAIC DEVICE FOR PERFORMANCE OPTIMIZATION

- INTRODUCTION
- LITERATURE SURVEY OF SOFT COMPUTING TOOLS APPLICABLE TO SOLAR CELLS
- THEORY OF ALGORITHMS RELATED TO SOLAR CELL PARAMETERS EXTRACTION
- MODELING AND OPTIMIZATION
- RESULT AND DISCUSSION
- REFERENCES

7.1 INTRODUCTION

Extraction of 'Energy' from the 'solar energy' 'irradiance' through 'solar photovoltaic' 'PV Module' is a very important task in the domain of renewable energy. The 'PV modules' comprise of numbers of 'solar cells' in 'series' and 'parallel' connections. The energy conversion ratios in 'solar cells' are very low, so it is always desirable to 'extract' the 'maximum power', minimizing the external 'losses'. 'Photovoltaic systems' consist of different 'PV modules' interconnected in 'series' and 'parallel' 'panels or arrays'. Accurate estimation of the commercial 'PV system' depends upon the conglomeration of extraction methods and the 'quality' of used 'solar module'. The 'lumped model' is recognized to provide modeling of as impeccable only if it placates the I-V characteristics curve at all operating points. In this context derivation of the 'electrical properties' from the non-linear 'current voltage' '(I-V) curve' of the 'solar cell' module is very critical in respect of 'efficiency', device 'performance' etc. Various

‘electrical models’ like ‘single diode’ and ‘double diode’ ‘electrical circuit’ models are used to describe the ‘solar cell’ curve in practice. ‘Different algorithms’ are used to extract these ‘parameters’ by different entity [1-2]. The ‘recently developed’ heuristic algorithms are like Fireflies Algorithm (FA), ‘Cuckoo Search’ (CS), Differential Algorithm and ‘Particle Swarm Optimization’ techniques are most popular.

Another critical part of ‘photovoltaic system’ is the ‘maximum power point’ tracking. For this purpose different controllers are designed and implemented in ‘Photovoltaic systems’. The fundamental operations of these controllers are depends on the output ‘current’ and ‘voltage’ of the ‘cell’ or ‘panel’. The objective of these controllers is to vary the ‘operating current’ and ‘voltage’ in respect of the ‘variable irradiance’ and ‘atmospheric conditions’, by which the accurate ‘maximum output power’ can be pull out in a very fast mode. These controllers are used in DC-DC, buck - boost converter with variable duty cycle. To pull out ‘maximum power’ from the ‘PV system’ so many approaches are proposed by different researchers in ‘recent years’ [3-6]. The approaches are can be ‘categorized’ like (a) Direct methods (b) Indirect methods & (c) Artificial intelligence methods. Under these methods the ‘Perturb and Observe’ (P&O), ‘Polynomial Curve fitting’, ‘Hill Climbing’ (HC), ‘Incremental Conductance’ (INC), ‘Fractional open circuit voltage’ and ‘short circuit techniques’, ‘Fuzzy logic’ and ‘Neural networks’ are observed in different works. The instantaneous values of current and voltages are assorted in order to strive for the ‘Maximum Power Point’ in ‘direct’ and ‘indirect’ methods. To ‘overcome the drawback’ of ‘these methods’ the artificial intelligence methods are becoming more popular. The ‘recently developed’ ‘swarm intelligence’ based ‘algorithms’ which are motivated from the ‘social behaviors’ and ‘biological evolutions’ of various species like ‘Fireflies’, ‘termites’, ‘ants’, ‘honey bees’. By the change in external parameters of the ‘solar modules’, these algorithmic

controllers generate the ‘duty cycle’ for the ‘operating point’. To operate the ‘Photovoltaic systems’ at its ‘maximum point’, it is required to have precise knowledge about the ‘PV module parameters’ or it is better to say the ‘solar cells’ parameters.

In this ‘research work’, we have used a ‘double diode’ circuit model and two non-linear optimization techniques like cuckoo search and ‘firefly algorithm’ have been employed to get the solar cell’s model parameters from the I-V characteristics curve. ‘Firefly algorithm’ (FA) is a recently developed computational optimization model widely applied in solving ‘global optimization’ mathematical problems. ‘Firefly Algorithm’ introduced by ‘Yang-sing’, which is simulated on the ‘social behavior’ of tropical ‘fireflies’ based upon their characteristic ‘flashing pattern’. ‘Cuckoo Search’ is a ‘meta-heuristic algorithms’ which is population driven and based on the obligate ‘brood parasitic’ behavior of the ‘cuckoo birds’. In the recent years this ‘cuckoo search algorithm’ is being applied in ‘different fields of engineering’ to ‘optimize the results’, with great ‘efficiency’.

It is also proposed an ‘intelligent technique’ based on ‘Swarm Intelligence’ based ‘optimization technique’ to track the ‘Maximum Power Point’ of a ‘solar cell’. We concentrated our focus on two most recently introduced ‘Swarm based algorithms’: .Artificial Bee Colony’ (ABC) and ‘Firefly Algorithm’ (FA). ‘Artificial Bee Colony’ is inspired from the ‘intelligent exploration’ for ‘food sources’ of ‘honey bees’. We have prepared a detailed overview of equivalent ‘models’ of ‘solar cell’, based on different ‘Intelligence based algorithms’ as already mentioned in the above paragraph, design of simulation model of MPP controller, simulation results and comparisons of different ‘Evolutionary Algorithms’.

7.2 LITERATURE SURVEY OF SOFT COMPUTING TOOLS APPLICABLE TO SOLAR CELLS

The 'current voltage' 'I-V characteristic' is an important parameter of Photovoltaic solar cell. The specific 'equivalent circuit' model of 'solar cell' is required for extraction of different parameters of 'solar cells' depending upon the 'Photo current' (I_{ph}), 'reverse saturation current' (I_s), the 'series Resistance' (R_s) and 'shunt resistance' (R_{sh}) and the 'ideality factor' (n). Among the models, 'single diode' or 'double diode' 'electrical equivalent circuit' considering the 'solar cell' as current generator are employed to demonstrate the non linear 'I-V curve' of 'solar cell' [4]. The 'I-V characteristic' equation can be deduced from the single diode equivalent circuit as follows:

$$I = I_L - I_s\left(e^{\frac{V+R_sI}{nkT}} - 1\right) - \left(\frac{V+R_sI}{R_{sh}}\right) \dots\dots\dots\dots\dots\dots\dots (7.1)$$

and $$P = V.(I_L - I_s\left(e^{\frac{V+R_sI}{nkT}} - 1\right) - \left(\frac{V+R_sI}{R_{sh}}\right) \dots\dots\dots\dots\dots (7.2)$$

The 'series resistance' arises due to 'ohmic contacts' of 'cells' and in the contrary the 'shunt resistance' is arises for the losses of 'solar cell' due to 'diffusion current' and 'recombination-losses'. The output 'performance' of 'photovoltaic system' is determined on the parameters like 'open circuit voltage', 'short circuit current density' and the formost other one is 'maximum power point' (MPP). In this respect different 'analytical models' are utilized in the prevailing research field, as "Nonlinear least square optimization algorithm" based on Newton Model [5], Modified analytical five point method, Gonzalez – Longatt is a 'circuit based' 'simulation model' in order to determine the 'electrical behavior' of 'PV module' [6].

In the previous few decades, enormous nature based algorithms are developed to optimize or analytical or numerical solution of different polynomials [7]. The "meta-heuristic optimization algorithms" are pulling the attention of researchers for investigation of 'different parameters' of

‘solar cells’ or any other real time investigations. The mainstream algorithms are ‘Genetic Algorithm’ (GA), ‘Artificial Neural Network’ (ANN), ‘Perturb and Observation’ (P&O), ‘Hill Climbing’ (HC), ‘Particle swarm Optimization’ (PSO), ‘Differential Evolution’ (DE), ‘Firefly Algorithm’(FA), ‘Artificial Bee Colony’ (ABC), ‘Cuckoo Search’ (CS), ‘Hunting and Search’ (HS) etc [3,7].

The Evolutionary Algorithm (EA) and Differential Algorithm (DE) are employed to optimize the critical parameters of solar cell. The DE has ‘some advantages’ over the EA. The DE can optimize the Global optimizations irrespective of initial parameters [8].

The continuous changes of atmospheric conditions like solar irradiance or temperature are the reason of vary the different parameters of solar cell. With the change of atmospheric conditions, the real time ‘maximum power point tracking’ is a predominant part of ‘Photovoltaic systems’ to get the best performance of any system. This extraction of real time MPP can be classified in different categories leads to Direct Method, Indirect Method or Artificial Intelligence Methods [3].

“FPGA controlled Power conditioning units” are used to attain the ‘maximum power point’ (MPP) is a direct method [4][9-10].

The ‘Cuckoo Search optimization’ was motivated by the ‘species of Cuckoo bird’ which was developed in the year of 2009 by ‘Yang and Deb’. The Cuckoos are very enthralling bird because of its peculiar aggressive reproduction system along with its beautiful sound making ability. The mature Cuckoo lays ‘eggs’ in a nest of other species bird. One ‘cuckoo’ can laid one egg at each time and dumped it randomly chosen other species bird nest. The ‘host bird’ either unknowingly can hatch the egg to chick or destroy the egg or abandoned the nest. Hence the chances of maturing the ‘Cuckoo egg’ to chick is $P \in (0,1)$. The ‘Cuckoo-search’ is an

'application of Levy Flights' for generation of new solution. The Cuckoo eggs are hatched before the 'host bird egg' and the 'Cuckoo eggs' are similar to look too. The 'Cuckoo egg in a nest' contemplated a 'solution' in the optimization technique [11-13].

'Artificial Bee Colony' was proposed by 'Karaboga' in 2005, imitates the 'foraging behavior' of a 'Honey Bee swarm'. This ABC algorithm becomes most popular as it can be utilized into many complex problems. ABC is a 'population' based 'stochastic algorithm', where the position of 'food source' of nectar amount represents the possible solution. Each 'cycle of search' subsists of 'three steps' to find the 'food source' that represent the 'possible solution' to the 'problem to be optimized', that is considered in the said algorithm. Selection of 'food source' is operated by a parameter called "limit" which is analogous to the mathematical limit of the problems.

The 'Firefly Algorithm' is 'meta-heuristic algorithm' for 'global optimization', which is motivated by the 'social behavior' of 'unisex firefly' insects' flashing pattern. This 'algorithm' was suggested by 'Xin She Yang' in 2008. The 'Firefly Algorithm' can 'efficiently' solve different engineering problems. It has the capability of dealing multimodality which makes it so efficient [2][14].

7.3 THEORY OF ALGORITHMS RELATED TO SOLAR CELL PARAMETERS EXTRACTION

In our research work, we concentrate our attention on two popular 'swarm intelligence based algorithms' like: (i) 'Artificial Bee Colony' (ABC) 'Algorithm' and (ii) 'Firefly Algorithm' (FA). We have applied another 'meta-heuristic' 'optimization technique' that is Cuckoo Search Algorithm, which are applied in our work to 'extract' the different 'electrical parameters' of 'solar cells'.

A. 'SWARM INTELLIGENCE (SI) BASED ALGORITHMS'

'Swarm intelligence' (SI) has drawn attention of the researchers in recent years. 'Swarm intelligence' is the 'collective behavior' of 'social insects' under certain rules. This concept was inspired from life-cycles of insects like ants, bees, termites, fireflies etc. 'Each individual' of the 'swarm' moves stochastically within the space around them as per its perception of the neighborhood. The motion of 'each individual' must be computed in accordance with space exploration knowledge of it and the knowledge shared and obtained from other individuals. The stochastic factor of 'each particle's velocity' enables the swarm to 'explore' the unknown and unexplored 'regions' of the 'search space'. So, good initial distribution of swarm and knowledge sharing enables the swarm to extensively 'explore' the 'search space' and move to the best solution very quickly. A swarm needs to satisfy the following principles in order to be characterized as an intelligent swarm [7]:

(a). "The proximity principle": The 'swarm' should be 'able to perform' simple 'space and time computations'.

(b). "The quality principle": The 'swarm' should be 'able to distinguish' between a good solution and a bad solution.

(c). "The principle of stability": The 'swarm' should not change its 'mode of behavior' when the environmental conditions fluctuate.

(d). "The principle of adaptability": The 'swarm' should be 'adaptable to environmental fluctuations' when the change is worth of investment of energy.

Considering all the above the 'Artificial Bee Colony' (ABC) and 'Firefly Algorithm' (FA) is developed for computation purpose.

(i) Artificial Bee Colony: It is one of the most recently developed algorithms and has been applied to many complex problems. [15]. In 'ABC algorithm', swarm of 'artificial bees' are made to fly around within the 'search space' to find 'probable food sources' (solutions) with high nectar amounts (better fitness) and finally find the 'best solution'. The colony of artificial bees is 'categorized' into 'three different components' namely Employed, onlooker and Scout bees in order to realize the concept of 'division of labor'. This component can be explained like this:

Employed bee–An employed bee is employed randomly at specific 'food source' and carries the 'information about that food source' (fitness). They share this information of 'fitness value' of 'food source' with the onlookers.

Onlookers – Onlookers select the 'food source' and recruit bees for the 'food source area' of higher nectar amount.

Scout bees – Scout bee looks for the 'food sources' which are yet to explore. It searches the 'food source' randomly. When it does not find a previously unexplored food source, it becomes employed.

In this algorithm, the 'number of employed bees' or 'artificial onlookers' is equal to the 'probable number of solutions' of the population. Initially 'artificial bees' are distributed within the 'search space' randomly using the equation as bellow:

$$x_{i,j} = x_{j:max} - \text{rand}(0,1) * (x_{j:max} - x_{j:min}) \qquad (7.3)$$

Where $x_{j:max}$ and $x_{j:min}$ are 'lower' and 'upper bounds' for the j^{th} dimension. The position is updated for them using the equation:

$$v_{i,j} = x_{i,j} + \varphi_{i,j} * (x_{i,j} - x_{k,j}) \qquad (7.4)$$

Where k has to be different from i. $\varphi_{i,j}$ is a 'random number' ranging from -1 to 1. Next the fitness values of new solution $v_{i,j}$ and old solution $x_{i,j}$ are compared and position with 'better fitness' value replaces the other. For each 'onlooker bee' a 'food source' is chosen by a probability which is given by:

$$p_i = \frac{fitness_{\ i}}{\sum_{i=1}^{N} fitness_{\ i}} \qquad (7.5)$$

Where $fitness_i$ is the fitness value for i^{th} individual. After selecting a 'food source' onlooker bees start exploitation. If any position of 'food source' cannot be improved over a predetermined number of cycles then that 'food source' is said to be 'abandoned' and new position is found using the equation (7.4). This 'process of iteration' is repeated until the 'termination criterion' attains and 'best position' of each iteration.

(ii) Firefly Algorithm*:* The 'Firefly Algorithm' is a 'meta-heuristic', 'stochastic search algorithm' inspiring from the 'social behavior' of 'tropical fireflies'. The Fireflies move with each other realizing the 'flashing patterns' that uses 'bio-luminescence'. The 'rate of flashing', 'rhythm and intensity of flashes' generates a 'pattern' which attracts both the 'males and females' to 'each other'. Another important function of flashing is to seduce potential prey. The 'flashing characteristics' of 'fireflies' can be encapsulated by following rules:

(a) 'Fireflies are unisex' and hence irrespective of sex 'every firefly' will proceed towards more appealing one.

(b) The more appealing firefly is proportional to its 'flashing intensity'. So among the flashing fireflies, will move towards the brighter one. If there is no brighter one, than it will move 'randomly' through the 'space'.

(c) As the 'intensity of the light' decreases with distance attractiveness will also decrease.

(d) The ‘flashing intensity’ of an individual firefly, corresponds to the ‘fitness value’ is to be optimized.

Thus for ‘firefly algorithm’ there are two predominant factors are involved, that is ‘variation of light intensity’ and ‘formulation of attractiveness’. In simplest cases ‘light intensity’ varies according to the ‘inverse square law’ [16]:

$$I(r)=\frac{I_0}{r^2} \quad \ldots\ldots\ldots\ldots\ldots\ldots\ldots (7.6)$$

Where, I_0 is the ‘intensity at the source’.

‘Light intensity’ also varies depending on the ‘medium properties’. For a medium having light absorbing coefficient γ, the variation in light intensity can be formulated as:

$$I(r)=I_0 e^{-\gamma r} \quad \ldots\ldots\ldots\ldots\ldots\ldots (7.7)$$

Singularity at r=0 can be avoided by combining the effects of ‘inverse square law’ and ‘light absorbing coefficient’, which derives Gaussian form as bellow:

$$I(r)=I_0 e^{-\gamma r^2} \quad \ldots\ldots\ldots\ldots\ldots\ldots\ldots (7.8)$$

As fireflies ‘attractiveness’ is proportional to the ‘light intensity’ observed by the adjacent fireflies. So, if we define a variable β for attractiveness then ‘variation of attractiveness’ will be quite similar to the variation in light intensity.

$$\beta=\beta_0 e^{-\gamma r^2} \quad \ldots\ldots\ldots\ldots\ldots\ldots\ldots (7.9)$$

Here β_0 is the ‘attractiveness’ at r=0 and ‘r’ is the ‘distance’ between two adjacent fireflies. The case r=0 implies two fireflies were found at the same exact point on the search space.

The value of light absorbing coefficient γ plays a critical role on the ‘performance’ of the ‘algorithm’ and the ‘speed of convergence’. Here, we assume the value of γ to be between 0.1 and 10. The ‘distance’ between two fireflies can be computed as the ‘Cartesian distance’ between them. For example, the ‘distance’ between i^{th} and j^{th} fireflies can be given as:

$$r_{ij} = |x_i - x_j| = \sqrt{\sum_{k=1}^{d} (x_{ik} - x_{jk})^2} \qquad (7.10)$$

The main position update formula for i^{th} firefly which is attracted to another more attractive (brighter) firefly j can be given as:

$$x_i^{t+1} = x_i^t + \beta_0 e^{-\gamma r_{ij}^2}(x_i - x_j) + \alpha\varepsilon_i \ldots\ldots\ldots\ldots\ldots\ldots\ldots\ldots\ldots (7.11)$$

Here ε_i is a randomization parameter and α is the parameter controlling the step size. In some variants of Firefly Algorithm, the 'movement' of the fireflies is gradually decreased by controlling the parameter α.

B. 'CUCKOO SEARCH OPTIMIZATION'

'Cuckoo search' is one of the most recent 'meta-heuristic', population driven 'algorithms' developed in 2009 by 'Xin-She Yang and Suash Deb' and it imitates the unique breeding characteristics of some 'cuckoo species'. Despite being fairly new CS has gathered attention of many researchers 'in recent years' for it can outperform many popular evolutionary and 'swarm' based 'optimization techniques' like 'Genetic Algorithm' (GA) and 'Particle Swarm Optimization' (PSO) [12].

(i). **Cuckoo breeding behavior**: 'Several species' of cuckoos are brood parasites, 'lay their eggs' in other birds' nests. Probability of survival of eggs depends upon the 'eggs' not getting 'discovered' by the 'host bird'. The female cuckoos adopt different strategies depending upon defensive strategies of host species. Some species of cuckoos lay eggs which closely resembles the 'host bird's eggs'. This ensures less chance of getting the 'alien eggs' 'discovered' by the 'host birds'. Some cuckoo species lay darker 'colored eggs' in the nests of host birds whose eggs are lighter in color. This strategy effectively hides the cuckoo's eggs from the host and reduces the chances of them getting abandoned.

(ii). Levy Flight: In natural world, many 'animals and insects' exhibit levy flight for efficient search for 'food sources'. Usually searching of food at 'current location' and a 'transition probability' is to next location. A 'levy flight' is a 'random walk'. This search pattern can be used in 'optimization algorithms' with good 'efficiency'.

Yang and Deb described 'cuckoo search algorithm' [12] based on 'three assumptions':

1. A cuckoo chooses a host nest randomly and lays 'one egg' at a time.
2. The 'best nests' with 'high quality eggs' (better fitness value) will move on to next generation.
3. The number of 'host nest' is constant and each egg will be associated with a probability p_a of getting 'discovered' by the 'host bird'. The discovered 'eggs' will be discarded'

The 'each cuckoo' is updated its position using 'Levy flights'

$x_i^{t+1}=x_i^t+\alpha\oplus\text{Levy}(\lambda)$ …… (7.12)

Where 'α' is a step scaling factor,

Levy flight 'provides' a 'random search' with 'random step length' is drawn from Levy distribution.

$$\text{Levy}\sim u=t^{-\lambda}(1<\lambda\leq 3) \text{ ……..(7.13)}$$

This Levy distribution has 'infinite mean' and 'infinite variance'.

7.4 MODELING AND OPTIMIZATION

The equivalent circuit diagram of a 'solar cell' is considered with 'double diode model' as it is given in figure 7.1. In this model, 'solar cell' has been 'modeled' as 'current source' parallel to rectifying diode for 'diffusion current' as 'diode current' (I_{d1}). The 'current source' has also

been connected by another ‘shunt diode’ for unveiling recombination current as diode current (I_{d2}). The resistance in series (R_s) accounts for ‘ohmic losses’. The ‘shunt resistance’ (R_{sh}) are represented for ‘current leakages’ across the ‘p-n junction’. The ‘ideality factor’ (n) is represented the ‘quality of the junction’.

In this ‘double-diode model’, the ‘cell terminal current’ is calculated as follows:

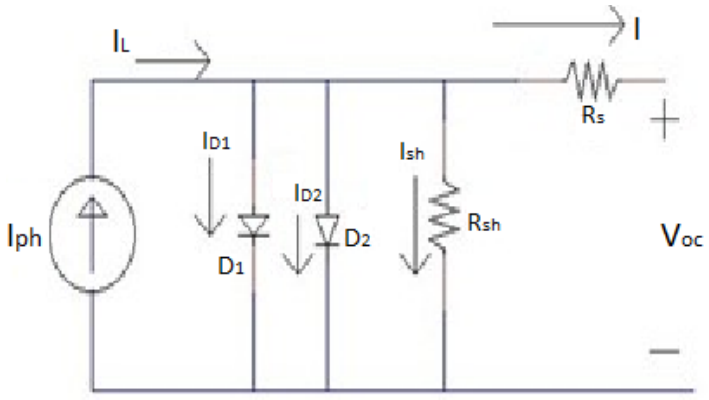

Figure-7.1:’Double diode solar cell equivalent circuit’

$$I = I_{ph} - I_{d1} - I_{d2} - I_{sh} \qquad (7.14)$$

Where

I= ‘Terminal current’

I_{ph}= ‘Cell generated photocurrent’

I_{d1}, I_{d2}= ‘Diode saturation currents’

I_{sh}= ‘Shunt resistor current’

The diode currents shown here can be derived from the Schottky diffusion model in P-N junction as shown in equation (7.15) and (7.16).

$$I_{d1} = I_{s1}(e^{\frac{V+R_sI}{\eta_1 V_t}} - 1) \qquad (7.15)$$

$$I_{d2} = I_{s2}(e^{\frac{V+R_sI}{\eta_2 V_t}} - 1) \qquad (7.16)$$

Thus the equation (7.14) can be modified as equation (7.18) after solving for the shunt current in equation (7.17):

$I_{sh} = (\frac{V+R_s I}{R_{sh}})$ …….. (7.17)

$I = I_{ph} - I_{s1}(e^{\frac{V+R_s I}{\eta_1 V_t}} - 1) - I_{s2}(e^{\frac{V+R_s I}{\eta_2 V_t}} - 1) - (\frac{V+R_s I}{R_{sh}})$ …… (7.18)

From the above equation power equation can be written as below:

$P = V * I$ where, V and I are'voltage' and 'output current' from the 'solar cell'

or, $P = V[I_{ph} - I_{s1}\left(e^{\frac{V+R_s I}{\eta_1 V_t}} - 1\right) - I_{s2}\left(e^{\frac{V+R_s I}{\eta_2 V_t}} - 1\right) - \left(\frac{V+R_s I}{R_{sh}}\right)]$ … … … … … (7.19)

The equation (7.18) is the characteristic curve equation for double diode model. The only difference in single diode model the 'diffusion' and 'recombination current' is accompanied in 'single diode current' and in double diode model, both the 'diffusion' and 'recombination current are shown separately.

(i). Methodology and Formulation of Fitness Function:

Thus equation (7.18) is the non-linear transcendent for the 'output current' involved form the 'solar cell circuit'. The fitness function for this optimization is the 'error criterion' which used in 'classical curve fitting' is based on the 'sum of the squared distances' between the experimental and calculated data [9].

$$E(x) = \sqrt{\frac{1}{p}\sum_{i=1}^{p} | I_i^{exp} - Y(I,V,\Phi)|^2} \qquad (7.20)$$

$$Y(I,V,\Phi) = I_{ph} - I_{s1}(e^{\frac{V+R_s I}{\eta_1 V_t}} - 1) - I_{s2}(e^{\frac{V+R_s I}{\eta_2 V_t}} - 1) - (\frac{V+R_s I}{R_{sh}}) \qquad (7.21)$$

Where $\Phi = \{I_{ph}, I_{s1}, I_{s2}, n_1, n_2, R_s, R_{sh}\}$

In this process, an initial population of model parameters generated randomly. Based on these parameters, a current value is calculated for each individuals using equation (7.21). As the

'current voltage equation' of a 'solar cell' (7.21) has seven unknown variables ($I_{ph}, I_{s1}, I_{s2}, n_1, n_2, R_s, R_{sh}$), so these variables were considered as the 'parameter for optimization'. These current values are then 'compared with the experimental value' through 'error criterion' equation (7.20) and the values of the 'model parameters' are get evaluated at each iteration. The 'objective' of this 'optimization' is to 'minimize' the 'error criterion' equation (7.20) so that the 'fitted curve' exactly matches the experimental curve. This iterative process goes on until the 'termination criterion' is fulfilled.

(ii) SWARM INTELLIGENCE BASED MPP TRACKING:

We have proposed an intelligent approach to track the 'Maximum Power Point' (MPP) of a 'solar cell'. The 'swarm intelligence' based 'algorithms' are used to track global MPP of a 'PV module'. The 'main objective' of the 'proposed model' is to deliver a constant power, which 'corresponds to P_{max}' of the 'solar cell' at that given 'irradiance level' and 'temperature'. The most 'important function' of the SI based 'controller' is to take 'output voltage' and 'current' of the 'PV module' as input and compute a 'duty cycle' corresponding to the 'peak power' at the particular 'G' and 'temperature' in which the 'PV module' is operating. Then this 'duty cycle' is fed to a boost type dc-dc converter which delivers the desired constant power to the load. Equation (7.19) is treated as the 'objective function' for the 'SI' based optimization purpose.

A simple schematic of the 'proposed approach' is highlighted in the figure 7.2. The figure 7.3(a) & 7.3(b) model was realized and effects of the parameters (irradiance level and temperature) on the P-V characteristics are observed.

For generating experimental 'I-V curve' of a 'PV module' a 'simulation model' was designed using MATLAB/SIMULINK environment. This model was used to generate 'I-V curves' at 'different environmental conditions' which were fitted using 'different evolutionary' and 'swarm

algorithms' to 'extract the parameters' required to generate the exact same curve using double diode model. Figure 7.4 depicted the 'simulation model' of a 'PV module'.

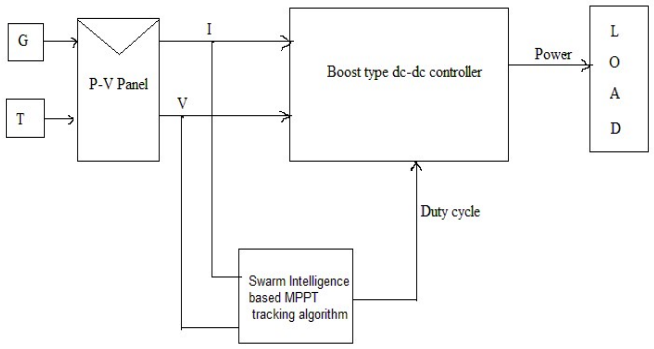

Fig 7.2 Schematic representation of the proposed approach

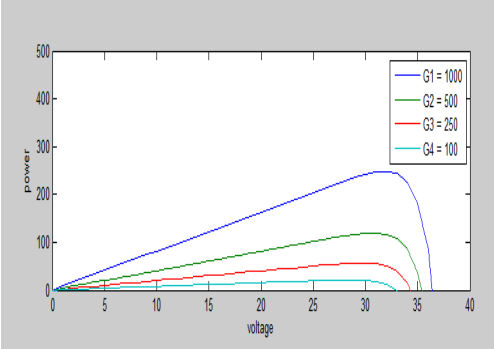

Fig 7.3(a) Change in P-V characteristic with the change in irradiance level

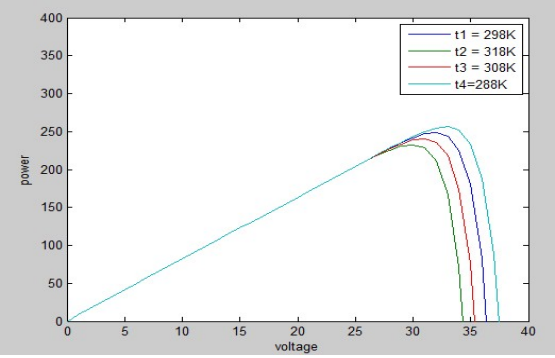

Fig 7.3(b) Change in P-V characteristic with temperature

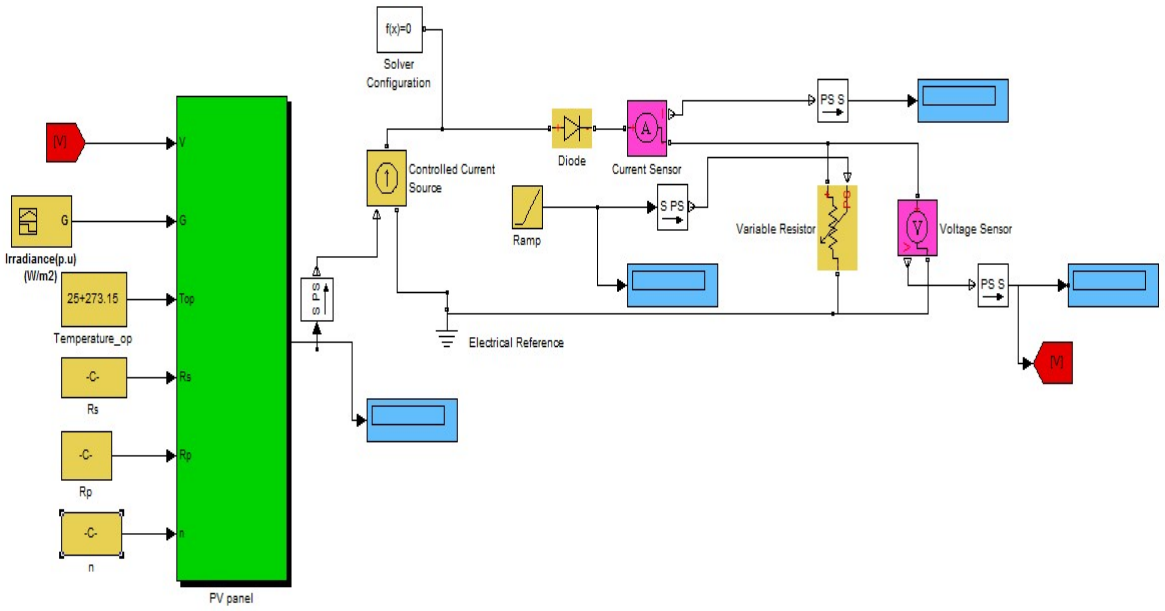

Fig. 7.4 MATLAB/SIMULINK model of a PV module

7.5 RESULTS AND DISCUSSION

The SIMULINK based 'solar cell' is used and simulated the 'I-V characteristics curves' are depicted in figure 7.5 and figure 7.6. The fitted 'I-V characteristics curves' are evaluated by using 'firefly algorithm' and 'cuckoo search optimization' respectively at different 'irradiance levels'. In each case, three different 'environmental conditions' (1000, 600 and 200 W/m^2) were considered and 'FA' and 'CS' were used to fit the 'curves' at different 'irradiance levels'. It can be seen clearly both the curves are exactly fitting with the synthetic SIMULINK curve. As a 'double diode model' has been used to 'characterize I-V curve', the total unknown parameters mount up to seven in the fitness function. Thus, the value of seven 'model parameters' values estimated using 'soft computing tools' like 'Firefly Algorithm' (FA) and 'Cuckoo Search' Algorithm (CS). The results are compared with 'DE' and 'PSO Algorithm' also in the Table 7.1.

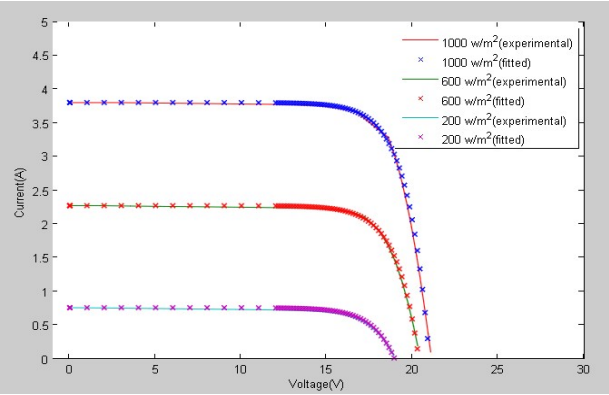

Fig 7.5: The Simulated fitted curve using firefly algorithm

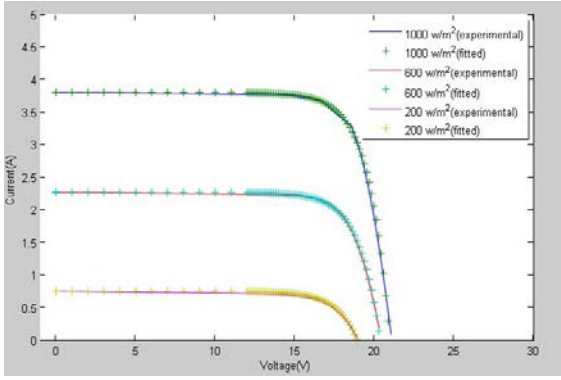

Fig 7.6: The Simulated fitted curve using Cuckoo Search Algorithm

Table 7.1: Estimated parameters for SIMULINK based solar cell at 200W/$m^2$and 25°C using different soft-computing algorithms

Parameters	FA	CS	DE	PSO
I_{ph}	0.7598	0.7598	0.76	0.7599
I_{s1}	1.1793×10^{-07}	8.8479×10^{-08}	1.1255×10^{-07}	6.4211×10^{-07}
I_{s2}	1.4264×10^{-04}	4.1191×10^{-05}	3.5181×10^{-05}	3.7482×10^{-05}
R_s	0.1093	0.1139	0.1717	0.1690
R_{sh}	381.68	353.6029	325.9318	379.8742
n_1	1.33	1.32	1.33	1.5
n_2	3.00	2.38	2.4	2.59
Fitness value	0.02	0.32	0.91	1.1
Computational time (sec)	1.82	1.87	1.94	1.91

'Artificial Bee Colony' (ABC) and 'Firefly Algorithm' (FA) were separately used in the proposed model. Simulation for each case has been given. Table 7.2 demonstrates MPP for a

given ‘solar cell’ at ‘different irradiance levels’ and ‘temperature’ and found analytically using the suggested model under ‘standard test condition’ along with the value of ‘parameters’ of I_s, I_{ph}, R_s & R_{sh} are 1.6×10^{-10}A, 8.206 A, 0.47Ω & 608 Ω respectively [11]. The numbers of cells considered in this analysis is 60. Figure7.8 demonstrates the controller output at 500 W/m^2& 25^0C when using ABC as ‘MPP tracking algorithm’. Fig 7.9 demonstrates the ‘controller output’ at same condition when ‘FA’ was used as ‘MPP tracking algorithm’. Finally table 7.3 and Table 7.4 compare the ‘performances’ of different ‘evolutionary algorithms’ in this context. During comparison, the number of individual in a ‘population’ in each algorithm was kept same 25. The figure 7.10 compares the ‘performances’ of different ‘evolutionary algorithms’ in terms of time taken to reach MPP.

Table 7.2: P_{max} (W) for different irradiance level and temp

	15°c	25°c	35°c	45°c
100 W/m^2	21.68	20.93	20.25	19.54
200 W/m^2	46.23	44.74	43.24	41.75
300 W/m^2	71.69	69.38	67.06	64.74
400 W/m^2	97.14	94.05	90.96	87.87
500 W/m^2	123.4	119.5	115.6	111.7
600 W/m^2	149.7	145	140.2	135.5
700 W/m^2	175.2	169.7	164.2	158.8
800 W/m^2	202.3	196	189.7	183.4
900 W/m^2	229.4	222.2	215.1	208
1000 W/m^2	256.5	248.5	240.6	232.7

Table 7.3: Comparison of performances of different evolutionary algorithms

Operating Condition		Power Delivered to the load (W)	
		ABC	FA
100 W/m^2	15^{0}C	21.65	21.62
	25^{0}C	20.9	20.8
	35^{0}C	20.2	20.15
	45^{0}C	19.5	19.5
300 W/m^2	15^{0}C	71.66	71.63
	25^{0}C	69.3	69.35
	35^{0}C	66.95	67.0
	45^{0}C	64.72	64.73
500 W/m^2	15^{0}C	123.3	123.1
	25^{0}C	119.3	119.1
	35^{0}C	115.5	115.5
	45^{0}C	111.6	111.5
1000 W/m^2	15^{0}C	256.4	256.1
	25^{0}C	248.29	248.42
	35^{0}C	240.5	240.35
	45^{0}C	232.6	232.65

Table 7.4: Comparison of Performance of different evolutionary algorithm

Algorithm	Time taken to reach MPP by the Controller (sec)	Convergence speed of algorithm (No. of iterations)
ABC	0.28	8
FA	0.57	12

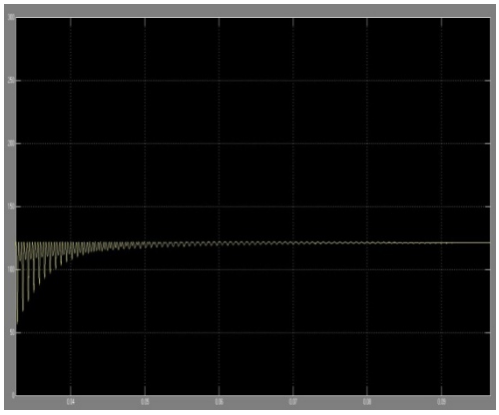

Fig.7.8. Controller output at 500 W/m^2&25°c using ABC as MPPT tracking algorithm

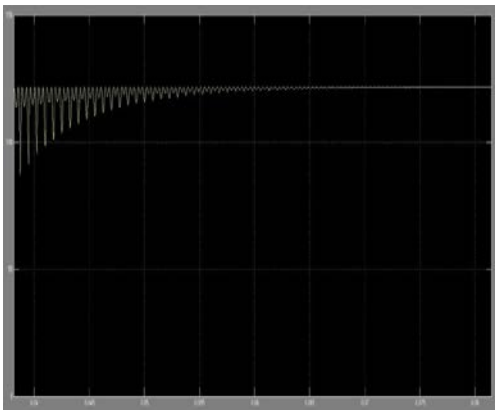

Fig 7.9: Controller output at 500 W/m^2&25°c using FA as MPPT tracking algorithm

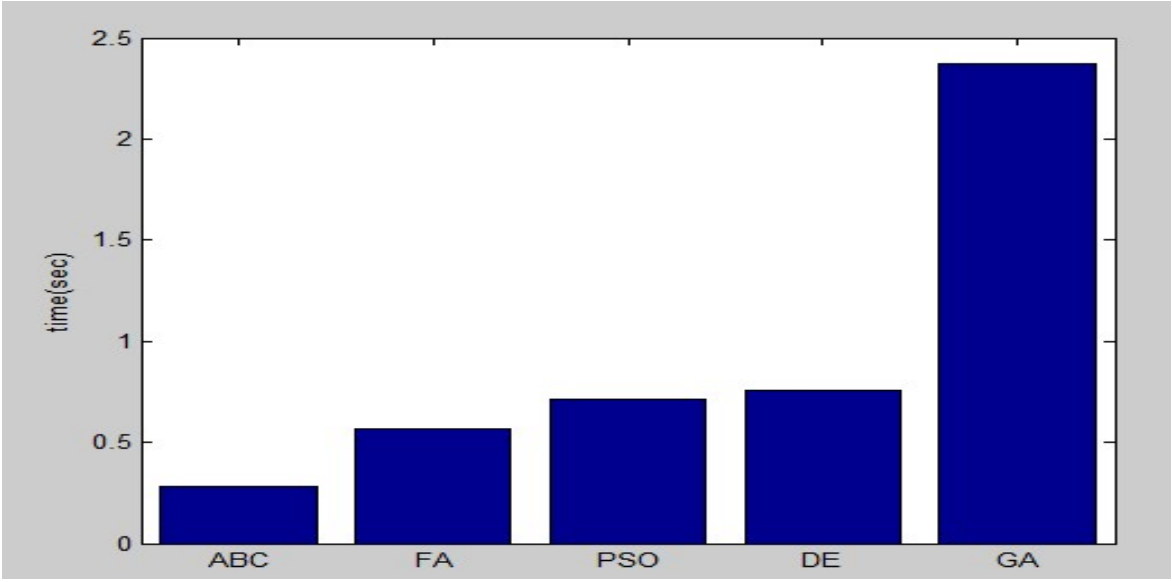

Fig 7.10: Comparison of performances of different evolutionary computing techniques for MPPT

7.6 REFERENCES

[1] Walker G. Evaluating MPPT converter topologies using a MATLAB PV model. JElectr Electron EngAust 2001;21:8.

[2] Sah CT, Noyce RN, Shockley W. Carrier generation and recombination in P–N junctions and P–N junction characteristics. Proc IRE 1957;45:1228–43.

[3] W. Xiao, N. Ozog, and W. G. Dunford, "Topology study of Photovoltaic interface for maximum power point tracking," *IEEE Trans. Ind.Electron.*,Vol.54, No.3,(2007), pp.1696–1704.

[4] E. Koutroulis, K. Kalaitzakis, and N. C. Voulgaris, "Development of a Microcontroller-based photovoltaic maximum power point tracking control System," IEEE Trans. Power Electron, Vol.16, No.1, (2001), pp.46–54.

[5] N. Femia, G. Petrone, G. Spagnuolon, and M. Vitelli, "Optimization of Perturb and observe maximum power point tracking method," *IEEE Trans.Power Electron*. Vol.20, No.4(2005), pp.963–973.

[6] I.William Christopher and R.Ramesh, "Comparative Study of P&O and InC MPPT Algorithms", American Journal of Engineering Research (AJER) , e-ISSN : 2320-0847 p-ISSN : 2320-0936, Volume-02, Issue-12, pp-402-408.

[7] M MMillonas, "Swarms, phase transitions and collective intelligence", *C. G. Langton, Ed., Artificial life III*, Addison Wesley, Reading, MA, 1994 .

[8] O. Wasynczuk, "Dynamic behavior of a class of photovoltaic power systems," *IEEE Trans. Power App. Syst.*, vol. 102, no. 9, pp. 3031–3037, Sep. 1983.

[9] Khomdram Jolson Singh and **Subir Kumar Sarkar**," Maximum Power Point Tracking Controller Using P and O Algorithm for Solar PV Array on FPGA " IEEE International

Conference on Communication and Signal Processing-2016 (IEEE-ICCSP'16),5-7 April, 2016 ,Melmaruvathur, Tamilnadu (India), Volume: IEEE Xplore

[10] Khomdram Jolson Singh, Terirama Thingujam and **Subir Kumar Sarkar**, "The Efficient FPGA-based Maximum Power Point Tracking (MPPT) Controller for Photovoltaic (PV) System", International Conference on Emerging Trends in Science and Engineering Research (ETSER-2015), 2-4 Dec, NIT Manipur.

[11] M. Ye, X. Wang, and Y. Xu, "Parameter extraction of solar cells using particle swarm optimization," Journal of Applied Physics, vol. 105, no.9, pp. 094502-094508, 2009.

[12] X.-S. Yang; S. Deb (December 2009). "Cuckoo search via Lévy flights". World Congress on Nature & Biologically Inspired Computing (NaBIC 2009). IEEE Publications. pp. 210–214.

[13] Tapas Chakrabarti, Suvrajit Manna, Udit Sharma, Tyajodeep Chakrabarti and **Subir Kumar Sarkar**, "Design of Intelligent Maximum Power Point Tracking (MPPT) technique based on Swarm Intelligence based Algorithms", 2015 International Conference on Power and Advanced Control Engineering (ICPACE), 12 – 14 Aug 2015.

[14] Tapas Chakrabarti, Tyajodeep Chakrabarti, Udit Sharma and **Subir Kumar Sarkar**, "Extraction of Efficient Electrical Parameters of SolarCell using Firefly and Cuckoo Search Algorithm", in IEEE-7th India 'International Conference on Power Electronics' (IICPE) 2016, 17th-19th November, Thapar University, Punjab, India, Volume: IEEE Xplore. (Ch-1/Ref20)

[15] D. Karaboga, B. Basturk, A powerful and efficient algorithm for numerical function optimization: artificial bee colony (ABC) algorithm, Journal of Global Optimization 39 (2007) 171–459.

[16] S. K. Pal, C. S. Rai, and A. P. Singh, "Comparative study of firefly algorithm and particle swarm optimization for noisy non-linear optimization problems," Int. J. Intelligent Systems and Applications, vol. 4, no. 10, pp. 50-57, 2012.

CHAPTER 8:

CONCLUDING REMARKS AND FUTURE SCOPE

- ❖ Conclusion and Remarks
- ❖ Future Scope of Work

1.1. CONCLUSION AND REMARKS

This research work can be demarcated in two boundaries among the ‘nanoscale devices’. In first part, the work is engrossed in the nanoscale DMDG SON MOSFET, where we have studied the reliability of ‘nanoscale devices’ and ‘other part’ is dedicated to ‘Photovoltaic solar devices’. Our research work is confined to develop novel structures using alternative optoelectronics materials, for cost effective and efficient ‘thin film’ ‘solar cells’.

1) The scaling is inevitable in domain of electronics devices and VLSI circuits. In this research work, the 2-D ‘Poisson equation’ and 1-D ‘Schrodinger equation’ is solved under ‘dual material’ ‘dual gate’ to realize the ‘overall potential’ and ‘inversion charge profile’, considering the ‘gate voltage’ as small signal of ‘AC’ ‘superimposed’ on ‘DC’ bias. Analytical studies have proven that the advanced DMDG SON structures are more unstable than the MOS counterparts, on application of a mixed supply in nano-regime. DMDG SON structures are capable of reducing ‘short channel effects’, thereby reducing threshold voltage, but this ‘threshold voltage’ which defines the operable range of any MOSFET and is a characteristic of that model, fluctuates appreciably at a single point in the channel on application of ac signals superimposed on dc, at the gate. Application of 10% to 30% ‘AC signal’ of the ‘original dc voltage’ is very common in practical circuits. Thus, if a small percentage of ac voltage, which may be the noise signal of circuits, is

leaked onto the gate of DMDG SON MOS structure the circuit may become fairly unstable. This fluctuation of threshold voltage will definitely oscillate the trans-conductance, drain-conductance, making the 'device behavior' utterly complex, and will definitely result in reduced 'battery life' and produce performance degradation. From the overall study, we 'may conclude' that, all the 'electrical parameters' of the 'device' gets 'affected' on the application of 'mixed supply voltage' at the gate. This instability may create a formost issue if advance 'MOS devices' are integrated in VLSI circuits.

2) The 'single junction' 'Silicon solar cells' are dominating the present solar cell industry. The 'extraction of silicon' from the 'silicon dioxide' is very complicated and very skillful technology also. The 'efficiency' of conventional 'silicon solar cells' have reached to their peak point of 20~22%. The productions of 'silicon solar cells' are also expensive, which leads the solar power tariff in upper side in comparison of conventional power. To break the bottleneck of this constraint the H-I-T 'solar cells' are very promising. But the H-I-T 'Solar cells' are basically made of c-Si and a-Si. In our 'research work', we substituted the a-Si by cheaper Zinc Oxide or Zinc Telluride as 'emitter layer' in the existing structure and achieved the significant 'improvement of efficiencies' of 25.54% and 27.71% respectively. The exhibited 'efficiency' of 'existing structure' with 'emitter layer' of a-Si is 23.04%. The 'short circuit current density' of ZnO(n) and ZnTe(p) (emitter layer) 'based solar cell' are 82mA/cm^2 and 85.03 mA/cm^2 respectively. The 'short circuit current density' is 81.11mA/cm^2, received from the existing structured solar cell of which the 'emitter layer' is made of a-Si. The 'thickness' of the 'emitter layer' is optimized to 10nm and perceived that the 'minimum optimum thickness' will give the better 'efficiency'. In this investigation of work in regards of HIT solar cell, it is

reconnoitered that the manoeuvre of silicon can be minimized with the incorporation of alternative materials in emitter layers. The best result of 'efficiency' is found with the application of ZnTe in the 'emitter laye'r of 'p' region, which is a novel idea in respect of improvement of efficiency.

3) In our 5^{th} chapter, we have explored on another form of 'solar cell' that is 'Dyesensitized solar cell', which is completely silicon free, made of 'low cost materials' and simple fabrication procedure. It is also an eco-friendly device. The light harvesting part of this type of 'solar cell' is the 'dye'. The inorganic and organic dyes like Red Colloid Dye, 'Red color dye' 'extracted from Hibiscus', 'Prussian Blue Dye', 'Blue dye' 'extracted from Clitoriaternatea', Green (Chlorophyll) Dyes are experimented in this 'research work' to develop efficient Dyesensitized solar cell. We have studied and fabricated five different 'Dyesensitized solar cells' with 'inorganic' and 'organic dyes'. The most significant result found is from the blue colored dyes of 'organic' and 'inorganic pigments' of Blue dye extracted from Clitoriaternatea and 'Prussian blue' dye. It is contemplated that the 'inorganic dye' based 'solar cells' are more stable 'with respect to' organic dyes.

4) Generally the 'Perovskite materials' 'Methyl ammonium leads Iodide' ($CH_3NH_3PbI_2$) is used in 'Perovskite solar cells'. As the Lead (Pb) is hazardous for health and environment too, we have replaced the Lead (Pb) by Tin (Sn) in the 'Perovskite material' as 'Methyl ammonium Tin Iodide' ($CH_3NH_3SnI_2$). Normally the 'hole transport layer' is popular with the 'organic compound material' 'spiro-MeOTAD'. But the material is too expensive. Hence the 'Perovskite solar cell' cost also will be increased. In our 'research work' we have proposed a novel structure with ZnTe as 'hole transport layer' (HTL) as

"*metal contact/TCO/ZnTe(p)/$CH_3NH_3SnI_3$/TiO_2(n)/TCO/metal contact"* and is achieved the simulated 'efficiency' of 23.54% with the 'short circuit current' of 36.88 mA/cm^2. We have fabricated the above structure in our 'Lab environment' and observed the 'efficiency' of 5.032% with the 'short circuit current' 11.57 mA/cm^2. We have simulated another structure of 'Perovskite solar cell' with the ETL of ZnO and got the 'efficiency' of 22.94% with the 'short circuit current' of 34.23 mA/cm^2. Another Perovskite ($CH_3NH_3SnI_3$) 'solar cell' applying 'ZnO as ETL' and 'ZnTe as HTL', has been fabricated and the 'efficiency' and 'short circuit current' observed 2.71% and 7.48 mA/cm^2. Our observations are that during fabrication the optimized 'layer thickness' are not maintained and the 'Perovskite materials' got the chance to get oxidized during change of chambers. Hence the fabricated results are not 'similar to simulated' results.

5) A comparison is illustrated in 'our work' on the 'performance' of 'Firefly' and 'Cuckoo Search Algorithm' in the estimation of model parameters. From fig (2) and (3) it can be 'concluded' that the curves obtained after calculating the parameters from the 'Firefly algorithm' and 'Cuckoo search algorithm' exactly fitting with the experimental curve of PV module. Swarm intelligence is gaining popularity among researchers for its 'fast convergence rate' that is also a necessary criterion for tracking 'Maximum Power Point' (MPP) of a 'solar cell'. Hence in this research work, we opted for swarm intelligence based optimization technique to track MPP of a solar cell. It is found that on an average 0.28 sec was taken 'by the model' to reach MPP when 'Artificial Bee Colony' was used as the MPP tracking algorithm in the controller. And 0.57 sec was the 'average time taken' by the 'model' when 'Firefly Algorithm' was used in the MPPT controller. It is also perceived that the power delivered to the load at 'different irradiance levels' and

'temperatures' are almost same as the 'Maximum Power Point' of the 'solar cell' found analytically at that condition (given in table 2).The controller outputs given in fig 4 and 5 suggest that there has been almost zero 'steady state oscillation' when 'ABC' and 'FA' are used as MPP tracking algorithm. From our results it may be concluded that 'ABC tracks MPP' at a much faster rate than other algorithms. So, faster response of the controller and efficient power delivery to load proved the 'validity of our work'.

8.2 FUTURE SCOPE OF WORKS:

1. The Analytical model of nanoscale DMDG SON MOSFET is carried out and viewed that application of 'AC supply' that is part of 'noise signals' along with DC supply in gate voltage, all the 'electrical parameters' are fluctuated which makes the devices instable. The validity should be verified in real life device structures and the applicability in VLSI circuits are to be done in future work.
2. The H-I-T 'solar cell' models are done applying ZnTe (p-layer) and ZnO (n-layer) 'emitter layer'. The remarkable 'efficiency' of 27.71% (ZnTe in emitter layer) and 25.54% (ZnO in emitter layer) are achieved by the 'Model solar cells'. In future the physics of enhanced efficiency in respect of current flow is to be studied and the Physical fabrications of these models are to be done, carrying the specific thickness considered in these two 'solar cells'.
3. The 'Dyesensitized solar cells' are fabricated employing different dyes on the 'TiO_2 semiconductor' layer. Alternative semiconductor materials like ZnO, CuO or any other similar materials can be used in the Dyesensitized solar cells in future. The alternative and substitutive solid materials are to be explored instead of liquid electrolyte. In future work the stability and 'DSSCs' life enhancement should be priority.

4. Lead free ‘Perovskite solar cells’ with ZnO as ‘electron transport layer’ and ZnTe the ‘hole transport layer’ are modeled and physically fabricated. The efficiency achieved is 22.94% (ZnO) and 23.54%(ZnTe) respectively in simulation software environment. But it is observed that the ‘efficiency’ drastically falls down in similar fabricated structure of ‘solar cells’ as 2.71% and 5.032%. Detailed investigation is required in future works. The thickness of each layer similar to the modeled structure should be taken care. More exploration with tuned ‘band gap’ of ‘Perovskite material’ is also to be done in future.
5. The different ‘soft computing tolls’ are used to extract the ‘electrical parameters’ of the ‘Photovoltaic solar panels’. The ‘Firefly Algorithm’ and ‘Cuckoo Search Algorithm’ are implemented to extract the ‘Short circuit current’, ‘open circuit voltage’ and ‘Fill Factor’. The ‘Cuckoo search algorithm’ shows the best result. The ‘particle swarm optimization’ algorithms like ‘Artificial Bee Colony’ and ‘Firefly Algorithm’ applied to find the ‘Maximum Power Point’. The ‘duty cycle’ of the controller has been found 0.28 sec and 0.57 sec using ABC and FA respectively. The controller for extraction of MPP is to be designed with ABC algorithm and physical implementation can satisfy the work, which can be done in future.